Australian Government
Department of Defence
Defence Science and
Technology Organisation

Fatigue Testing of AA7050-T7451 with Various Corrosion Prevention Surface Treatments

Marcus McDonald, Robert Boykett and Michael Jones *

Air Vehicles Division
Defence Science and Technology Organisation
* QinetiQ Aerostructures

DSTO-TR-2851

ABSTRACT

The aluminium components of combat aircraft are usually manufactured with corrosion preventative surface treatments. This report presents the results of a fatigue coupon testing program carried out on AA7050-T7451 that was used to aid in the understanding of the fatigue life effect that anodising and an etching surface treatment can have in comparison to as-machined surfaces. The testing program included both high and low stress concentration geometry coupons that were subjected to a combat wing root bending moment spectrum. The results of the fatigue testing showed a reduction in the fatigue lives of anodised and etched coupons, especially in the low stress concentration geometry coupons. An investigation into the anodising process indicated the cause of the pitting found was likely chemical attack during a chemical cleaning process prior to the anodic layer being applied. These pits, which were numerous, acted as relatively large crack initiation discontinuities.

RELEASE LIMITATION

Approved for Public Release

Fatigue Testing of AA7050-T7451 with Various Corrosion Prevention Surface Treatments

Executive Summary

Corrosion preventative surface treatments are commonly used on metallic components of modern combat aircraft to help prevent environmental effects from degrading the integrity of the structure. However, some metals are known to be susceptible to surface degradation due to the surface treatments themselves. A common outcome of a chemical surface treatment is pitting of the material surface resulting in more frequent and larger fatigue crack initiation sites, which can in turn potentially reduce the fatigue life of the component. This is significant since fatigue cracking is an important life-limiting factor which can be pertinent to the structural integrity of an aircraft.

This report presents the results of a fatigue coupon test program undertaken to investigate the potential life effects of four different surface treatments on aluminium alloy (AA)7050-T7451, a material commonly used in modern combat aircraft and known to be susceptible to chemical pitting attack. The surface treatments investigated and tested in this fatigue program were bare machined, machined and polished, anodised and etched. The tested coupons consisted of two different geometries representing both high and low stress concentration geometries. The coupons were subjected to a combat wing root bending moment spectrum that had the addition of marker loads to allow for the crack-growth progression to be measured post test. An assessment of the type, size and effectiveness of the fatigue crack initiation discontinuities was also undertaken.

The results of the coupon test program showed the fatigue life of the anodised and etched coupons were shorter than those of the machined coupons, especially in the lower stress concentration geometries. An assessment of the crack initiation sites in the anodised coupons showed that they were larger and more frequent than those found in the machined coupons and that this accounted for the difference in the fatigue lives. An investigation into the anodising process indicated the cause of the pitting found was likely chemical attack during a chemical cleaning process prior to the anodic layer being applied.

This project was carried out to aid in RAAF understanding of the effects that surface treatments have on the fatigue performance of the AA7050-T7451. The account of this effect can vary significantly between aircraft manufacturers; therefore this work may assist in the conduct of compliance finding, planning and technical risk assessments.

This page is intentionally blank

Authors

Marcus McDonald
Air Vehicles Division

Marcus McDonald initially spent 3 years working in the oil & gas, steel and railway industries for structural design projects and failure investigations. He has since worked a further 14 years in the aeronautical field at DSTO as a Structural Integrity engineer. Marcus' research fields include metallic fatigue analysis and structural optimisation. He was attached to the US Naval Air Command (2005-2008) as an Air Worthiness engineer for the new F-35 combat aircraft. He currently leads S&T activities in support of certification compliance on new combat aircraft, and provides structural integrity advice to the RAAF on numerous aircraft including F-35 Lightning II, F/A-18 Hornet and F/A18F Super Hornet.

Robert Boykett
Air Vehicles Division

Mr Rob Boykett is a senior engineer in Air Vehicles Division of DSTO. He holds a Bachelor in Aeronautical Engineering and a Masters in Systems Engineering from RMIT University.
Throughout his career, which began at Government Aircraft Factories in 1986 on missiles and civil airliners, he has worked in the field of structural analysis. Since 1990, he has worked at DSTO in a range of areas from F/A-18 & F-111 Full Scale Fatigue Testing, Bonded Repair Certification and Helicopter Airframe Fatigue. After managing Structural Integrity for both Army and Navy helicopters and the F-111 up to its retirement, he now supports the acquisition of the Joint Strike Fighter.

Michael Jones
QinetiQ Aerostructures

Mr Michael Jones graduated from Monash University in 2007 with a double degree in Engineering (Mechanical) and Technology (Aersopace). In 2009 he completed his Masters in Engineering Science (Research). He has since worked for QinetiQ Aerostructures providing engineering support to DSTO in the field of aircraft structural integrity, primarily supporting the acquisition of the F-35.

This page is intentionally blank

Contents

Abbreviations and Notations

a	Crack depth
AA	Aluminium Alloy
CF	Canadian Forces
FT55	IFOSTP centre fuselage full-scale fatigue test
FT55m5	FT55 spectrum with five compressive marker loads added
IFOSTP	International Follow-On Structural Test Program
IVD	Ion Vapour Deposition
K_t	Stress Concentration Factor
M5	Marker band representing 5 compressive loads
N6	Roughness grade number equivalent to 0.8 µm roughness value
NATA	National Association of Testing Authorities
Ra	Surface Roughness – mean
RAAF	Royal Australian Air Force
SEM	Scanning Electron Microscope
QF	Quantitative Fractography

This page is intentionally blank

1. Introduction

The aluminium alloy components of combat aircraft are usually finished with corrosion preventative surface treatments to help prevent environmental degradation of the surface that may lead to structural integrity issues. However, some metals are known to be susceptible to surface degradation due to the surface treatments themselves. Such degradation may include pitting of the material. These pits although usually small, can act as fatigue initiators in service and therefore can have an influence on the fatigue life of the structure. Some materials in certain forms may be more susceptible to pitting than others during chemical surface finishing treatments. When these pits are larger than other inherent discontinuities (inclusions etc.) from which fatigue cracking may grow, they can reduce the fatigue life of the component below that which may be expected or demonstrated during tests of the material without the final surface treatment. In order to understand the potential effect on fatigue life that typical chemical surface treatments can have on high strength aircraft aluminium alloys, coupon tests have been performed on Aluminium Alloy (AA)7050-T7451, a material commonly used in modern combat aircraft and known to be susceptible to chemical attack [1].

AA7050-T7451 coupons with four different surface treatments were tested. Two "base-line" treatments that would not normally be used in service without other treatments: machined and polished (with #400 grit paper) and bare-machined (N6 surface finish) and two finishing treatments that are used on aircraft components: pre- Ion Vapour Deposition (IVD) etched, and anodised. The main interest of the coupon testing program was the analysis of the anodised coupons, whilst the pre-IVD etched coupons (in service, such components would be coated with aluminium via the IVD method to give corrosion protection) were tested to allow the anodised results to be compared with previous IVD etched coupon results [2]. The polished coupons were prepared, tested and analysed for research purposes, primarily to determine the correlation effect between surface condition and fatigue life.

Two types of coupon for this testing program were manufactured; two to represent high, and another to represent a low stress concentration factor (K_t). The geometries were; centre-hole, side-notched, and dogbone. The coupons were subjected to a combat wing bending moment loading spectrum derived from the F/A-18 International Follow-On Structural Test Project (IFOSTP) that is designated FT55m5 [2, 3]. Five marker loads [4] were inserted into the spectrum to simplify post test quantitative fractography (QF) to be undertaken to determine crack growth curves for the tested coupons. The crack growth curves were measured to assist with related Royal Australian Air Force (RAAF) structural compliance finding activities.

2. Background

Aluminium alloys are often anodised for better wear and corrosion protection. Anodising is an electrolytic passivation process used to increase the thickness of the natural oxide layer on the surface of metal parts. In the case of aluminium alloys, the process produces controlled columnar growth of an amorphous aluminium oxide on the surface of the aluminium substrate [5]. When the aluminium substrate is electrochemically oxidised under constant, or increasing (typical for chromic acid methods) potential, the surface of the aluminium alloy is covered by the formation of a thick (thicker than the natural oxide) and strongly adherent oxide layer with a high hardness [6, 7]. There are several types of anodising, with some of the most common types being based on chromic acid anodising (the type used in this coupon test program), sulphuric acid anodising and hard anodising. Each of these is described in US Military Specification MIL-A-8625, as Type I, Type II and Type III. Each type of anodising utilises different electrolyte temperatures, current densities, and oxidising chemicals. The chromic acid anodising process produces a thinner [8] softer coating than the Type II & III coatings. This gives this type of coating better fatigue resistance than sulphuric acid and hard anodising [8-10]. Additionally, the hardness of the coating, in comparison to the aluminium alloy that it coats, gives the coated parts better wear resistance. The retention of some of the chromate ions in the coating improves its corrosion resistance through a measure of self-oxidative self-healing – if the coating is damaged the chromate can re-oxidise the surface to help prevent further damage.

Despite the increase in wear and corrosion protection, it is well documented that the anodising process decreases the fatigue life of aluminium alloys [5, 6, 8-13]. Three contributing factors to this reduction in fatigue strength are discussed in the literature. Firstly, the oxide layer is brittle compared to the aluminium substrate and may easily crack under cyclic stress [6, 12]. The load bearing ability of the coating results in these cracks acting as if they were cracks in the aluminium. Since they are sharp they produce high stress intensities (depending on the coating thickness and the applied stress) at their tips, allowing fatigue crack initiation at the interface with the aluminium. These cracks can then propagate into the base metal [6]. Another cause for a reduction in fatigue strength due to anodising is that tensile residual stresses can be created in the substrate during the anodising process [6, 8]. These tensile stresses raise the mean stress at the interface aiding early fatigue crack growth. Finally, the most reported cause for the reduced fatigue life is pitting caused by the pre-anodising process. The depth of the pitting also increases the stress intensities, partially if the anodic coating is cracked in these pits. Since the anodised layers are typically thin compared to such pits, the stress intensity increase at the base of the pits may be considerably greater than those at the base of the cracks in the layer on a smooth surface, hence pitting is more damaging to the fatigue strength. Pitting is formed primarily in the preliminary cleaning and preparation stages prior to the anodic layer being applied [5, 10, 11, 13].

Compared to a machined surface finish on high strength aluminium alloys, where the surface breaking inclusions (particularly those that have been cracked in the machining operation) act as crack initiators, the pits created from the anodising process are larger in size and number [11]. As a result, the initiation of fatigue cracks is promoted and the cracks start off at larger sizes than those that may be generated from other types of discontinuities. The result is

shorter total fatigue lives. As noted, a survey of the literature indicated that the degreasing and pickling (deoxidisation) stages are when the pitting may most commonly occur. Degreasing is performed to remove oils and grease from the metal surface [11]. Pickling removes the natural oxides and other compounds from the metal surface by utilising a solution which chemically removes (dissolves) the compounds, resulting in a more conductive clean surface for the anodisation process [11] that will give a consistent coating. The literature differs in the effect that each of these processes can have on the fatigue life of high strength aluminium alloys, with [5] concluding that the degreasing stage can result in a small decrease in fatigue life, whilst [11, 13] conclude that degreasing had no effect on the fatigue life. This is probably largely dependent on the degreasing method used i.e. either solvent or alkaline degreasing. However, they all agree that pickling had a significant effect on fatigue life, with the anodising process producing a further slight decrease in fatigue life [5, 10, 11, 13].

In [11], the pickling solution was shown to attack grain boundaries and inclusions forming pits. It was also concluded in that study, with the aid of a probabilistic analysis, that the distribution of fatigue life is strongly correlated to the distribution in the nucleating pit size [14]. References [5, 15] also show that the effect of the anodising process is dependent on, to a degree, additional variables - primarily the stress level, where lower stresses show a greater relative decrease in fatigue life compared to machined coupons. The time that the crack spends when it is small depends on the cyclic stress intensity level at the tip of the discontinuity from which is has initiated. If pitting effectively increases the starting size and therefore the cyclic stress intensity at the tip of the fatigue crack, it will spend less time while it is small compared to a crack initiating from a smaller discontinuity. For that reason it will have a shorter life when compared to a crack that starts from a crack in the anodic coating that occurs on a smooth surface and therefore with a lower cyclic stress intensity at its crack tip due to its smaller depth.

Other important considerations in the effect of anodising include the type of anodising [5, 11, 13], the grain direction [13] since it can play a significant role in the size of the pits created and the prior processing history and type and size of the microstructure [10], which again can effect the size and shape of the pits on the surface of the metal.

3. AA7050-T7451 Coupon Design

3.1 Material

The high K_t side-notched and low K_t dogbone coupons for these tests were cut from a rolled plate of AA7050-T7451 manufactured to AMS4050 specifications. The 6″ thick plate was supplied by Airport Metals (Pechiney) in 2004 and was labelled LM by the Defence Science and Technology Organisation (DSTO). The dimensions of the LM plate were 48″ x 144″ x 6.0″ but it was cut in half (72″) for transportation purposes.

The high K_t centre-hole coupons were cut from an AA7050-T7451 plate provided by Alcoa through AMI Metal Inc. in 1992. It was labelled KK by DSTO and had dimensions of 18″x 37.5″x 5″. The KK plate was also manufactured to AMS4050 specifications. It should also be noted that one high Kt centre-hole coupon that was tested, designated KF2B8, was cut from an AA7050-T7452 forging per MMS-146 by International Light Metals. Table 1 shows the AMS4050 specifications and the results of a chemical composition analysis performed by DSTO on the LM and KY plates.

Table 1 Chemical composition analysis by DSTO compared to specification AMS 4050E

Element	Min	Max	Analysis of LM plate	Analysis of KK plate
Zinc	5.7	6.7	6.2	6.06
Copper	2	2.6	2.2	2.12
Magnesium	1.9	2.6	2.1	2.25
Zirconium	0.08	0.15	0.09	0.11
Iron	--	0.15	0.07	0.08
Silicon	--	0.12	0.05	0.03
Manganese	--	0.1	0.01	0.01
Titanium	--	0.06	0.04	0.03
Chromium	--	0.04		0.005
Other Impurities, each	--	0.05		Ni <0.01
Other Impurities, total	--	0.15		<0.15
Aluminium		Remainder	Remainder	Remainder

3.2 Coupon Geometry

For the fatigue life coupon tests, both high and low stress concentration (K_t) coupons were manufactured and the coupon geometries are shown in Figures 1, 2 and 3.
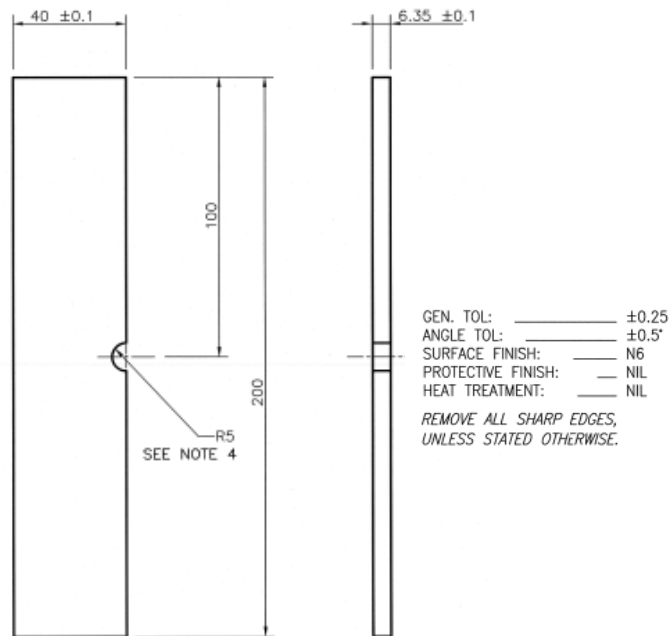
Figure 1: High K_t Side-notch Coupon
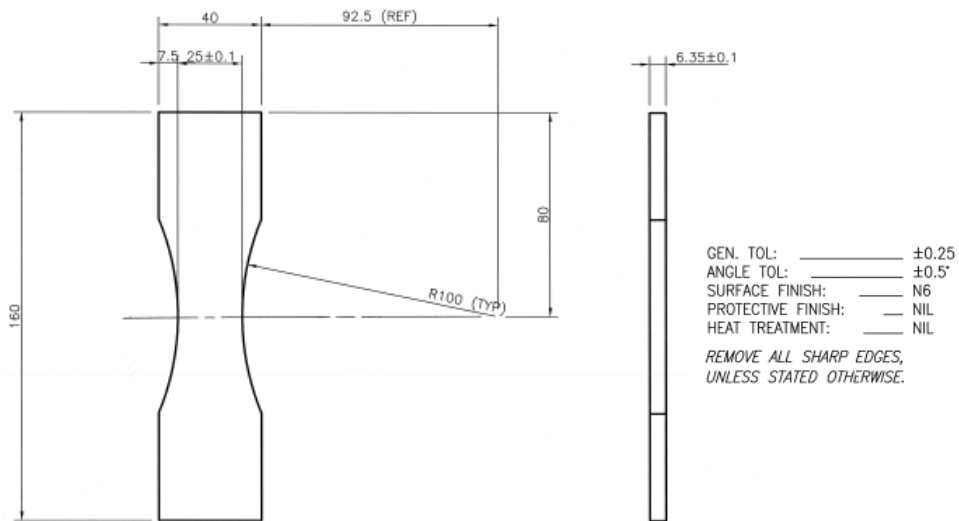
Figure 2: Low K_t Dogbone Coupon
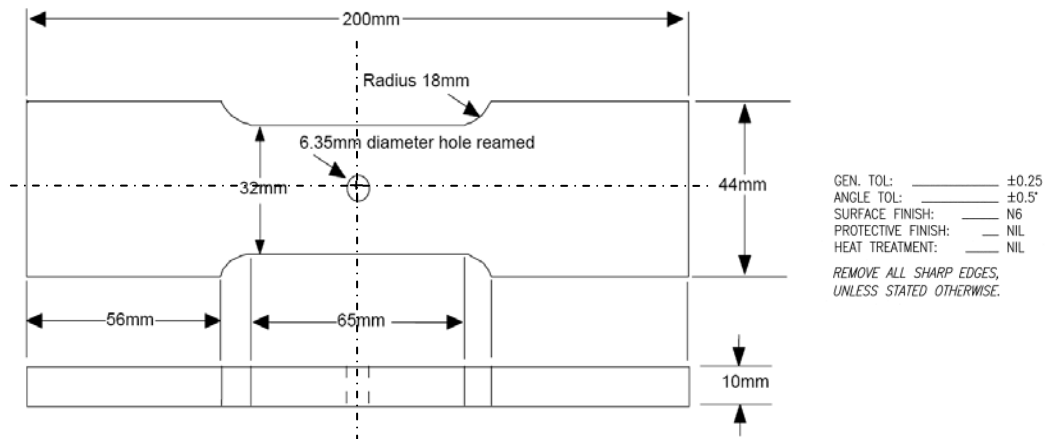
Figure 3: High K_t Centre-Hole Coupon

The high K_t centre-hole coupons were tested to allow for comparisons to be made to previous work including comparisons between the fatigue life of material produced circa 2000 and circa 1990 (not reported here; to be published).

The location and depth that each coupon was cut from within the original plate was designated in some coupon labels. The cutup plans for the LM coupons can be found in Appendix A. For more information on the cutup plan of the KK coupons see [3]. The depth and location of the single KF coupon within its forging was unknown. The grain orientation of the coupons is shown in Figure 4. For these tests the L-T (shorthand for L-LT indicating [loading]-[crack direction]) coupons were chosen.
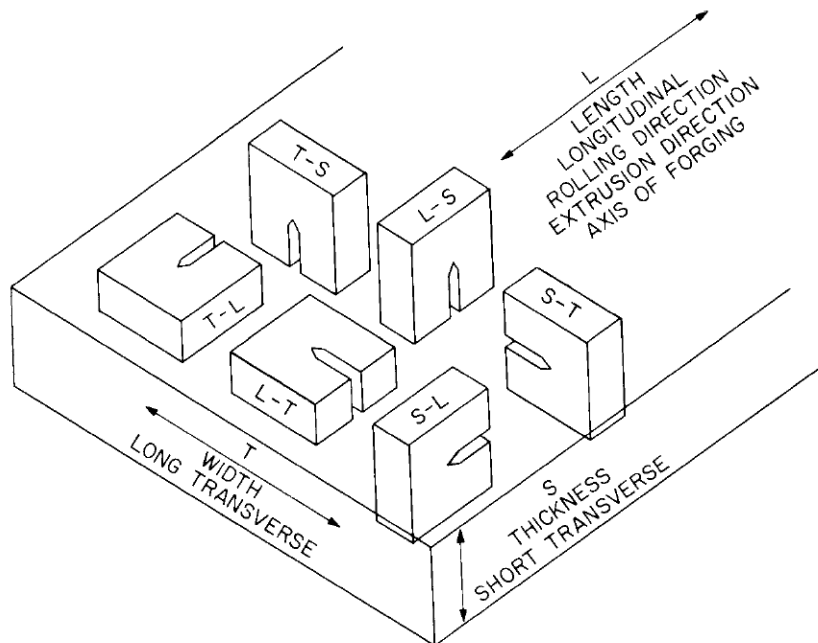
Figure 4: Grain orientation for coupon manufacture [16]

3.3 Stress Concentration Factors

The K_t for each specimen was calculated using finite element analyses. Figures 5 and 6 show the results of the first principal stress analysis which were undertaken utilising StressCheck^{TM} version 8.0 with tetrahedral polynomial-order elements. The low K_t (dogbone) specimens were found to have a net-section K_t of 1.08. The high K_t (side-notched) specimens had a net-section K_t of 2.97 (or a gross K_t of 3.39). The net-section K_t for the centre-hole coupons was 2.66 (or from previous work [17] a gross K_t of 3.32).
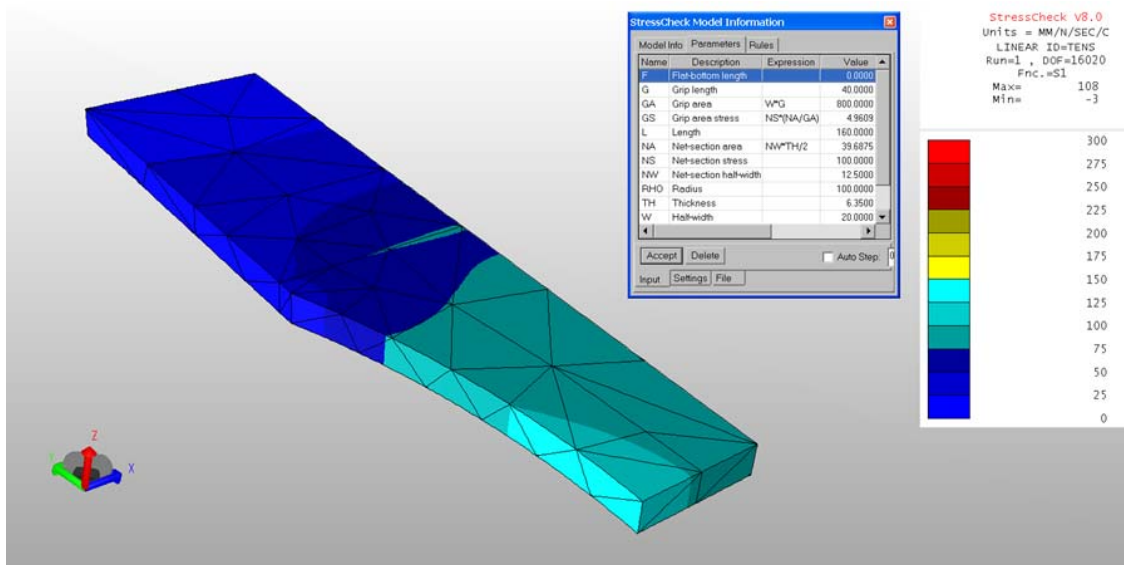
Figure 5: First principal stress results for Dogbone coupons
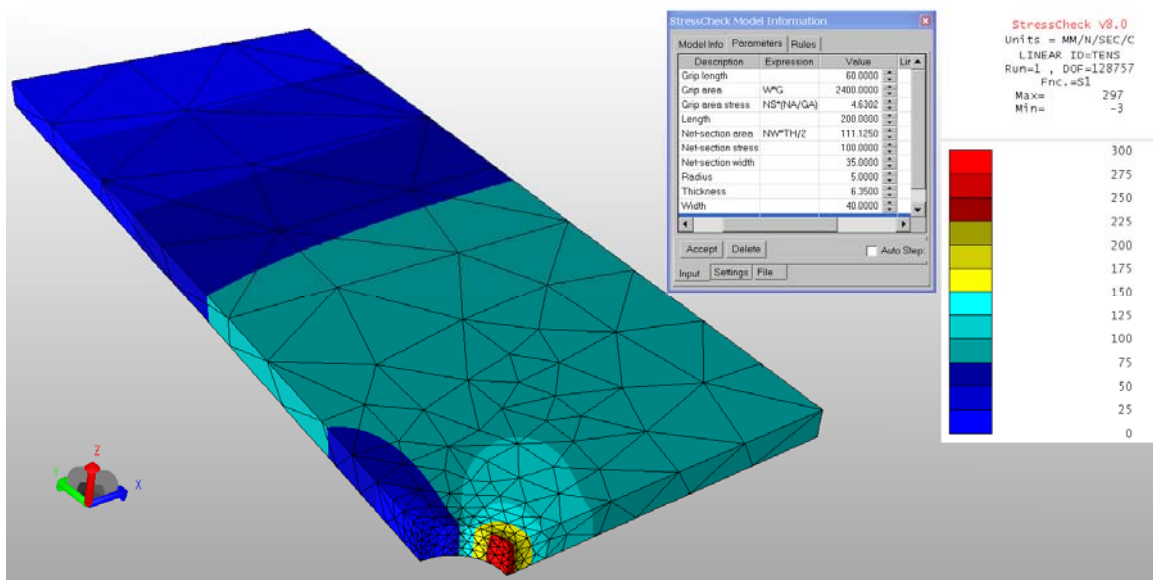
Figure 6: First principal stress results for Side-notched coupons

4. Surface Treatments

Four different surface treatments were used in the fatigue testing program; Machined (N6 surface finish), machined and polished with #400 grit paper, pre-IVD etched, and anodised. The following sections provide information on each of the surface treatments. The surface roughness of the coupons was tested following these treatments and these results may be found in Section 4.5.

4.1 Machined (N6 Surface Finish)

Ten coupons (five high and five low K_t) were tested in the as-machined to the N6 surface finish condition. Table 2 provides further information on the surface roughness equivalence of N6. In the test schedule in Table 4 these coupons are referred to as Machined (N6).

4.2 Machined and polished (#400 Grit Paper Finish)

Ten coupons (five high and five low K_t) were machined to an N6 finish, then polished using #400 grit papers. These coupons were tested to provide information on a pristine machined surface finish for comparative purposes. These specimens were not expected to represent typical airframe component surface conditions. In the test schedule in Table 4 these coupons are referred to as Machined (#400).

4.3 Pre-IVD Etched

Ten coupons (five high and five low K_t), cut from the LM plate, were etched with a solution of 50% HNO_3 and 1% HF (remainder water) at room temperature for five minutes (see [3], this is the solution used in the MACAIR P.S. 12050.1 Method B, which is used as a preparation for Ion Vapour Deposition (IVD) of aluminium on service AA7050-T7451 structures in the F/A-18 family of aircraft).

The duration that the etching process was applied was sufficient so as to ensure no evidence of the original as-machined surface remained. Time variations were required in the etching time to balance the reduction in chemical concentration of the relatively small acid bath (about a litre) used at DSTO, as compared to a bath in a commercial finishing facility (several thousand litres) that would be involved in the application of IVD to aircraft components. In the DSTO bath, as more specimens were treated, the chemicals were consumed and slightly longer times were required for subsequent coupons. For further details of etch pits produced by the etching process refer to [4]. In the test schedule in Table 4 these coupons are identified as Pre-IVD Etched.

4.4 Wash and Anodise

Ten coupons (five high and five low K_t), cut from the LM plate, were anodised in October 2007. The anodising process was completed as a Class 1 non-dyed general coating according to specification MIL-A-8625 TYPE 1B. The Type IB Chromic acid anodizing process is a low voltage process, with a peak voltage applied of 22 +/- 2V.

The anodising process was carried out in accordance with the steps set out in Boeing specification BSOPM 20-43-01[1]. These are outlined below:

1. Ensure all organic coatings have been removed prior to the initial degreasing step.
2. Vapour degrease or manually solvent clean the area to be coated per BSOPM 20-30-03[2] using Acetone – Technical Grade (87°C-90 °C).
3. Dry the area to be coated fully.
4. Alkaline clean (Turco 4215 NC-LT)[3] per BSOPM 20-30-03 for 3-5 minutes at 49°C-60°C.
5. Cold water rinse for minimum 5 times. Check for water break free surface.
6. Fully immerse in deoxidising solution (Deoxidiser #7)[4] for 1-10 minutes at 10°C- 27°C. Deoxidiser #7 is a powdered chemical, which, after addition to a dilute solution of nitric or sulphuric acid, produces a bath for deoxidising, desmutting or slight etching of aluminium alloys. Deoxidiser #7 is a product of Henkel Pty. Ltd. In this process, the deoxidiser #7 was mixed in the following composition per litre: 800mL water, 100mL nitric acid (57%), and 23 grams of deoxidiser #7.
7. Cold water rinse for minimum 5 times. Check for water break free surface.
8. Anodise at a maximum of 22 volts. Start at 5 volts and increase the voltage at a rate of 7 volts per minute.
9. Lower the part into the anodising solution and commence the current within two minutes after the start of immersion. Anodise for 35-60 minutes after the final operating voltage is obtained. Agitate by use of air.
10. Remove the parts from the anodising tank within two minutes of the voltage being switched off.
11. Cold water rinse for minimum 5-10 times. Check for water break free surface.
12. Dilute chromic seal[5] for 23-28 minutes at 82°C-88 °C. Class 1 anodising only.
13. Cold water rinse for minimum 5-10 times. Check for water break free surface.
14. Chromate conversion coat all rack and jigging marks greater than 0.094 inches across for 5-60 seconds.
15. Cold water rinse for minimum 5-10 times. Check for water break free surface.
16. Hot water rinse a minimum of five times.
17. Dry using clean compressed air.

---

[1] BSOPM 20-43-01 is a Boeing Standard Overhaul Practices Manual for chromic acid anodising.

[2] BSOPM 20-30-03 is a Boeing Standard Overhaul Practices Manual for general cleaning procedures.

[3] Turco 4215 NC-LT is composed of 30-60% Borax, 10-30% Pentasodium Triphosphate, 5-10% Sodium Nitrate, 5-10% Nonylphenol Ethoxylate, 1-5% Fatty Alcohol Ethoxylate/Propoxylate, 1-5% Diethylene Glycol Monobutyl Ether, and 1-5% Disodium Hexaflourosilicate.

[4] Deoxidiser #7 is composed of >60% Potassium Dichromate, 10-30% Potassium Nitrate, and 1-10% Sodium Biflouride.

[5] The chemical composition of the dilute chromic seal was unknown.

Several examples of the anodic coating produced by the anodising process applied to the coupons tested here were examined using a scanning electron microscope (SEM) to determine the thickness of the coating. Figure 7 shows a typical image obtained to measure the coating thickness. The coating thickness was found to be consistent between the high and low K_t coupons with a thickness of between 2-4µm. The thickness of the anodic coating is an important consideration when analysing the fatigue crack initiations as thicker coatings are more susceptible to micro cracking, and these cracks can act as fatigue crack initiators. The chromic acid anodising process generally produces relatively thin coatings compared to other anodising processes, therefore minimising the effect on fatigue life should the coating crack. In the test schedule in Table 4 these coupons are referred to as Anodised.
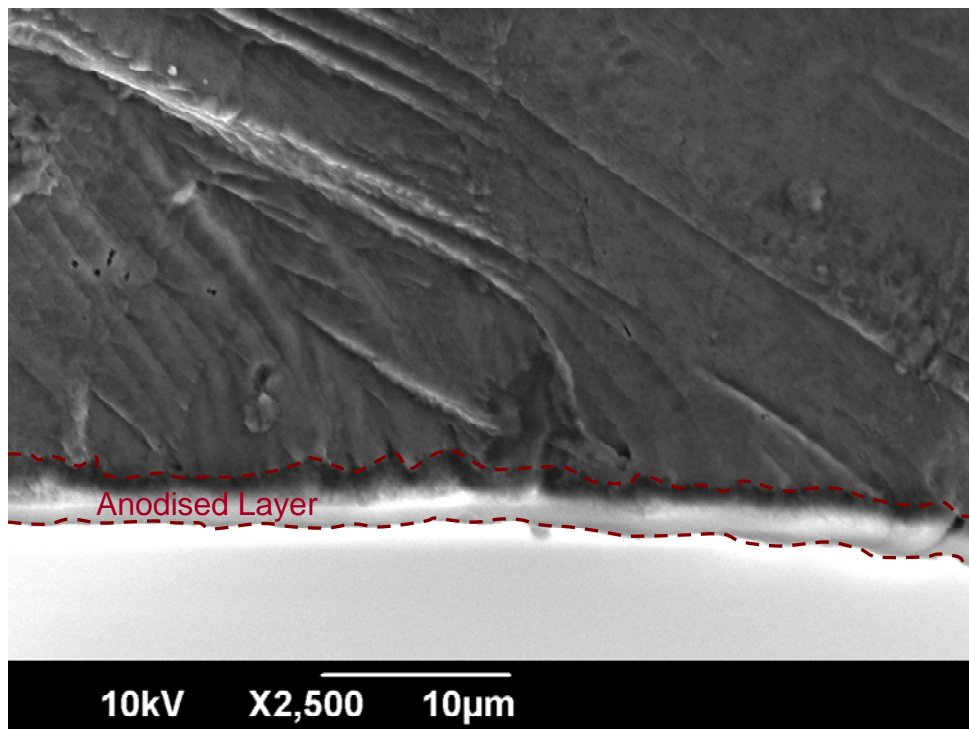
Figure 7: An example SEM photograph showing the thickness of the oxide layer produced by the anodising process

4.5 Surface Roughness Measurements

A metrology examination was undertaken on all tested coupons. This was carried out to allow for potential future comparisons of surface roughness between this test program and other programs on airframe components. A Mahr Perthometer with Focodyn laser probe was used to determine the surface roughness by utilising a linear scan with the average surface roughness taken over the length of the scan.

Surface roughness is usually measured along a line perpendicular to the machining marks; however, this representation of the surface roughness may not be pertinent to the onset of fatigue cracking, rather, the roughness along a path parallel to the loading direction, is more

relevant. For all coupons in this test program, the machining marks lay parallel with the loaded direction, as shown in Figure 8. It was anticipated that the roughness measured along this path would be lower compared to the usual roughness values quoted (i.e. when the surface roughness is measured perpendicular to the machining marks). Since measuring in one direction is relevant to the roughness achieved by the machining process and the other to the roughness that may affect the fatigue life, the roughness was measured in both directions. Additionally, where possible, the surface roughness on the radius of the side-notch or hourglass side was also recorded. Figure 8 illustrates the directions where surface roughness measurements were made. The complete results of the analysis can be found in Appendix B. For comparison, roughness grade numbers and their equivalent roughness values are provided in Table 2 according to ISO-1302 [18].
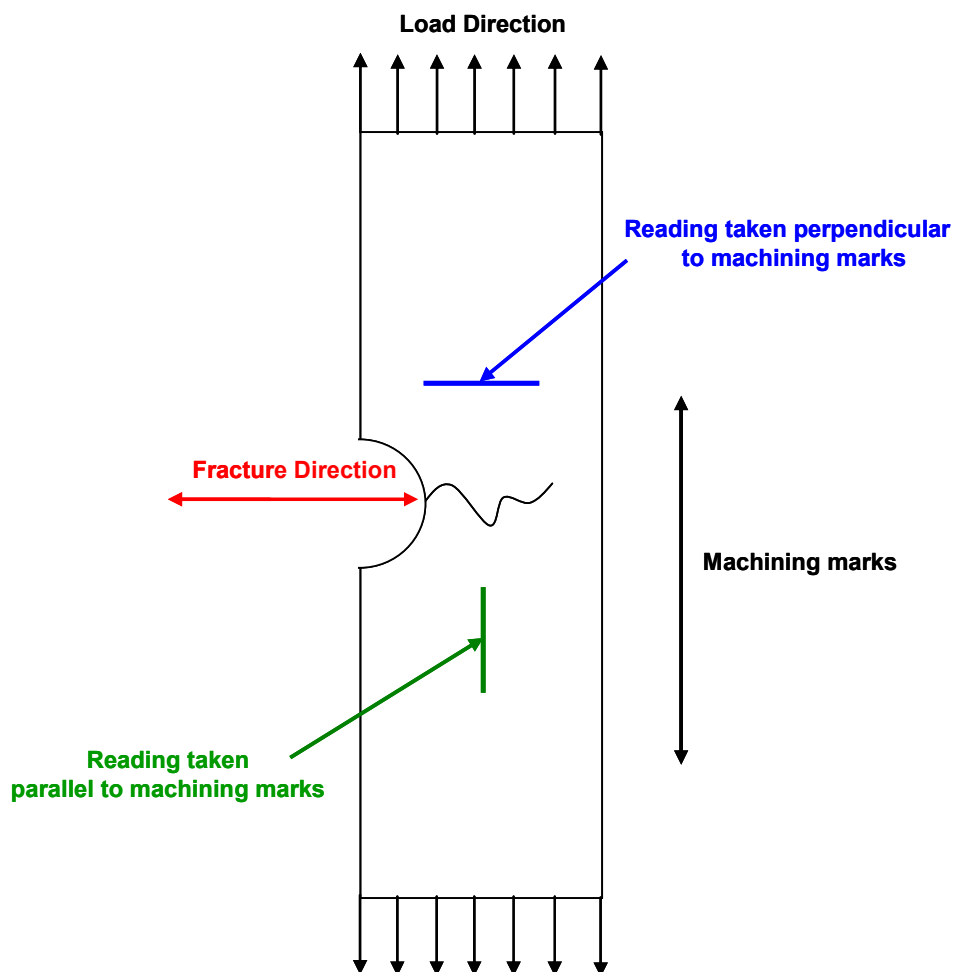
Figure 8: Surface roughness measurement directions in relation to the direction of the machining marks

Table 2: Comparison of arithmetical mean surface roughness (Ra) and roughness grade numbers

Roughness Value (Ra) - 1302:2002 (E)		(Superseded) Roughness Grade Numbers – 1302:1992
μm	μin	
50	2000	N 12
25	1000	N 11
12.5	500	N 10
6.3	250	N 9
3.2	125	N 8
1.6	63	N 7
0.8	32	N 6
0.4	16	N 5
0.2	8	N 4
0.1	4	N 3
0.05	2	N 2
0.025	1	N 1

Figure 9 shows the results of the surface roughness metrology examination parallel and perpendicular to the machining marks. The results for the machined and polished (#400) coupons show a significantly higher surface roughness parallel to the machining marks compared to perpendicular. This result was unexpected and could be due to the surface roughness measurements being performed after fracture for these coupons - during the fracture process, it is possible that micro-cracks that had formed on the surface, that were in the path of the measurements taken, may have affected the accuracy of the surface roughness tests parallel to the machining marks since such cracks would have been perpendicular to the measuring direction. In comparison, the machined (N6) coupons surface roughness tests were performed prior to the fatigue testing and the surface roughness results were more typical of what was expected. Perpendicular to the machining marks the Ra value was 0.92 μm, representing a good representation with the N6 roughness grade number shown in Table 2. As expected, measurements taken parallel to the machining marks showed a reduction in the surface roughness compared to those taken perpendicular to the marks.

For the pre-IVD etched coupons the surface roughness values were similar for both parallel and perpendicular directions to the machining marks. This was expected since the etching process removed the machining marks on the surface leaving a constant surface roughness on all directions on the coupons. The anodised coupons showed a slightly higher surface roughness value parallel to the machining marks compared to perpendicular.
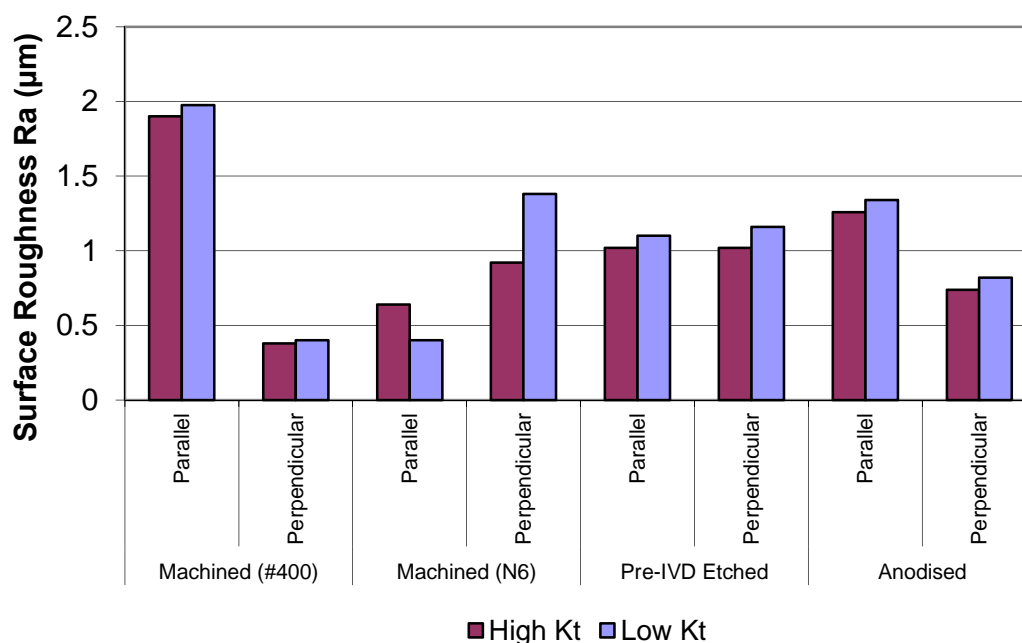
Figure 9: Average surface roughness results for the tested coupons, perpendicular and parallel to the machining marks

5. Loading Spectrum

5.1 Spectrum Information

The loading spectrum used for these tests was the F/A-18 wing root bending moment load spectrum identified herein as the FT55m5 spectrum. Unlike the name would suggest, the FT55m5 spectrum was not the spectrum that was applied to the F/A-18 International Follow-On Structural Test Project (IFOSTP) full-scale centre fuselage fatigue test, designated FT55, but was drawn from this test by the National Research Council (NRC) of Canada for application to the DSTO FS488 bulkhead component fatigue test FT488/2 [2, 19]. To derive the spectrum, NRC used FT55 WRBM and Wing Root Torque (WRTQ) spectra to predict the strain expected to occur on the centreline of the FS488 bulkhead Outboard Mold-Line OML flange on the FT55 test article, specifically at Gauge 488001263. Further details of this spectrum can be found in [3]. FT55m5 was given the FT55 prefix when it was combined with the M5 marker band inserted in the middle of each block.

The FT55m5 spectrum, with the marker band is shown in Figure 10. The spectrum has a total of 13,480 load lines including the five compression load lines for the M5 marker loads to make a block that represents 324.92 flight hours. It should be noted that the 13,480 load lines of the FT55m5 sequence consists of 13,456 turning points plus 24 intermediate points, or points with a continual increase/decrease in stress (i.e. no load reversal).
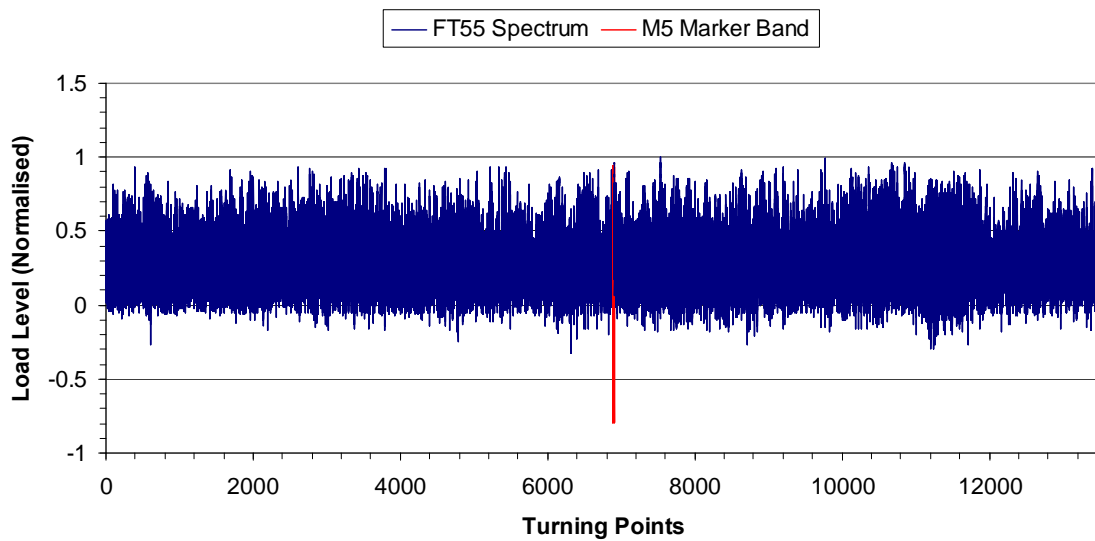
Figure 10: The FT55m5 loading spectrum

The M5 marker band was inserted in the spectrum to make QF easier for the measurement of crack growth curves. The M5 marker band consisted of ten turning points, including five compression loads, varying from a normalised load level of -0.795 to 0.963 (last peak). The marker loads can be seen in Figure 11. Previous tests conducted at DSTO have demonstrated that these marker loads have a negligible effect on the fatigue crack growth rate produced by this spectrum when applied to the types of AA7050-T7451 coupons tested here [4].
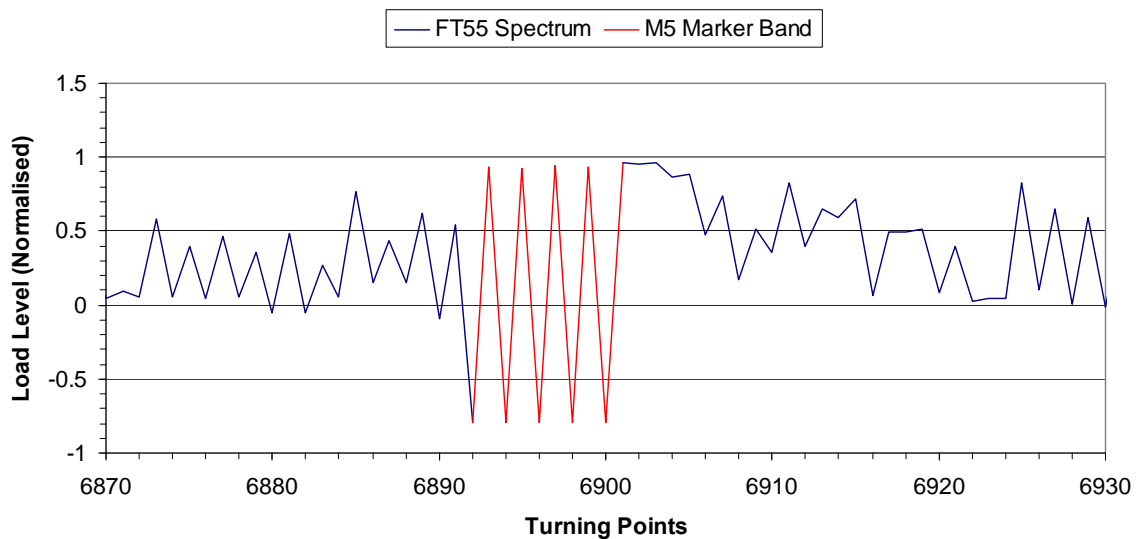
Figure 11: The M5 marker loads

5.2 Stress Scale Levels

The high K_t coupons were tested at an applied peak spectrum stress of 180 MPa. The low K_t coupons were tested at an applied peak spectrum stress of 300 MPa. The applied stress levels were net-section stresses that were based on the net-section area at the narrowest width of each coupon. The width was measured before each test, and the applied test load adjusted, to ensure the nominal net-section stress was applied to individual specimens. These stress levels were anticipated to result in a test life of around 20,000 equivalent flight hours for the machined specimens. This total life generally represents a combat aircraft design target without uncertainty (fatigue scatter) factors applied. The stress levels applied to the coupons can be seen in Table 3.

Table 3: Stress scale levels for fatigue coupon tests

Coupon Geometry	Gross-Section Stress (MPa)	Net-Section Stress (MPa)	K_t Stress (MPa)
Centre-hole	144.3	180.0	478.8
Side-notched	157.5	180.0	534.6
Dogbone	N/A	300.0	324.0

5.3 Test Schedule

Table 4 shows the coupons, geometries and stress scale levels that were tested. The coupons were tested in a National Association of Testing (NATA) certified 100 kN, MTS computer-controlled, servo-hydraulic fatigue test machine at ambient room temperature. Humidity was typically about 70%.

Table 4 Coupon test schedule

Geometry	Surface Finish	[Load-Cracking] Grain Direction	Nominal Net-Section Width (mm)	Net- Section Stress (MPa)	Coupon Label
High K_t Centre Hole	Machined (N6)	L-T	25.65	180	KK1H100
"	"	"	"	"	KK1H159
"	"	"	"	"	KK1H147
"	"	"	"	"	KK1H172
"	"	"	"	"	KF2B8
High K_t Side-notched	Machined (#400)	L-T	35	180	LM-8
"	"	"	"	"	LM-62
"	"	"	"	"	LM-98
"	"	"	"	"	LM-135
"	"	"	"	"	LM-189
High K_t Side-notched	Machined (N6)	L-T	35	180	LMAE-01-L-T
"	"	"	"	"	LMAE-03-L-T
"	"	"	"	"	LMAE-05-L-T
"	"	"	"	"	LMAE-07-L-T
"	"	"	'	"	LMAE-09-L-T
High K_t Side-notched	Pre-IVD Etched	L-T	35	180	LM-17
"	"	"	'	"	LM-151
"	"	"	"	"	LM-188
"	"	"	'	"	LM-214
"	"	"	"	"	LM-223
High K_t Side-notched	Anodised	L-T	35	180	LM-87
"	"	"	"	"	LM-102
"	"	"	"	"	LM-136
"	"	"	"	"	LM-149
"	"	"	"	"	LM-175
Low K_t Dogbone	Machined (#400)	L-T	25	300	LM-244
"	"	"	"	"	LM-344
"	"	"	"	"	LM-371
"	"	"	"	"	LM-398
"	"	"	"	"	LM-442
Low K_t Dogbone	Machined (N6)	L-T	25	300	LMAA-01-L-T
"	"	"	"	"	LMAA-03-L-T
"	"	"	"	"	LMAA-06-L-T
"	"	"	"	"	LMAA-08-L-T
"	"	"	"	"	LMAA-10-L-T
Low K_t Dogbone	Pre-IVD Etched	L-T	25	300	LM-309
"	"	"	"	"	LM-329
"	"	"	"	"	LM-364
"	"	"	"	"	LM-372
"	"	"	"	"	LM-440
Low K_t Dogbone	Anodised	L-T	25	300	LM-233
"	"	"	"	"	LM-301
"	"	"	"	"	LM-303
"	"	"	"	"	LM-317
"	"	"	"	"	LM-418

6. Results

6.1 Test Results

The test results are summarised in Table 5. Specimen LM-442 and LMAA-08-L-T failed in the grips during testing and the specimens were not subjected to QF, however, the life result (as a minimum) is assumed to be valid for analysis purposes because the failure in the grips occurred before the failure in the test section. In other words, the test section had not failed at the time of the failure in the grips; therefore, the results can be considered a conservative result for the fatigue life of the coupon.

Table 5 Total life to failure for each tested coupon

Geometry	Surface Finish	Coupon Label	Total Life to Failure		
			Load Lines	Blocks	Flight Hours
High K_t Centre Hole	Machined (N6)	KK1H100	855,776	63.48	20,628
"	"	KK1H147	734,825	54.51	17,712
"	"	KK1H159	944,846	70.09	22,774
"	"	KK1H172	791,259	58.70	19,072
"	"	KF2B8	1,047,753	77.73	25,255
High K_t Side-notched	Machined (#400)	LM-8	292,187	21.68	7,043
"	"	LM-62	273,400	20.28	6,590
"	"	LM-98	234,394	17.39	5,650
"	"	LM-135	238,955	17.73	5,760
"	"	LM-189	283,021	21.00	6,822
High K_t Side-notched	Machined (N6)	LMAE-01-L-T	370,872	27.51	8,939
"	"	LMAE-03-L-T	267,822	19.87	6,456
"	"	LMAE-05-L-T	282,294	20.94	6,804
"	"	LMAE-07-L-T	263,665	19.56	6,355
"	"	LMAE-09-L-T	276,509	20.51	6,665
High K_t Side-notched	Pre-IVD Etched	LM-17	225,473	16.73	5,435
"	"	LM-151	230,842	17.12	5,564
"	"	LM-188	249,555	18.51	6,015
"	"	LM-214	223,223	16.56	5,381
"	"	LM-223	249,555	18.51	6,015
High K_t Side-notched	Anodised	LM-87	172,635	12.81	4,161
"	"	LM-102	197,939	14.68	4,771
"	"	LM-136	258,644	19.19	6,234
"	"	LM-149	204,174	15.15	4,921
"	"	LM-175	179,040	13.28	4,316
Low K_t Dogbone	Machined (#400)	LM-244	1,758,540	130.46	42,388
"	"	LM-344	1,109,164	82.28	26,735
"	"	LM-371	1,274,027	94.51	30,709
"	"	LM-398	1,566,018	116.17	37,747
"	"	LM-442*	1,558,859	115.64	37,575
Low K_t Dogbone	Machined (N6)	LMAA-01-L-T	919,132	68.18	22,155
"	"	LMAA-03-L-T	710,755	52.73	17,132
"	"	LMAA-06-L-T	602,914	44.73	14,533
"	"	LMAA-08-L-T*	1,287,515	95.51	31,034
"	"	LMAA-10-L-T	646,016	47.92	15,571
Low K_t Dogbone	Pre-IVD Etched	LM-309	498,697	37.00	12,021
"	"	LM-329	488,056	36.21	11,764
"	"	LM-364	427,673	31.73	10,309
"	"	LM-372	515,686	38.26	12,430
"	"	LM-440	500,734	37.15	12,070
Low K_t Dogbone	Anodised	LM-233	480,421	35.64	11,580
"	"	LM-301	378,754	28.10	9,129
"	"	LM-303	353,922	26.26	8,531
"	"	LM-317	438,269	32.51	10,564
"	"	LM-418	333,313	24.73	8,034

*Failed in grips, not necessarily valid.

Graphical representations of the total-life results are displayed in Figures 12 and 13. These include the log-averaged life results for each surface treatment.
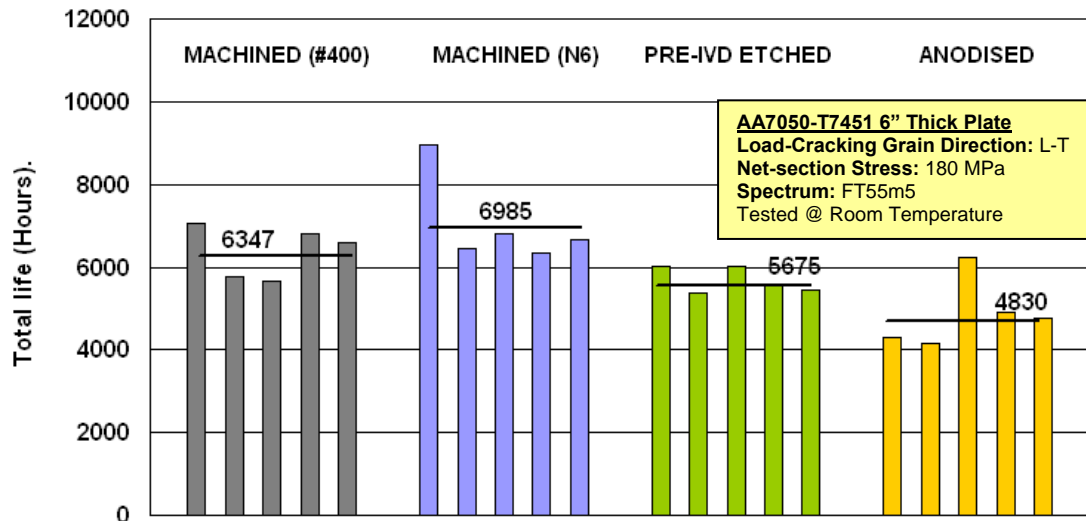
Figure 12: Results summary for high K_t side-notched coupons
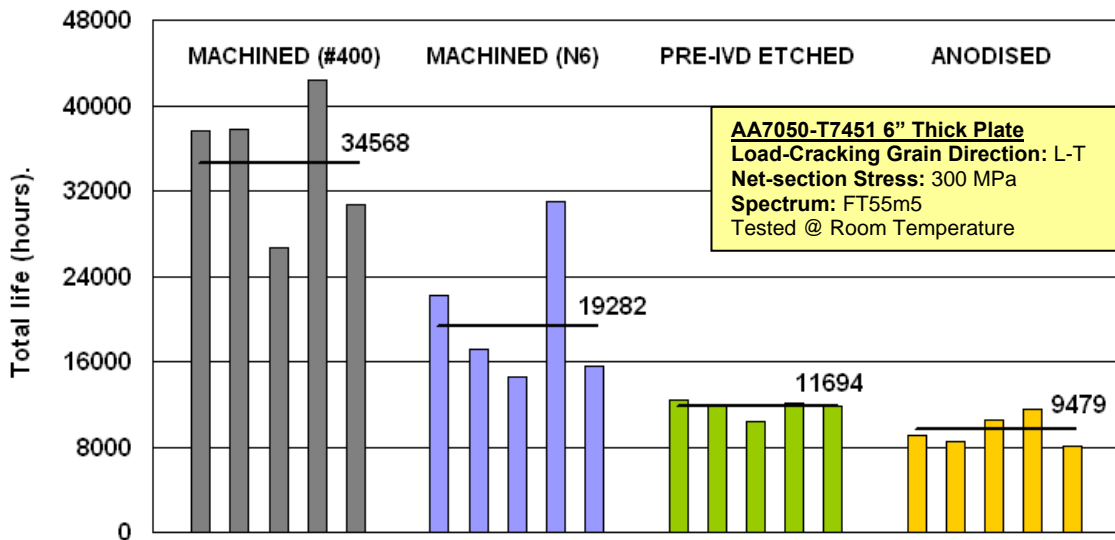
Figure 13: Results summary for low K_t dogbone coupons

The log means and standard deviations of each surface treatment and geometry are shown in Table 6.

Table 6: Statistical analysis results on the total life of each surface treatment and geometry

Geometry	Surface Finish	Number of Samples	Log_{10} Mean Total Life (Flight Hours)	Log_{10} Standard Deviation
High Kt Side-notched	Machined (#400)	5	6,347.5	0.04364
High Kt Side-notched	Machined (N6)	5	6,985.3	0.06098
High Kt Side-notched	Pre-IVD Etched	5	5,675.2	0.02365
High Kt Side-notched	Anodised	5	4,829.9	0.06884
Low Kt Dogbone	Machined (#400)	5	34,568.0	0.08018
Low Kt Dogbone	Machined (N6)	5	19,282.3	0.13481
Low Kt Dogbone	Pre-IVD Etched	5	11,694.4	0.03178
Low Kt Dogbone	Anodised	5	9,479.3	0.06576

A *t*-test using the normal distribution of the log values was used to compare the log mean total lives of each surface treatment for both geometry types. The total lives were compared using a 95% confidence interval, or in other words, the analyses shows, with 95% confidence that the total lives are different by the amounts shown. The *t*-test analysis was performed assuming equal variance for each surface treatment. A *t* value of higher than 2.2 shows there is a significant difference in the means of the fatigue lives of the surface treatments being compared. The *t*-test comparisons are shown in Table 7.

Table 7: T-test results for difference of means between each surface treatment

Geometry	Surface Treatments	t	Degrees of Freedom	Mean Difference	95% Confidence Interval of the Difference	
					Lower	Upper
High Kt Side-notched	Machined (#400) Machined (N6)	-1.204	8	-670.80	-1,955.64	614.04
High Kt Side-notched	Machined (#400) Pre-IVD Etched	2.194	8	691.00	-35.19	1,417.19
High Kt Side-notched	Machined (#400) Anodised	3.227	8	1,492.40	425.89	2,558.91
High Kt Side-notched	Machined (N6) Pre-IVD Etched	2.724	8	1,361.80	208.79	2,514.81
High Kt Side-notched	Machined (N6) Anodised	3.582	8	2,163.20	770.53	3,555.87
High Kt Side-notched	Pre-IVD Etched Anodised	2.046	8	801.40	-101.96	1,704.76
Low Kt Dogbone	Machined (#400) Machined (N6)	3.627	8	14,945.80	5,444.00	24,447.60
Low Kt Dogbone	Machined (#400) Pre-IVD Etched	8.289	8	23,312.00	16,826.69	29,797.31
Low Kt Dogbone	Machined (#400) Anodised	8.888	8	25,463.20	18,857.02	32,069.38
Low Kt Dogbone	Machined (N6) Pre-IVD Etched	2.738	8	8,366.20	1,318.79	15,413.61
Low Kt Dogbone	Machined (N6) Anodised	3.388	8	10,517.40	3,358.60	17,676.20
Low Kt Dogbone	Pre-IVD Etched Anodised	2.853	8	2,151.20	412.39	3,890.01

*A '*t*' value of higher than 2.2 shows the mean fatigue live of the compared surface treatments is significantly different.

The t-test results showed that the surface treatment had a much larger effect on the fatigue life of low K_t coupons than it did for high K_t coupons. The high K_t t-test results showed there was no significant statistical variation in the means between the two machined surface treatments (#400 and N6), as well as between the pre-IVD etched coupons and the anodised coupons. Significant variations in the means were shown between the two machined surface treatments and the anodised coupons; however, for the low K_t coupons this variation was significantly larger. The same trend was seen between the machined surface treatments and the pre-IVD etched coupons. For the high K_t coupons, the variation in the means produced t values of 2.194 and 2.724. For the low K_t coupons, these t values became 8.289 and 2.738.

6.2 Initiating discontinuities

The crack initiation locations were analysed using QF to determine the characteristics of the intrinsic feature from which each of the main fatigue cracks grew. These characteristics included the maximum depth (measured from the free surface to the deepest point of the discontinuity), the area of the discontinuity and an assessment of the cause(s) of the intrinsic feature. By collecting these parameters, an assessment on the surface treatment could be undertaken to understand the link between the surface treatment and the fatigue life of the coupons. Photographs of the crack initiating discontinuities, from which the largest cracks grew, are shown in Appendix C.

For the machined surfaces, the discontinuity from which the main fatigue crack grew was usually a surface-breaking inclusion, inclusion cluster and/or porosity created during the casting of the original ingot that had been exposed to the free surface during the manufacturing of the coupon. Figure 14 shows an example of a surface-breaking inclusion and Figure 15 shows an example of a surface-breaking inclusion with porosity, both of these had initiated fatigue cracks.
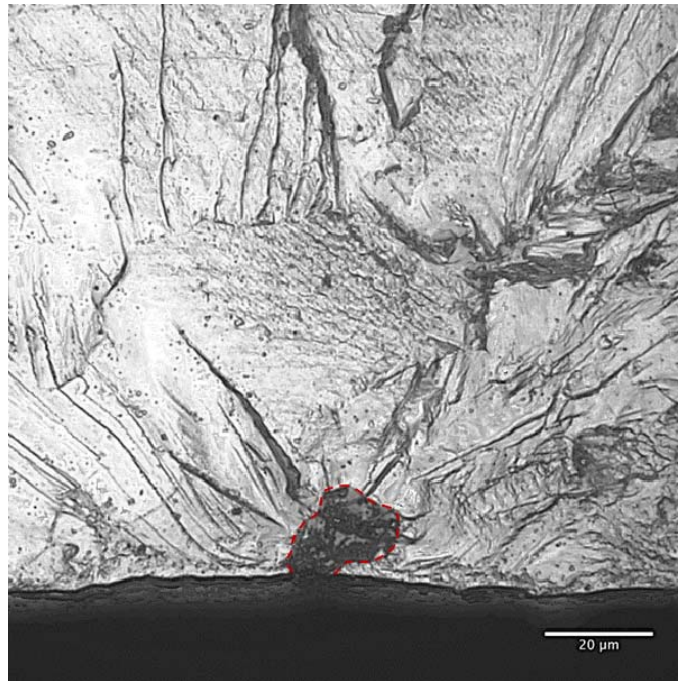
Figure 14: Coupon KF2B8 with a surface-breaking inclusion initiating cracking
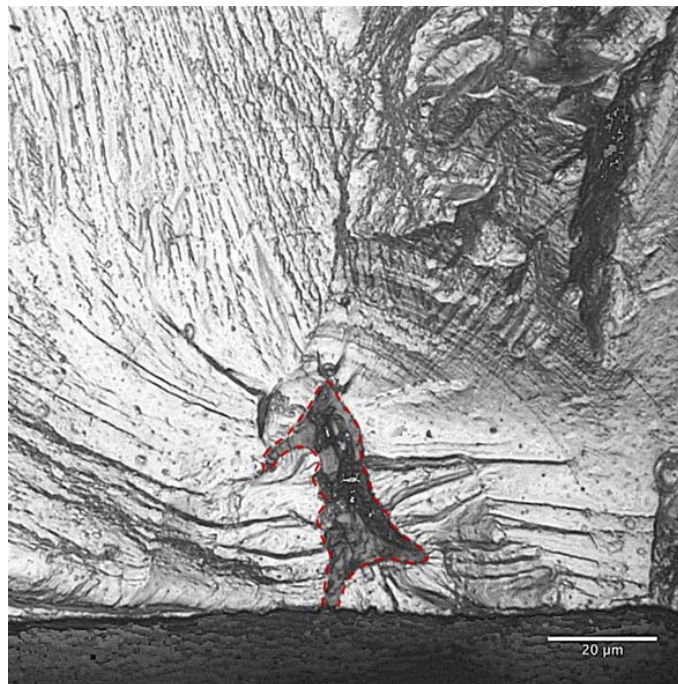
Figure 15: Coupon LMAE-07-L-T with a surface-breaking inclusion cluster associated with porosity causing the onset of fatigue cracking

For the etched coupons the discontinuities, usually associated with crack initiation, were pits caused by chemical attack during the etching process. An example of an etch pit is shown in Figure 16. These pits were associated with grain boundaries and sub-grain boundaries, surface breaking inclusions and any associated porosity.

The anodised surfaces also had pits that had lead to fatigue crack onset. These were also caused by chemical attack during one of the water based chemical treatments: caustic degreasing, de-oxidising or anodising. The pits in the anodised coupons were larger than the pits caused by the pre-IVD etching process, in both depth and area, and they were larger than the inclusions in the machined surfaces. Figure 17 shows an example of an anodised pit. The anodising pits tended to be associated with surface breaking inclusions or inclusion clusters and grain boundaries to a lesser extent.
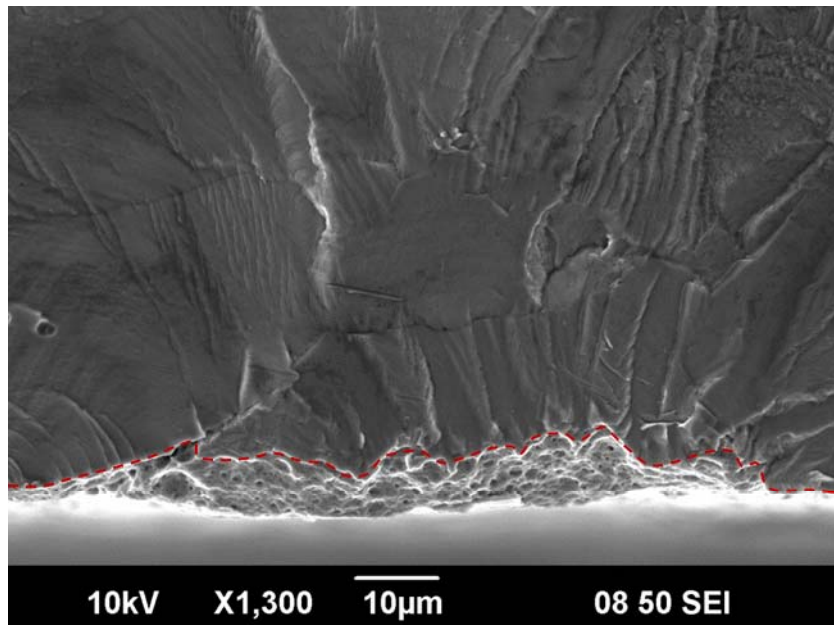
Figure 16: Coupon LM-372 with a shallow pit caused from the etching process highlighted
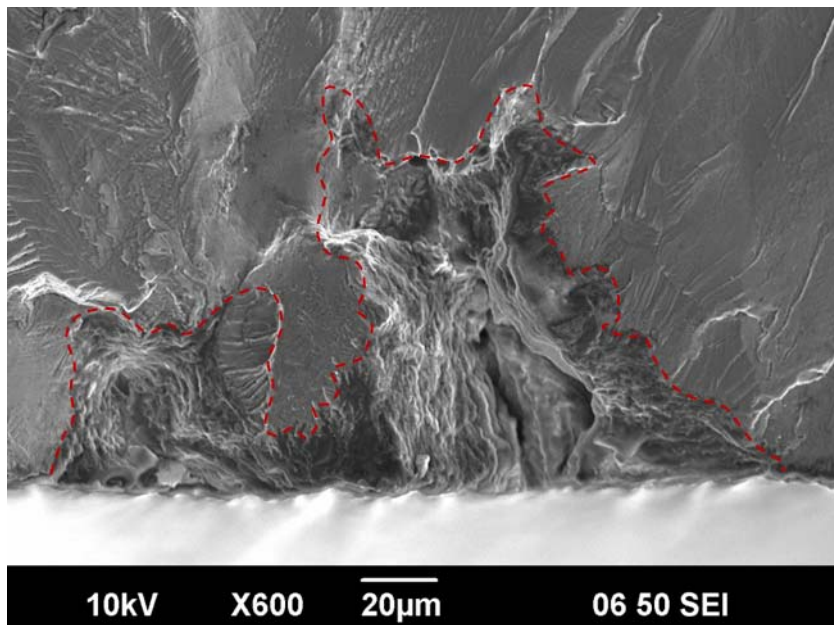
Figure 17: LM-303 with a pit caused from the anodising process leading to the onset of fatigue cracking

The depth and area of the initiating flaws were measured (listed in Table 8) to determine if there was a link between the surface treatments and the fatigue life of the coupons.

Table 8: Size of the intrinsic feature from which the main fatigue cracks grew in each coupon

Geometry	Surface Finish	Coupon Label	Maximium Discontinuity Depth (mm)	Average Depth (mm)	Discontinuity Area (mm²)	Average Area (mm²)
High Kt Centre Hole	Machined (N6)	KF2B8	0.0158		2.26E-04	
"	"	KK1H100	*		*	
"	"	KK1H147	0.0268	0.0169	1.88E-04	1.97E-04
"	"	KK1H159	0.0165		3.55E-04	
"	"	KK1H172	0.0084		1.75E-05	
High Kt Side-Notched	Machined (#400)	LM-8	0.0145		2.52E-04	
"	"	LM-62	0.0252		4.59E-04	
"	"	LM-98	0.0111	0.0233	1.17E-04	3.78E-04
"	"	LM-135	0.053		5.39E-04	
"	"	LM-189	0.0126		1.45E-04	
High Kt Side-Notched	Machined (N6)	LMAE-01-L-T	0.0166		1.60E-04	
"	"	LMAE-03-L-T	0.0207		3.54E-04	
"	"	LMAE-05-L-T	0.0417	0.0290	7.66E-04	3.81E-04
"	"	LMAE-07-L-T	0.041		4.04E-04	
"	"	LMAE-09-L-T	0.0248		2.22E-04	
High Kt Side-Notched	Anodised	LM-87	0.1535		1.89E-02	
"	"	LM-102	0.0594		2.47E-03	
"	"	LM-136	0.0322	0.0764	3.70E-04	6.89E-03
"	"	LM-149	0.0672		7.52E-03	
"	"	LM-175	0.0698		5.19E-03	
High Kt Side-Notched	Pre-IVD Etched	LM-17	0.0201		1.09E-03	
"	"	LM-151	0.0183		5.30E-04	
"	"	LM-188	0.0202	0.0268	6.20E-04	1.09E-03
"	"	LM-214	0.0442		2.81E-03	
"	"	LM-223	0.0311		4.15E-04	
High Kt Side-Notched	Machined (#400)	LM-244	0.0082		7.80E-05	
"	"	LM-344	0.0163		2.09E-04	
"	"	LM-371	0.0262	0.0148	1.79E-04	1.24E-04
"	"	LM-398	0.0086		3.01E-05	
"	"	LM-442	Failed in Grips		Failed in Grips	
High Kt Side-Notched	Machined (N6)	LMAA-01-L-T	0.0204		4.64E-04	
"	"	LMAA-03-L-T	0.0707		1.53E-03	
"	"	LMAA-06-L-T	0.0184	0.0302	3.16E-04	6.13E-04
"	"	LMAA-08-L-T	Failed in Grips		Failed in Grips	
"	"	LMAA-10-L-T	0.0114		1.45E-04	
High Kt Side-Notched	Anodised	LM-233	0.0819		4.59E-03	
"	"	LM-301	0.03		6.81E-03	
"	"	LM-303	0.1091	0.0672	1.17E-02	6.15E-03
"	"	LM-317	0.0407		3.20E-03	
"	"	LM-418	0.0744		4.41E-03	
High Kt Side-Notched	Pre-IVD Etched	LM-309	0.0098		3.81E-04	
"	"	LM-329	0.0241		1.06E-03	
"	"	LM-364	0.03	0.0235	1.72E-03	9.87E-04
"	"	LM-372	0.0108		5.62E-04	
"	"	LM-440	0.0427		1.22E-03	

* The initiating discontinuity could not be identified on coupon KK1H100 since the initiation appeared to start from a burr created during the machining process of the coupon.

6.3 Crack growth measurements

QF was utilised to generate crack growth curves for each of the fractured specimens. The crack-growth curves were produced by first finding the crack initiation location on the fracture surface and zeroing the microscope measurements at the free surface. The marker loads were then visually located and measured relative to the free surface at the crack initiation point. In some circumstances, the first marker band measurement was smaller than the maximum depth of the initiating discontinuity quoted in Table 8. This situation arose when the crack was measured at a location where it was growing faster and therefore the marker bands were more visible. This could occur at certain areas around the boundary of the discontinuity, since, initially several cracks initiate about each discontinuity and the fastest growth is not necessarily from the deepest point of the discontinuity. An example of this is illustrated in Figure 18.
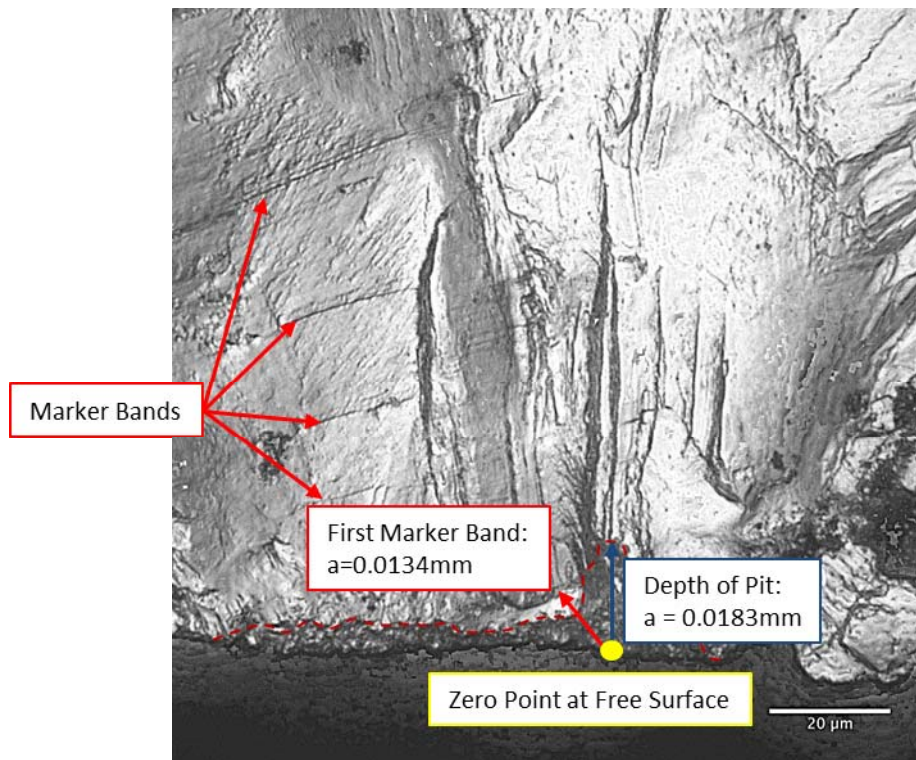
Figure 18: Example of first marker band measurement being smaller than the maximum depth of the initiating discontinuity from coupon LM-151

In certain circumstances, where the marker band significantly changed shape or direction at various depths of the cracking being measured, multiple measurements were taken, with the average result quoted herein. Each measurement provided an *x* and *y* distance as well as a total '*R*' (radial) distance, where *R* is defined mathematically with the following equation.

$$R = \sqrt{x^2 + y^2}$$

Figure 19 indicates the method used for generating crack growth curves. It should be noted that crack growth curves were not generated for the two coupons that failed in the grip area. This method was used to produce the crack-growth curves shown in Figures 20 and 21, which, as discussed previously, are measurements of the marker bands measured from an origin at the free surface of the initiating discontinuity. The initiating discontinuities are not shown on the crack growth curves but were analysed separately in Sections 6.2 and 7.2.

Track to deepest point of the crack along which the crack growth is measured

Deepest point of crack

y

Some of the progression marks

Idealised region from which depth data is collected

Fatigue crack surface

Zero point for measurement at free surface

Surface

x

Initiating Flaw
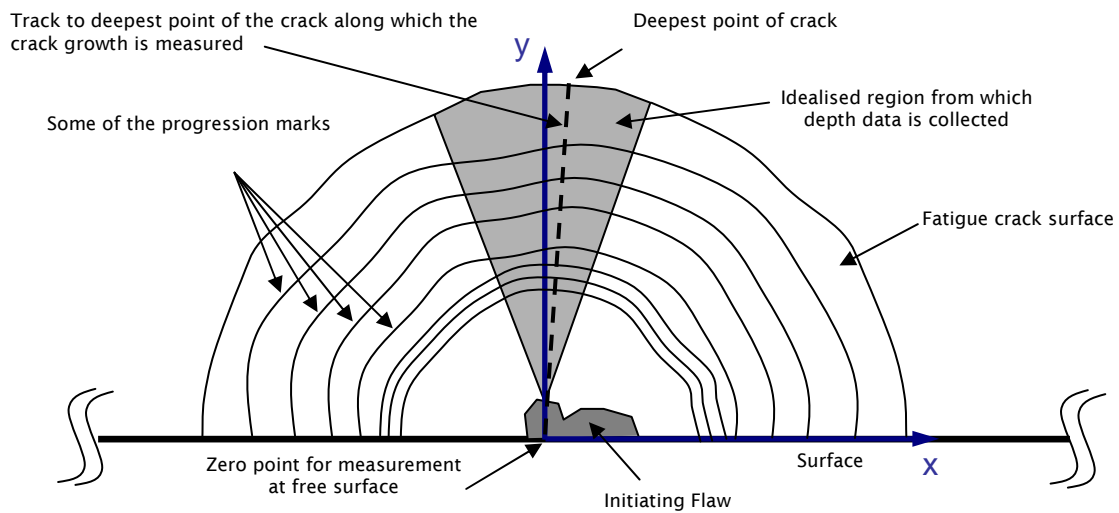
Figure 19: A schematic drawing of the method and track used to measure the fatigue crack growth by quantitative fractography [4]
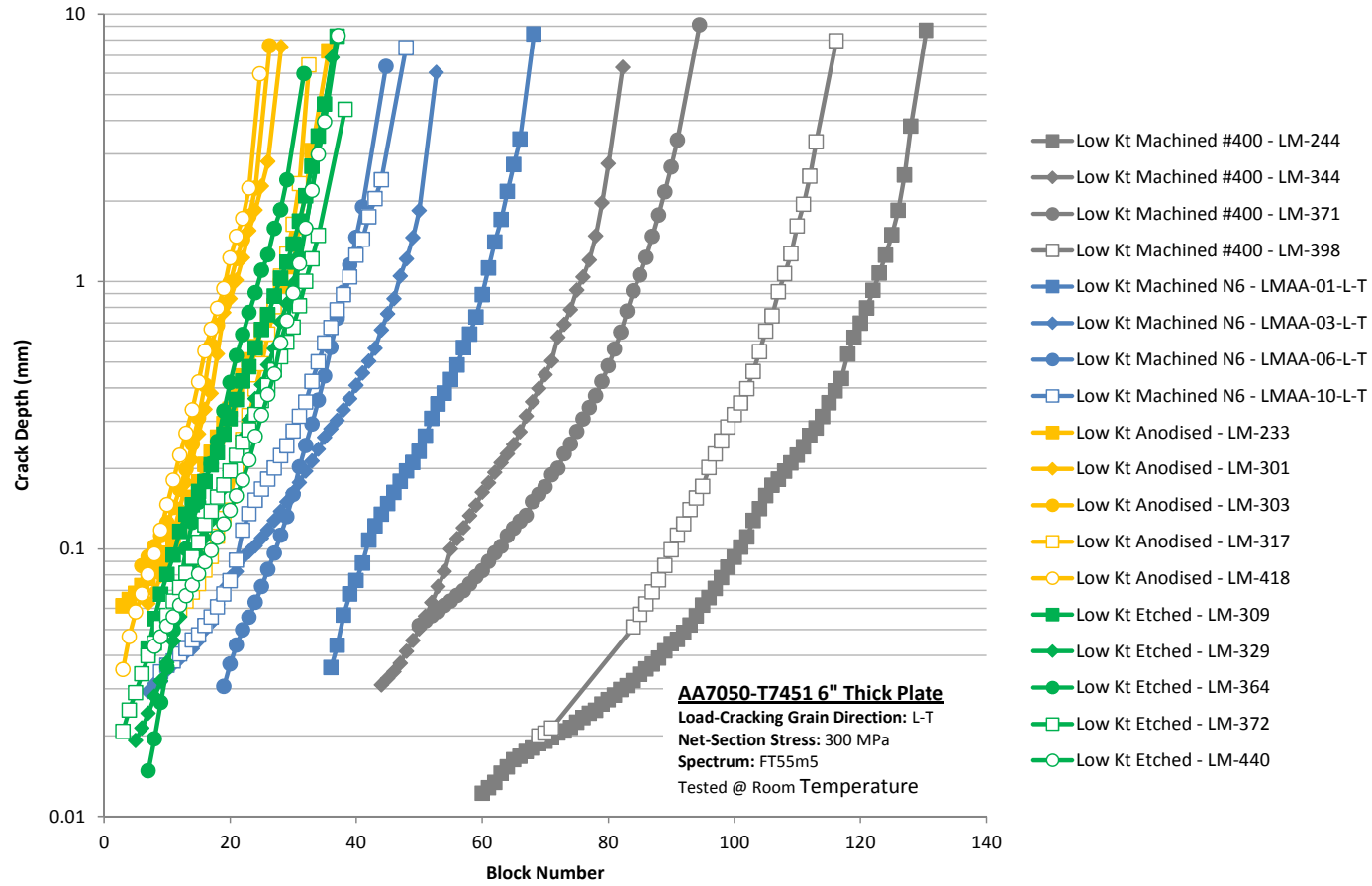
Figure 20: Crack growth curves for low K$_t$ coupons
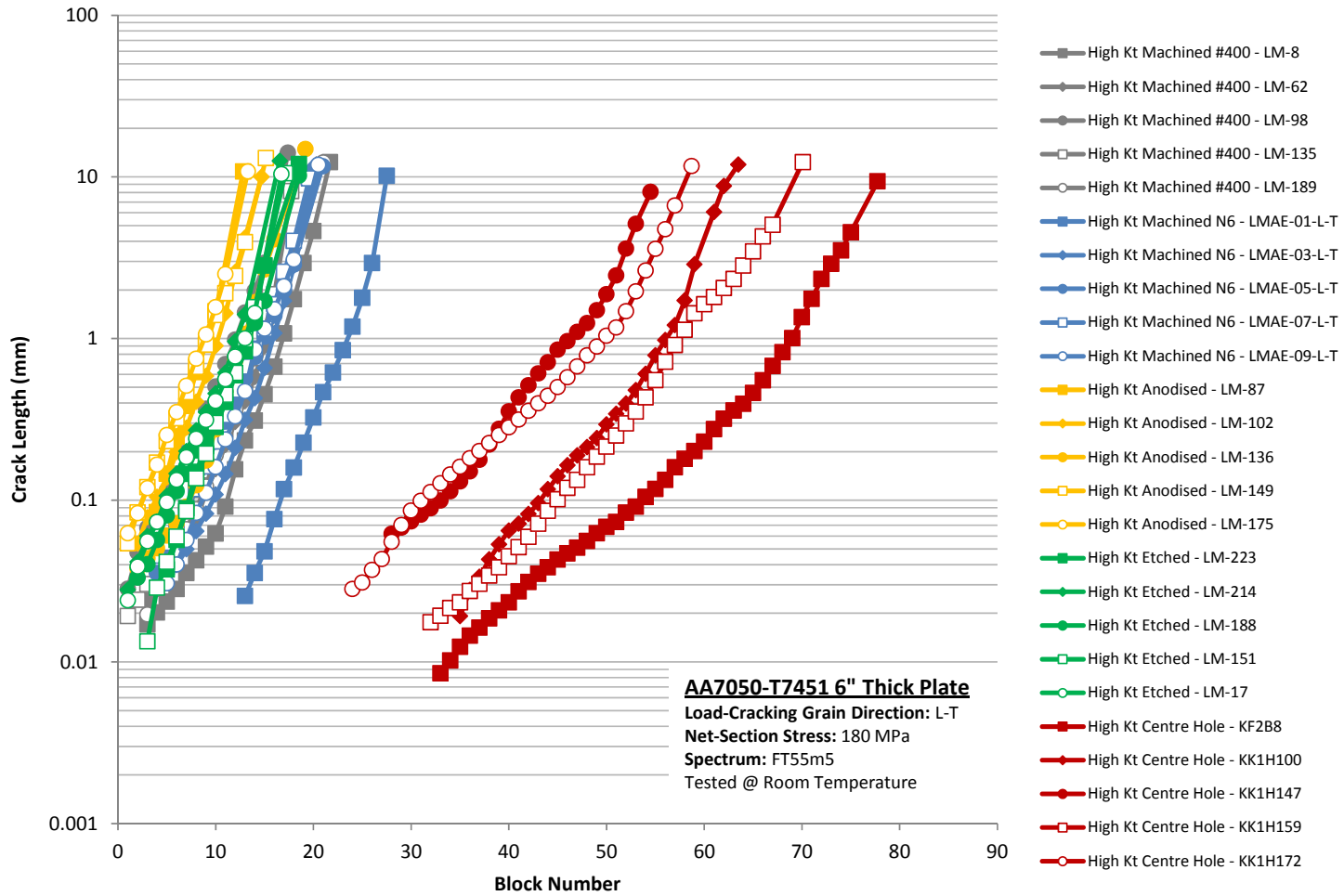
Figure 21: Crack-growth curves for high K$_t$ coupons

7. Discussion

7.1 Life Variation

An examination of the total life results (Figures 12 and 13) shows a marked difference between the machined (N6) and machined and polished (#400) coupons in comparison to the pre-IVD etched and anodised coupons. The results of the Student's t-test statistical analysis showed that the effect of the surface treatments was more prevalent in the low K_t geometries than the high K_t geometries. Table 7 shows the variations in the means of the fatigue lives were significantly larger for the low K_t coupons. It should be pointed out however that the target life for the machined (N6) coupons was ~20,000 flight hours as previously explained in Section 5. The machined (N6) high K_t specimens lasted a log-average of 6,985 flight hours, with the machined and polished (#400), pre-IVD etched and anodised coupons lasting log-averages of 6,347, 5,675 and 4,830 flight hours respectively. Whereas, for the low K_t specimens, the machined (N6) and the machined and polished (#400) coupons lasted a log-average of 34,568 and 19,282 flight hours respectively, and the pre-IVD etched and anodised coupons failed after 11,694 and 9,479 flight hours respectively. These results demonstrated that the applied stress levels might have been higher than a general combat aircraft design condition (for an open hole). This will have affected the representation of the relative life differences for the high Kt coupons, since it is expected that the life differences will be greater at lower stresses (longer lives) as was demonstrated by the low Kt data. The high stress levels applied to the high K_t coupons probably contributed to the smaller variation between the fatigue life means of those coupons. In other words, it can be expected that higher stresses will reduce fatigue life scatter and this is well document in the literature [5, 15], or put another way, high stresses reduce the effect that surface treatments can have on the fatigue life.

7.2 Initiating Discontinuities

Each of the fatigue cracks examined here initiated from a discontinuity on the surface or just below the surface of the coupons. Typically, several fatigue cracks grew from discontinuities in each coupon, although many cracks initiated in the case of the pre-IVD etched and anodised coupons when compared to the machined (N6) or machined and polished (#400) coupons. These discontinuities were found to be mostly associated with inclusions in the case of the machined (N6) and machined and polished (#400) coupons and pits formed by chemical etching in the case of the pre-IVD etched and anodised coupons.

The crack initiation discontinuities in the coupons were measured: see Table 8. This showed that in the machined coupons they were significantly smaller in depth and area than the discontinuities caused by the anodising process. The larger size of the discontinuities had the effect that those fatigue cracks that grew from them spent less time in growing whilst they were small, because the crack started at what was a larger effective initial size. This appears to be the major reason behind the reduced fatigue life of the anodised coupons.
Although the depth of the discontinuities was found to be important, it did not appear to correlate accurately with the reduction in fatigue life since the pre-IVD etched coupons (as illustrated in Figure 16) had similar depth flaws as the machined coupons, but significantly

shorter lives, more akin to the anodised coupons. The areas of the discontinuities may account for this in that they were much greater than the discontinuity areas of the machined coupons, therefore the area of the flaws appears to be a more accurate metric that would link the surface treatment with the fatigue life. This was examined in Figures 22 and 23 which summarise the average depth and area of the discontinuities in terms of the surface treatment and the geometry of the coupon. An examination of these results along with the results plotted in Figures 24 and 25 found that although the area of the discontinuities was more closely related to the lives of the discontinuities the correlation was again weak.
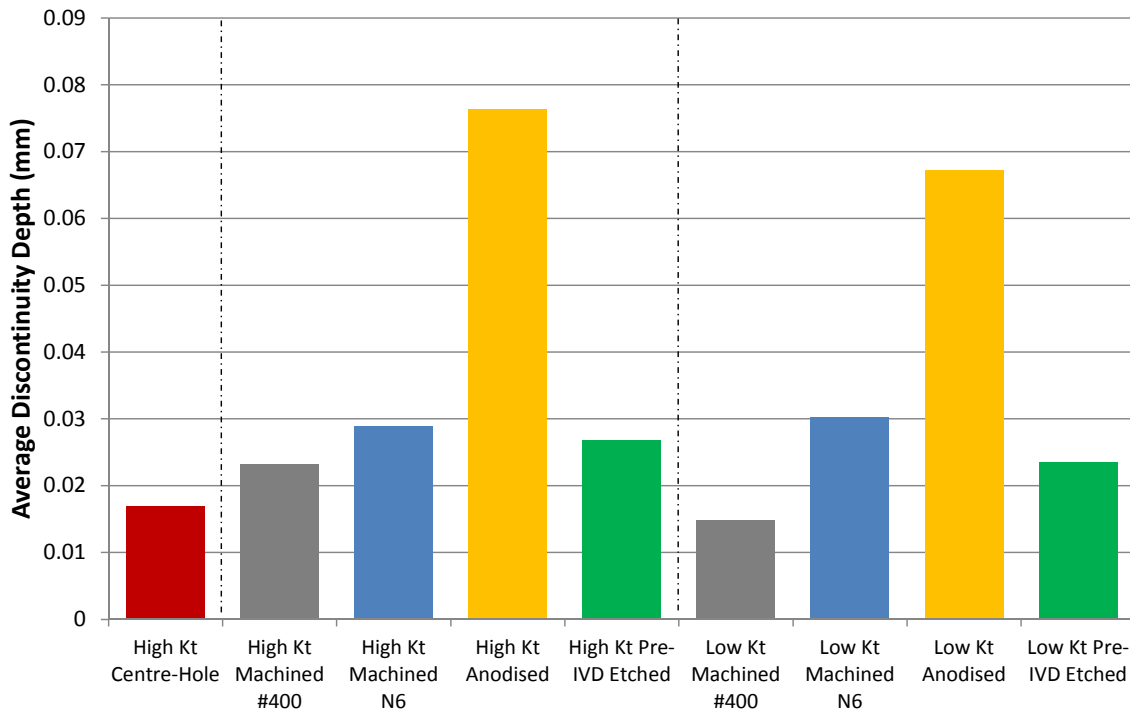
Figure 22: Summary of the average depths of each of the initiating discontinuities
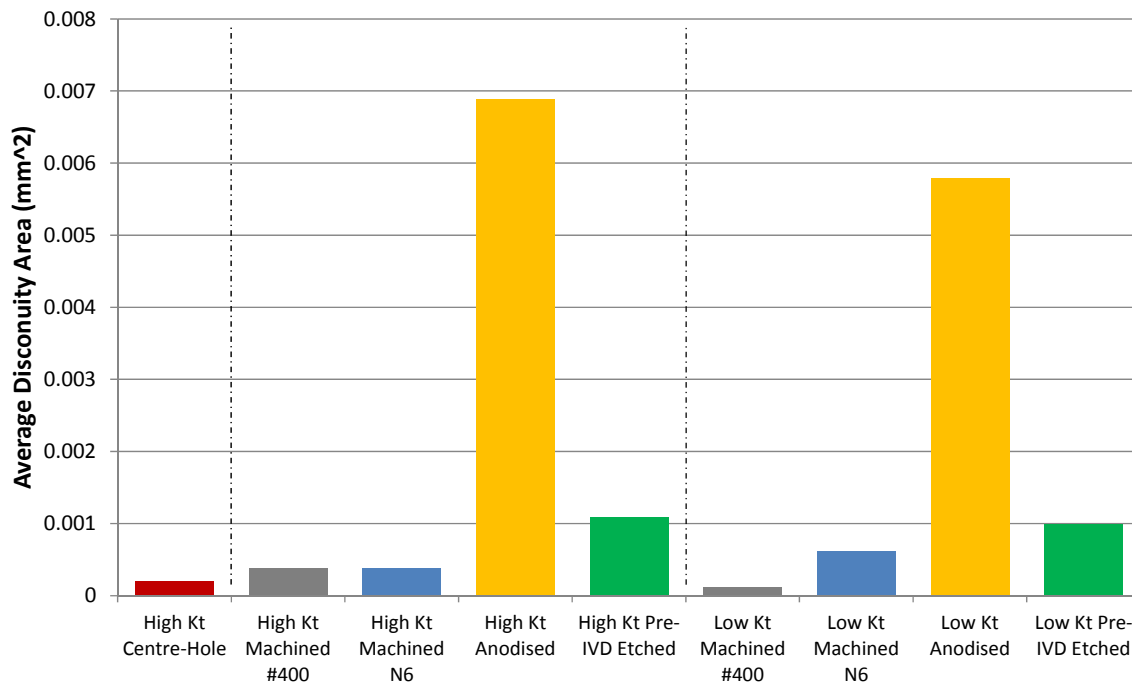
Figure 23: Summary of the average areas of each of the initiating discontinuities

Figures 24 and 25 show the link between the average flaw area and the fatigue life of each surface treatment, indicating that the fatigue lives of the low K_t coupons are much more susceptible to surface treatments than the high K_t coupons. This was expected since the high K_t coupons spend less time growing about their initiating feature, which is a function of surface treatment, due to the higher stress concentrations. The low K_t coupons spend significantly longer initially growing about the initiating discontinuities and therefore the total fatigue life is strongly affected by any potential shortening of this phase of the life, which in this case is caused by larger initial flaws. This result was verified in the Student's T-test results in Section 6.1.
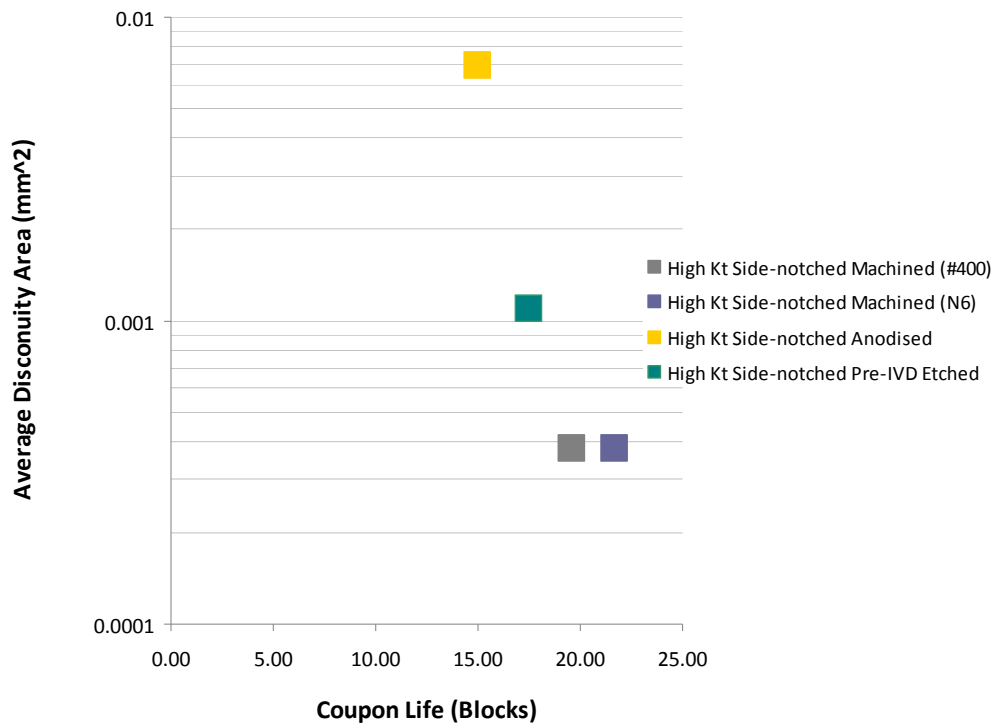
Figure 24: A plot showing the relationship between fatigue life and the average initial flaw area caused by the different surface treatments for the high K_t coupons
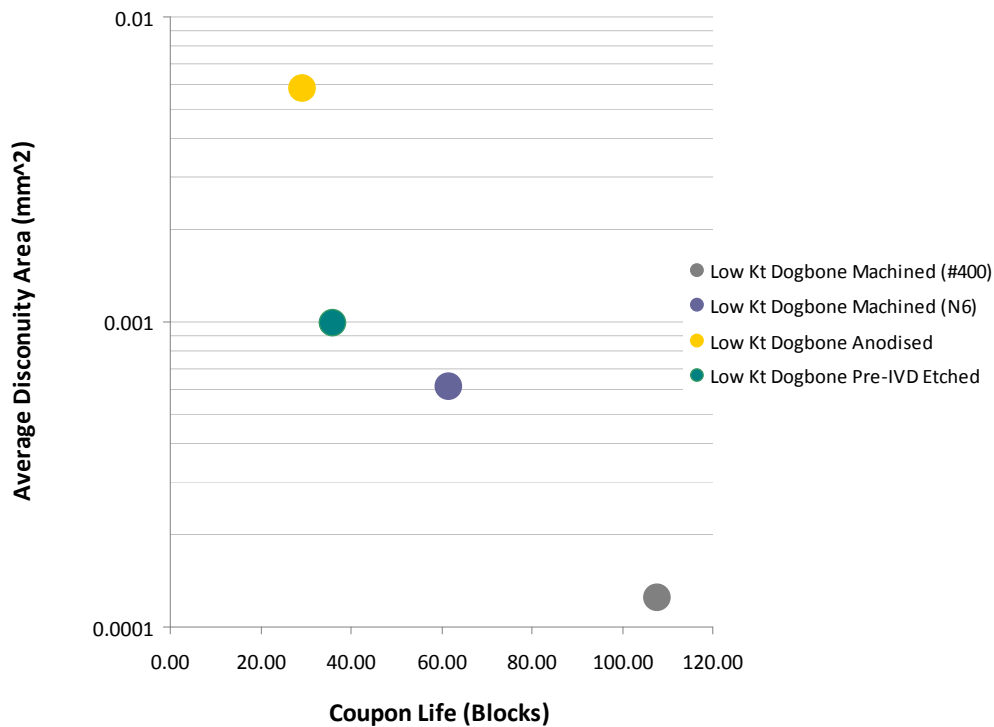
Figure 25: A plot showing the relationship between the fatigue life and the average initial flaw area caused by the different surface treatments for the low K_t coupons

7.3 Cause of the Discontinuities for the Anodised Surface Treatment

An assessment was undertaken to understand the reasons behind the formation of the larger pits in the anodised coupons. The originating discontinuities for the anodised coupons were examined in the SEM. The example in Figure 26, a SEM photograph of coupon LM-301, shows that the anodic layer could be found within the pit, although it did not completely fill the pit. From this, it can be deduced that the pit was present before the anodic layer was applied. This indicates that the pitting was caused by chemical attack of the surface prior to the anodising process. This observation was verified in other coupons, as shown in Figure 27 from coupon LM-418.
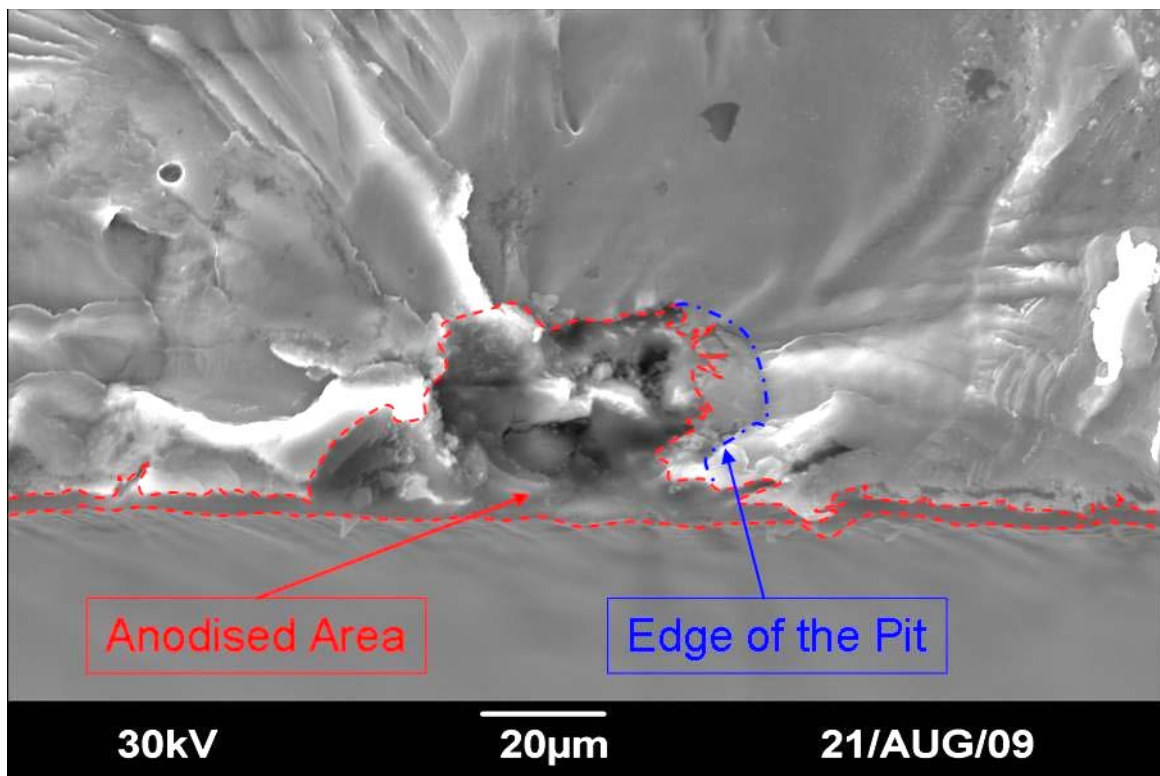
Figure 26: An anodised pit from LM-301 showing the edge of the pit is larger than the anodised area
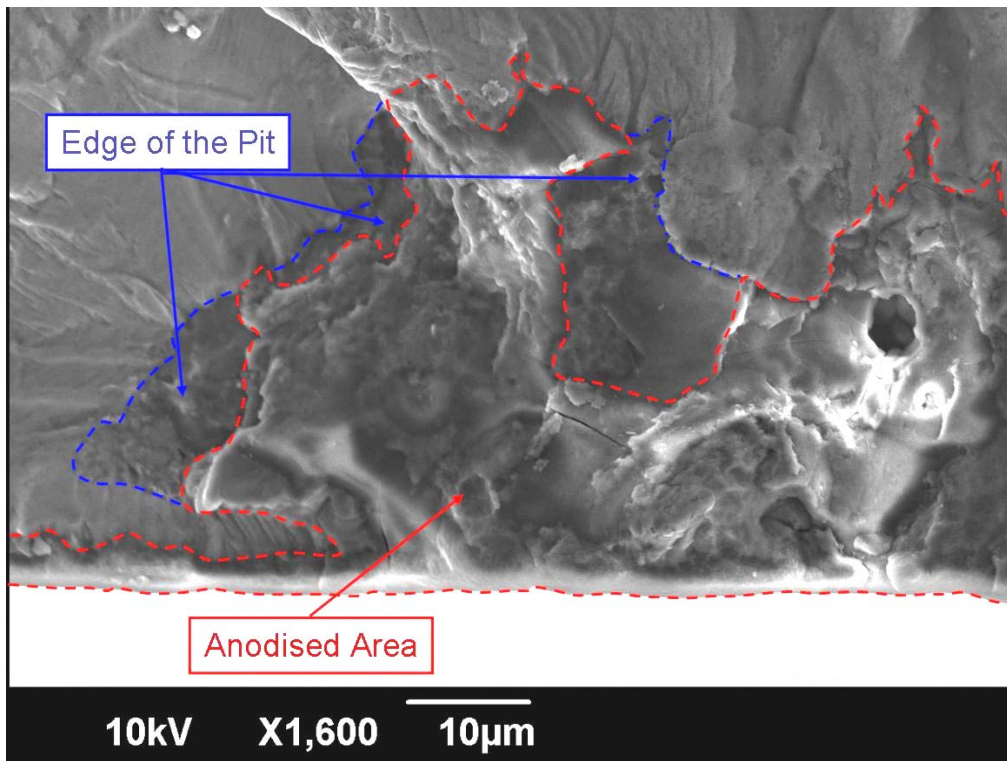
Figure 27: An anodised pit from LM-418 showing the edge of the pit is larger than the anodised area

The types of pits caused during the anodising process were also investigated. It was found that the pits were typically associated with surface breaking inclusions or grain boundaries. Figure 28 of coupon LM-136 shows a pit that has formed by the dissolution of an inclusion. Figure 29 from coupon LM-87 shows a pit which has formed at a grain boundary. These larger pits were more frequently the source of crack initiation in the anodised coupons compared to the etched coupons, where the pitting was generally shallower. These pits tended to be long on the surface and were found to be an important source of crack initiation for the anodised coupons. Figure 30 shows an example of the fracture surface from LM-418 where multiple cracks have started as a result of multiple large pits formed during the anodising process. In general, both the pre-IVD etched coupons and the anodised coupons had many more initiation sites than the machined (N6) and the machined and polished (#400) coupons, most notably in the case of the low Kt coupons.
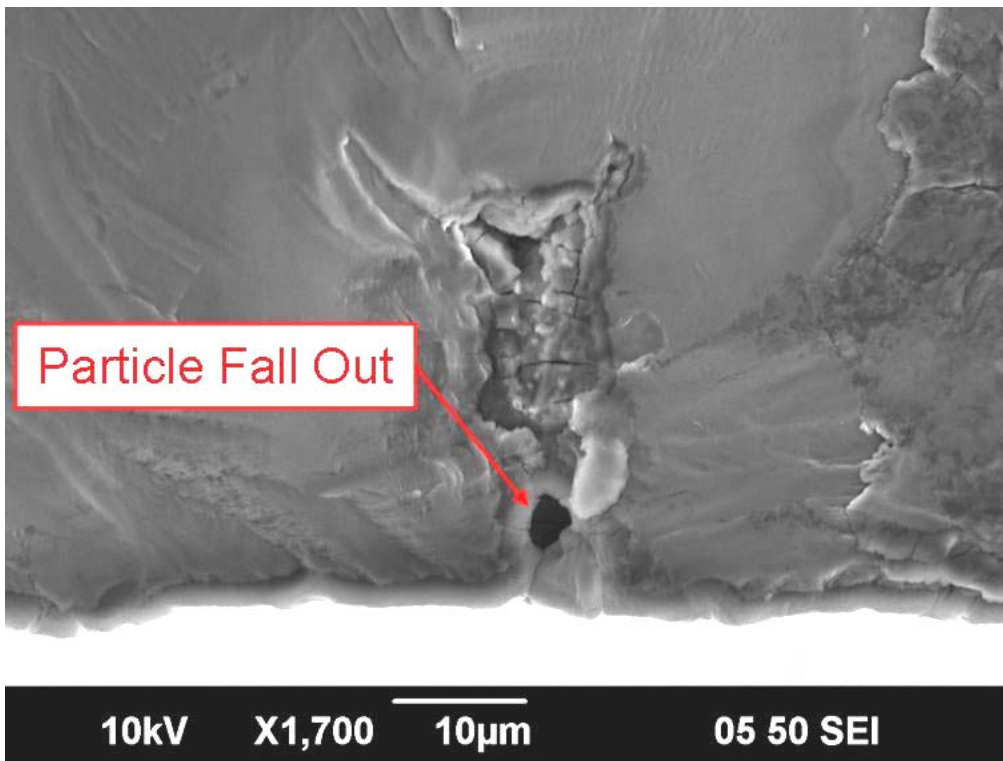
Figure 28: A pit formed from the dissolution of a particle inclusion on coupon LM-136
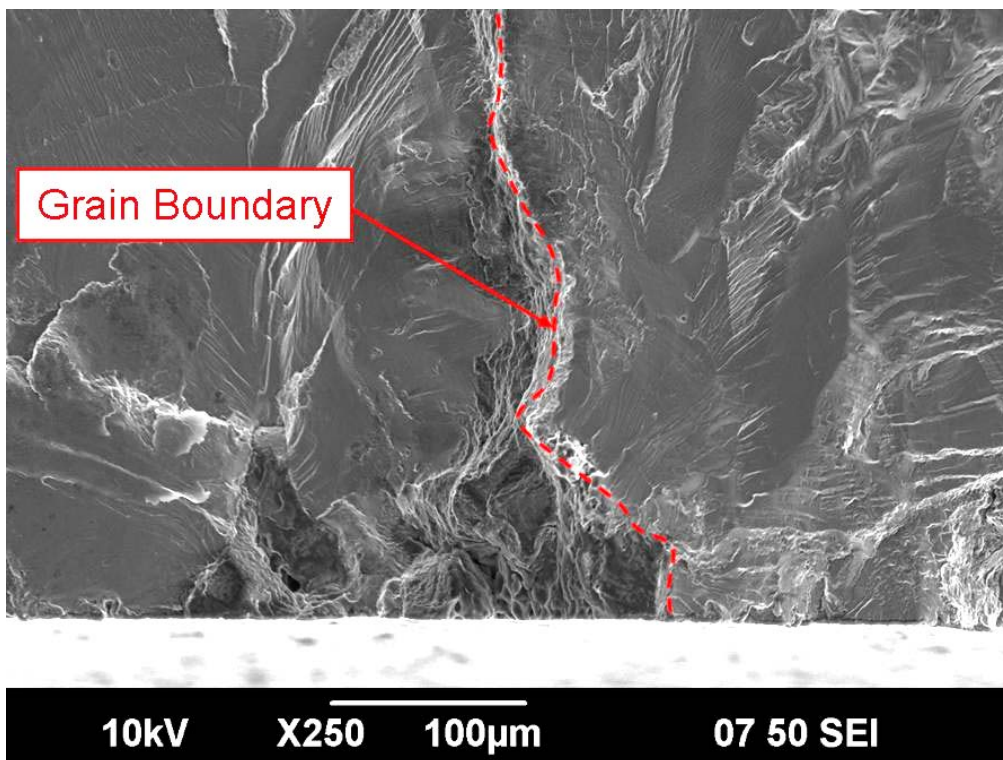
Figure 29: A pit formed by attacking a grain boundary on coupon LM-87
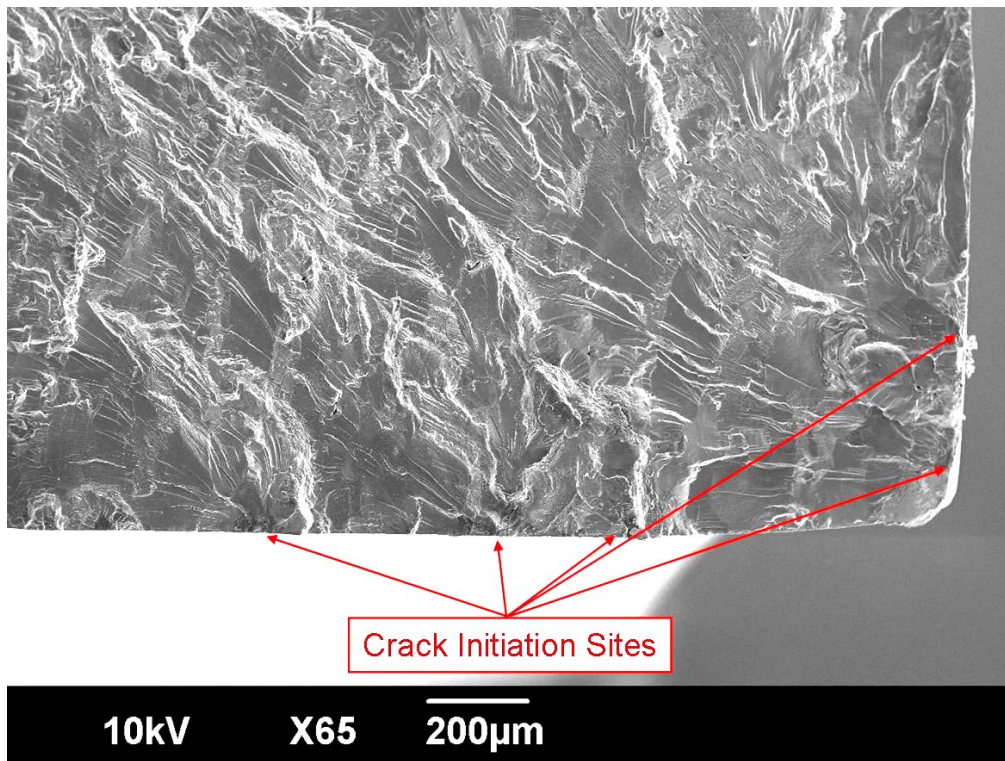
Figure 30: Multiple crack initiation sites on coupon LM-418

7.4 Crack-Growth

The crack-growth rates measured by QF were similar for each surface condition and geometry for each separate Kt, as indicated by the near-parallel growth curves over a large proportion of the crack growth length, within Figures 20 and 21 (excluding the different centre-hole geometry results). This indicates that the difference in fatigue lives is primarily due to the surface features from which the cracks initiated. The crack growth curves for each surface treatment were normalised to a crack length of 0.1mm at zero time (blocks) so an exponential line of best fit could be calculated from the data to analytically compare the crack growth results. The results of the analysis are shown in Figures 31 and 32.
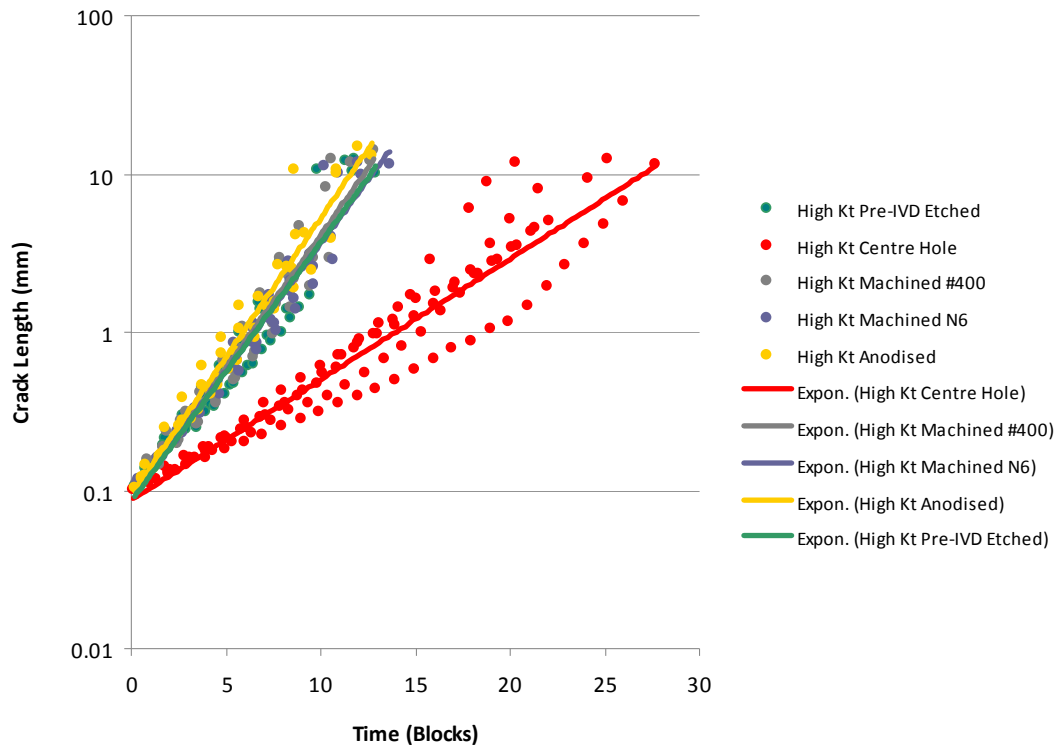
Figure 31: Exponential best-fit line fitted to high K_t coupon results
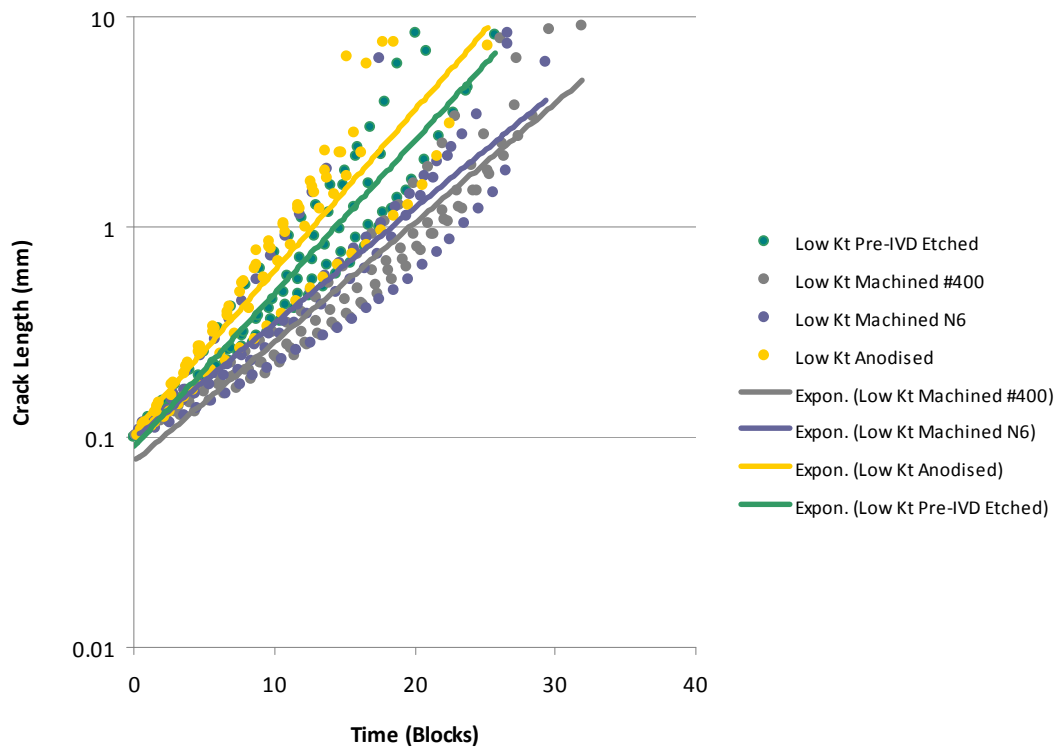
Figure 32: Exponential best-fit line fitted to low K_t coupon results

Figure 31 shows the crack growth curves of all four surface treatments are very similar for the high K_t coupons with the exception of the high K_t centre hole coupons which are noticeably different in crack growth rates compared to the side notched coupons. This may have been caused by the difference in stress intensity factors which can be a result of the different beta functions for the two geometries. Since the applied net-section stresses were the same, the total fatigue life of the centre hole coupons were longer due to the smaller local stress gradient which may have caused the cracks to grow slower. It is also possible that the recorded crack growth rate was slower than the other geometries and surface treatments due to the uneven growth of the cracks on either side of the hole retarding the growth rate of the lead crack.

For the low K_t coupons, the curves appeared to be relatively consistent between the surface treatments. What is notable is the slower growth recorded for the early parts of the crack in the machined coupons, similar to the centre hole coupons discussed previously. This could be contributed to the location of the cracks, where less crack initiation sites makes for slower crack growth rates on average whilst the cracks are small, compared to the pre-IVD etched and anodised coupons where multiple cracks were initiated from a larger number of pits. As the cracks grew longer the growth rate appears to match the other surface treatments more accurately.

8. Conclusions

AA7050-T7451 coupons, subjected to a combat aircraft wing root bending loading spectrum, were tested to analyse the fatigue life effects of four different surface treatments; machined to a N6 surface finish, machined and polished with #400 grit paper, pre-IVD etched, and anodised. The results showed a reduction in the fatigue life for pre-IVD etched and anodised coupons compared to the machined coupons. The reductions in fatigue life were greater in the low Kt specimens compared to the high K_t specimens, although the effect of the local stress levels may have influenced the relative severity between the low and high K_t coupons. The anodising and etching processes caused pitting on the AA7050 surfaces which lead to fatigue cracking that had an advantage due to the larger discontinuities compared to the smaller discontinuities in the "machined" coupons. This indicated that the control of surface discontinuities, particularly pits, is important to the fatigue lives achieved. In the low K_t coupons, the early crack growth contributed more to the total fatigue life than in the high K_t coupons, which resulted in the difference in the relative lives between surface finishes.

The discontinuities that lead to the onset of each of the main fatigue cracks were examined. These observations showed that significantly larger (in depth and area) and more frequent pits occurred in the anodised coupons when compared to the "machined" coupons. This part of the investigation indicated that the pits were produced prior to the anodic layer being applied, most likely during one of the pre-treatment stages in the anodising process.

This test program showed that caution must be taken when applying anodised coatings to this aluminium alloy, since significant pitting may occur, not during anodising but in the pre-treatments. Failure to control these pre-treatments has in this case resulted in a significant reduction in the fatigue life, and this can be expected to flow onto fatigue critical areas in aircraft. The consideration of fatigue life reduction effects may be pertinent during design, inspection (where chemical cleaning may be performed), validation and in-service maintenance of airframe components subjected to these and similar surface treatments.

9. Acknowledgements

10. References

1. Wanhill, R. J. H. (1995) *Damage tolerance engineering property evaluations of aerospace aluminium alloys with emphasis on fatigue crack growth*. National Aerospace Laboratory Report NLR TP 94177U, NLR Amsterdam, The Netherlands

2. Athiniotis, N., Barter, S.A., Bohret, D.D., Green, A.J., Houston, M.I., and Stimson, M.G. (2003) *Final report for the component fatigue test of a F/A-18 Centre Fuselage FS488 Bulkhead - FT488/2*. DSTO-TR-0948, Melbourne, DSTO

3. Molent, L., Barter, S.A., Green, A.J. (2004) *Comparison of two F/A-18 aluminium alloy 7050-T7451 bulkhead coupon fatigue tests*. DSTO-TR-1646, Melbourne, DSTO

4. Barter, S. A. (2003) *Fatigue Crack Growth in 7050-T7451 Aluminium Alloy Thick Section Plate with a Surface Condition Simulating Some Regions of the F/A-18 Structure*. DSTO-TR-1458, Melbourne, DSTO

5. Chaussumier, M., Shahzad, M., Mabru, C., Chieragatti, R., Rezai-Aria, F. (2010) *A fatigue multi-site cracks model using coalescence, short and long crack growth laws, for anodised aluminium alloys*. Procedia Engineering **2** pp 995-1004

6. Lonyuk, B., Apachitei, I., Duszczyk, J. (2007) *The effect of oxide coatings on fatigue properties of 7475-T6 aluminium alloy*. Surface & Coatings Technology **201** pp 8688-8694

7. Kyaw, T. T., Naing, K.M., Win, N. (2011) *Study on Anodizing Processes for formation of Nano porous Aluminium oxide Thin Films*. Advanced Materials Research **236-238** pp 3061-3064

8. Camargo, J. A. M., Cornelis, H.J., Cioffi, V. M. O. H., Costa, M. Y. P (2007) *Coating residual stress effects on fatigue performance of 7050-T7451 aluminium alloy*. Surface & Coatings Technology **201** pp 9448-9455

9. Camargo, A., Voorwald, H. (2007) *Influence of anodization on the fatigue strength of 7050-T7451 aluminium alloy*. Fatigue & Fracture of Engineering Materials & Structures **30** pp 993-1007

10. Rateick, R. G., Griffith, R.J., Hall, D.A., Thompson, K.A. (2005) *Relationship of microstructure to fatigue strength loss in anodised aluminium-copper alloys*. Institute of Materials, Minerals and Mining **21** pp 1227-1235

11. Shahzad, M., Chaussumier, M., Chieragatti, R., Mabru, C., Rezai-Aria, F. (2010) *Influence of Anodizing Process on Fatigue Life of Machined Aluminium Alloy*. Procedia Engineering **2** pp 1015-1024

12. Cirik, E., Genel, K. (2008) *Effect of anodic oxidation on fatigue performance of 7075-T6 alloy*. Surface & Coatings Technology **202** pp 5190-5201

13. Shahzad, M., Chaussumier, M., Chieragatti, R., Mabru, C., Rezai-Aria, F. (2011) *Surface characterization and influence of anodising process on fatigue life of Al 7050 alloy*. Materials and Design **32** pp 3328-3335

14. Dolley, E. J., Lee, B., Wei, R.P. (2000) *The effect of pitting corrosion on fatigue life*. Fatigue & Fracture of Engineering Materials & Structures **23** pp 550-560

15. Barter, S. A., Sharp, P.K., Holden, G., Clark, G. (2001) *Initiation and early growth of fatigue cracks in an aerospace aluminium alloy*. Fatigue & Fracture of Engineering Materials & Structures **25** pp 111-125

16. ASTM-E399 (2009) *Standard Test Method for Linear-Elastic Plane-Strain Fracture Toughness of K_{Ic} of Metallic Materials*. American Society for Testing and Materials.

17. Barter, S., Huynh, J. (2006) *Fatigue Crack Growth in 7050-T7451 Aluminium Alloy Open Hole Coupons*. DSTO-TN-0677, Melbourne, DSTO

18. *ISO 1302:2002(E) - Geometrical Product Specifications (GPS) - Indication of surface texture in technical product documentation.* (2002). ISO1302.

19. Sullivan, A. B., Zavitz, D., Hiscocks, R.J., and Simpson, D.L. (1992) *Post-LEX Sample Mission Block (IARPO), A Sub-Task of CF-18, F/A-18 IFOSTP Usage Processing Task WBS D.A.* LTR-ST-1881, National Research Council Canada

Appendix A: LM Cut-up Plan

A.1   LM-001 to LM-408
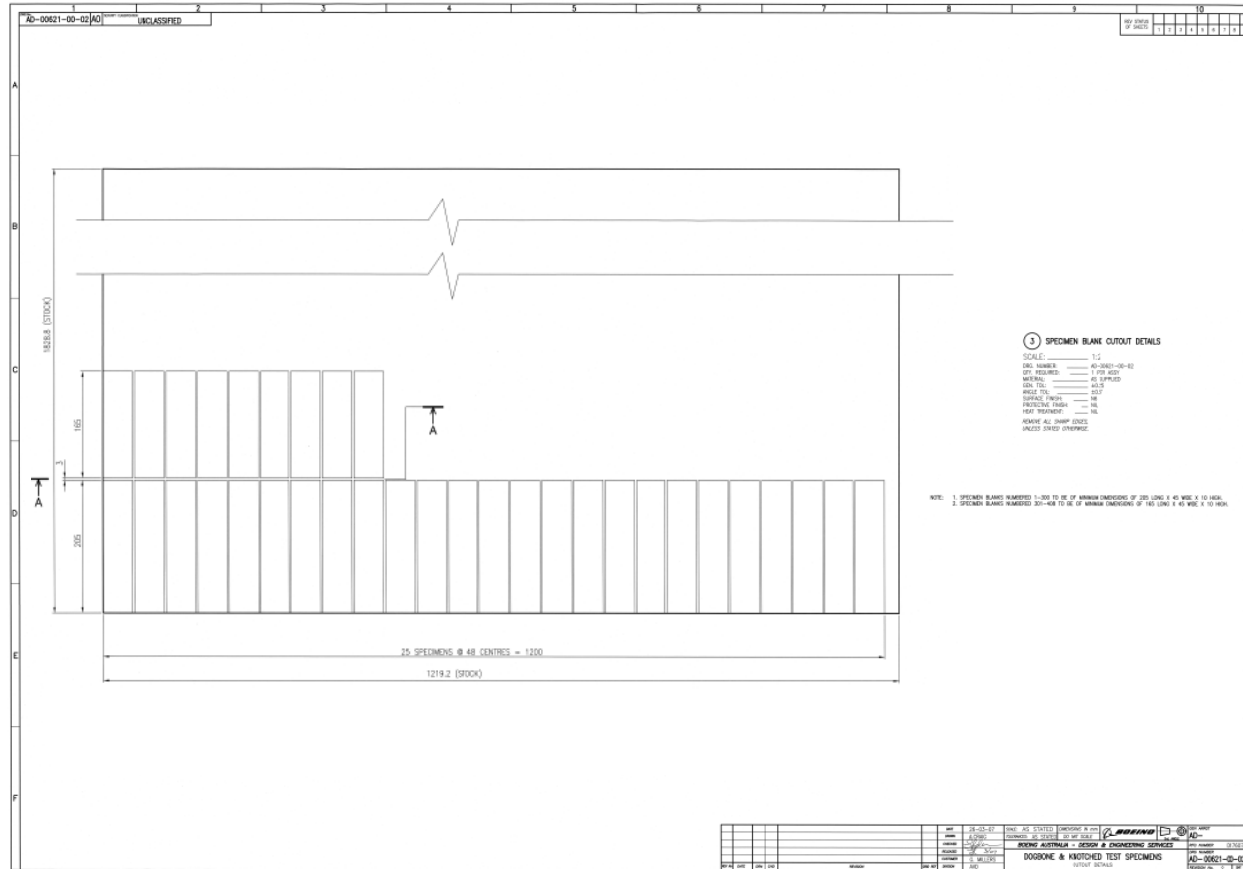
Figure A1: Cutup plan for LM coupons LM-001 to LM-408

Figure A2:Cross-section cutup plan for LM coupons LM-001 to LM-408

A.2   LMAA-01-L-T to LMBM-10-T-L
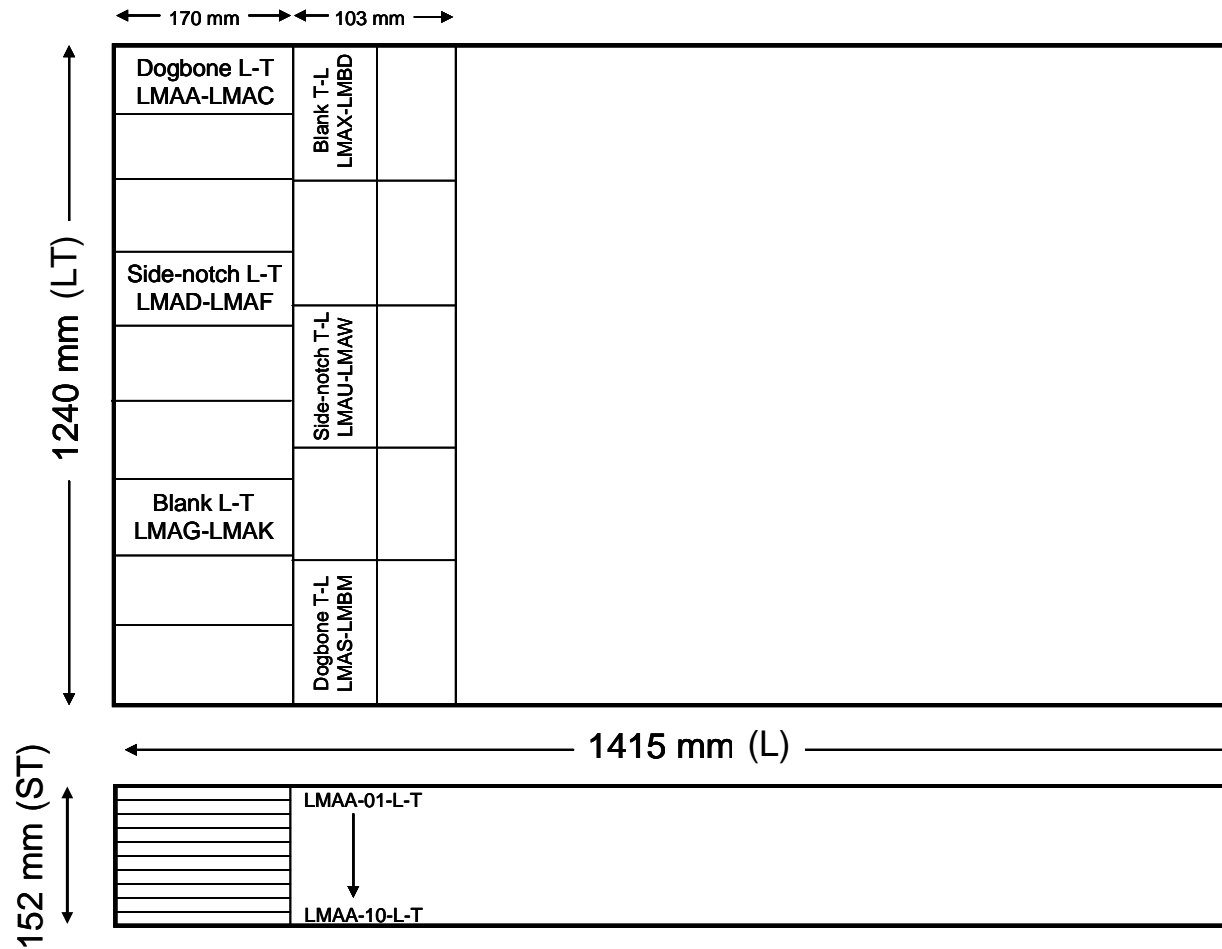
Figure A3: Cutup plan for LM coupons LMAA-01-L-T to LMBM-10-T-L

Appendix B: Surface Roughness Test Results

Specimen ID	Specimen Geometry	Plate ID	Plate Year	Load Dir.	Lay Direction	Spectrum	Surface Condition Description	Surface Texture (Average Profile Roughness) ISO 1302:2002(E)				
								Flat Area (on surface near notch)				Radius Area
								90 Degrees to Fracture		Parallel to Fracture		Longitudinal
								Front Face Ra (µm)	Back Face Ra (µm)	Front Face Ra (µm)	Back Face Ra (µm)	Ra (µm)
LM-8	Sidenotch200R5	LM	2004	L	L	FT55m5	Machined (#400)	1.7	1.3	0.3	0.3	0.3
LM-135	Sidenotch200R5	LM	2004	L	L	FT55m5	Machined (#400)	1.9	2.3	0.4	0.4	0.2
LM-98	Sidenotch200R5	LM	2004	L	L	FT55m5	Machined (#400)	1.8	1.6	0.3	0.3	0.3
LM-189	Sidenotch200R5	LM	2004	L	L	FT55m5	Machined (#400)	2.2	2.3	0.4	0.5	0.2
LM-62	Sidenotch200R5	LM	2004	L	L	FT55m5	Machined (#400)	1.9	1.9	0.5	0.3	0.2
LMAE-01-L-T	Sidenotch160R5	LM	2004	L	L	FT55m5	Machined (N6)	0.7	-	1	-	-
LMAE-03-L-T	Sidenotch160R5	LM	2004	L	L	FT55m5	Machined (N6)	0.6	-	1	-	-
LMAE-05-L-T	Sidenotch160R5	LM	2004	L	L	FT55m5	Machined (N6)	0.6	-	0.9	-	-
LMAE-07-L-T	Sidenotch160R5	LM	2004	L	L	FT55m5	Machined (N6)	0.6	-	0.8	-	-
LMAE-09-L-T	Sidenotch160R5	LM	2004	L	L	FT55m5	Machined (N6)	0.7	-	0.9	-	-
LM-223	Sidenotch200R5	LM	2004	L	L	FT55m5	Pre-IVD Etched	0.9	0.8	0.9	0.9	0.7
LM-214	Sidenotch200R5	LM	2004	L	L	FT55m5	Pre-IVD Etched	1.1	1.1	1.1	1.2	1.2
LM-188	Sidenotch200R5	LM	2004	L	L	FT55m5	Pre-IVD Etched	1	1	1	1.1	0.9
LM-151	Sidenotch200R5	LM	2004	L	L	FT55m5	Pre-IVD Etched	1.1	1	1	1	0.9
LM-17	Sidenotch200R5	LM	2004	L	L	FT55m5	Pre-IVD Etched	1	1	1.1	1.1	1.2
LM-175	Sidenotch200R5	LM	2004	L	L	FT55m5	Anodised	1.1	1.1	0.8	0.8	0.3
LM-87	Sidenotch200R5	LM	2004	L	L	FT55m5	Anodised	1.2	1.4	0.8	0.8	0.3
LM-136	Sidenotch200R5	LM	2004	L	L	FT55m5	Anodised	1.7	2	0.6	0.5	0.2
LM-149	Sidenotch200R5	LM	2004	L	L	FT55m5	Anodised	1.2	1.3	0.8	0.7	0.3
LM-102	Sidenotch200R5	LM	2004	L	L	FT55m5	Anodised	1.1	1.2	0.7	0.8	0.3
LM-442*	Dogbone160RAD	LM	2004	L	L	FT55m5	Machined (#400)	-	-	-	-	-
LM-398	Dogbone160RAD	LM	2004	L	L	FT55m5	Machined (#400)	2.1	2	0.4	0.4	-

Specimen ID	Specimen Geometry	Plate ID	Plate Year	Load Dir.	Lay Direction	Spectrum	Surface Condition Description	Surface Texture (Average Profile Roughness) ISO 1302:2002(E)				
								Flat Area (on surface near notch)				Radius Area
								90 Degrees to Fracture		Parallel to Fracture		Longitudinal
								Front Face Ra (µm)	Back Face Ra (µm)	Front Face Ra (µm)	Back Face Ra (µm)	Ra (µm)
LM-344	Dogbone160RAD	LM	2004	L	L	FT55m5	Machined (#400)	1.6	1.8	0.4	0.4	-
LM-244	Dogbone160RAD	LM	2004	L	L	FT55m5	Machined (#400)	1.9	2.1	0.4	0.4	-
LM-371	Dogbone160RAD	LM	2004	L	L	FT55m5	Machined (#400)	2.3	1.7	0.4	0.4	-
LMAA01-L-T	Dogbone160RAD	LM	2004	L	L	FT55m5	Machined (N6)	0.5	-	1.4	-	-
LMAA03-L-T	Dogbone160RAD	LM	2004	L	L	FT55m5	Machined (N6)	0.4	-	1.5	-	-
LMAA06-L-T	Dogbone160RAD	LM	2004	L	L	FT55m5	Machined (N6)	0.5	-	1.6	-	-
LMAA08-L-T	Dogbone160RAD	LM	2004	L	L	FT55m5	Machined (N6)	0.4	-	1.5	-	-
LMAA10-L-T	Dogbone160RAD	LM	2004	L	L	FT55m5	Machined (N6)	0.2	-	0.9	-	-
LM-372	Dogbone160RAD	LM	2004	L	L	FT55m5	Pre-IVD Etched	1.1	1	1.2	1.1	-
LM-309	Dogbone160RAD	LM	2004	L	L	FT55m5	Pre-IVD Etched	1.1	1.3	1.1	1.1	-
LM-364	Dogbone160RAD	LM	2004	L	L	FT55m5	Pre-IVD Etched	1.1	1.2	1.1	1.1	-
LM-440	Dogbone160RAD	LM	2004	L	L	FT55m5	Pre-IVD Etched	1.1	1.3	1.3	1.2	-
LM-329	Dogbone160RAD	LM	2004	L	L	FT55m5	Pre-IVD Etched	1.1	1.1	1.1	1.2	-
LM-301	Dogbone160RAD	LM	2004	L	L	FT55m5	Anodised	1.2	1.2	0.9	0.9	-
LM-303	Dogbone160RAD	LM	2004	L	L	FT55m5	Anodised	1.3	1.1	0.7	0.7	-
LM-317	Dogbone160RAD	LM	2004	L	L	FT55m5	Anodised	1.5	1.5	0.9	0.7	-
LM-233	Dogbone160RAD	LM	2004	L	L	FT55m5	Anodised	1.3	1.3	0.6	0.7	-
LM-418	Dogbone160RAD	LM	2004	L	L	FT55m5	Anodised	1.4	1.2	1	0.9	-
KK1H159*	Centre-Hole	KK	~1992	L	L	FT55m5	Machined (N6)	0.4	0.2	0.7	0.8	0.2
KK1H172	Centre-Hole	KK	~1992	L	L	FT55m5	Machined (N6)	0.3	0.3	0.7	0.6	0.3
KK1H100	Centre-Hole	KK	~1992	L	L	FT55m5	Machined (N6)	0.2	0.4	0.7	0.6	0.1
KK1H147	Centre-Hole	KK	~1992	L	L	FT55m5	Machined (N6)	0.3	0.3	0.6	0.7	0.1
KF2B8	Centre-Hole	KF	1990	?	L	FT55m5	Machined (N6)	0.2	0.3	0.8	0.6	1.4

Appendix C: Initial Flaw Photographs

C.1 High Kt Centre Hole – Machined (N6)
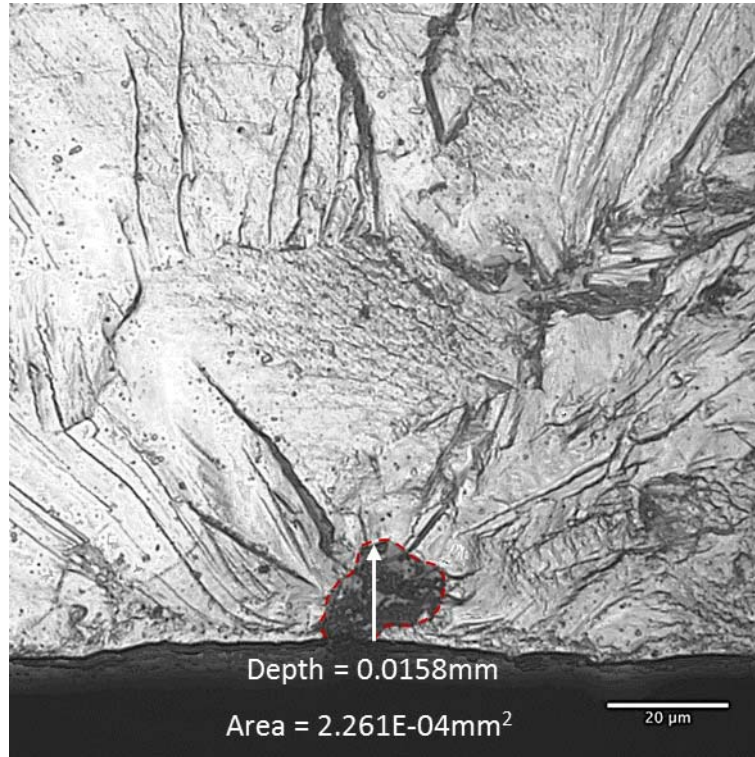
Figure C1: Initiating flaw of KF2B8
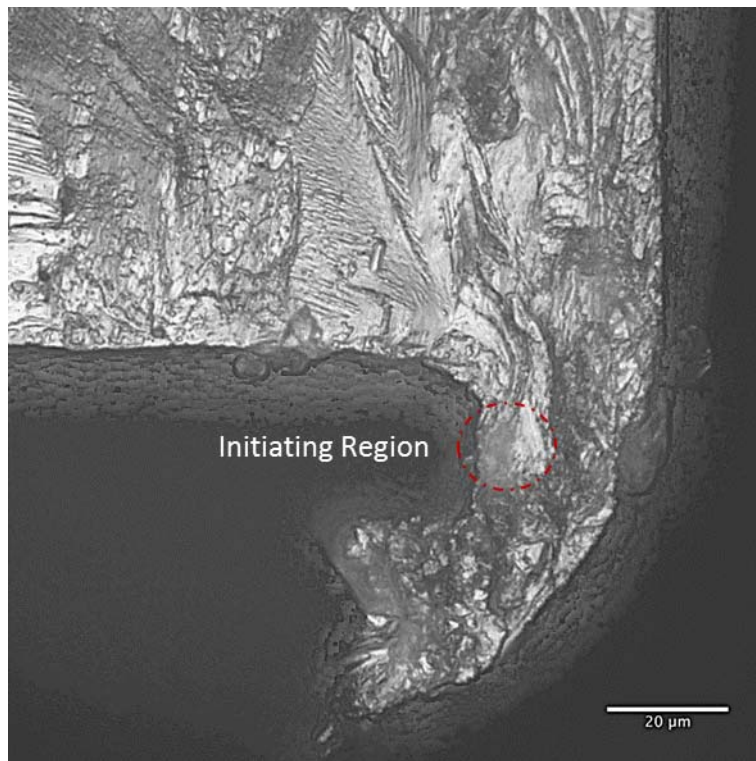
Figure C2: Initiating flaw of KK1H100 (the crack initiated from a machining burr and therefore the exact initiation point and features were difficult to determine)
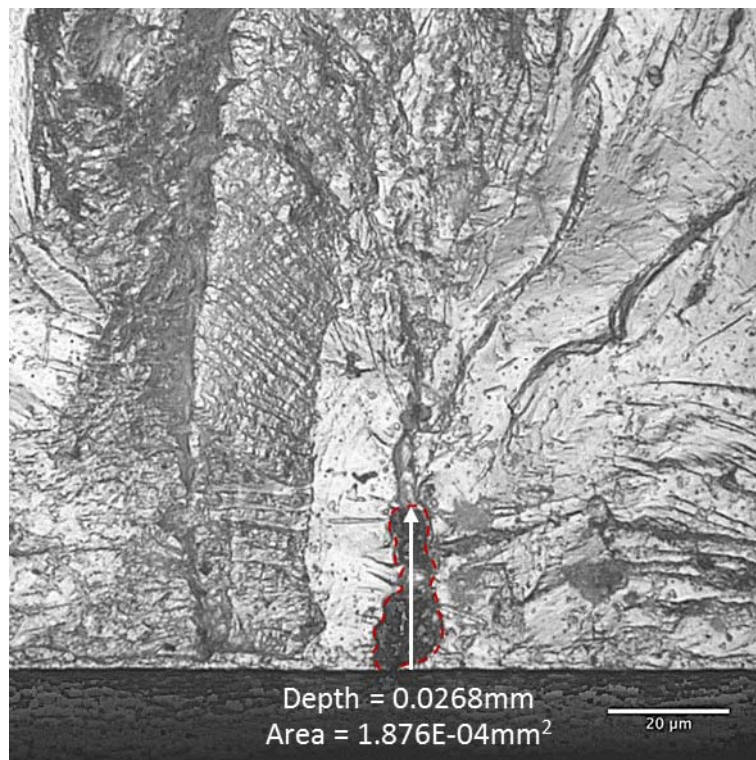
Figure C3: Initiating flaw of KK1H147
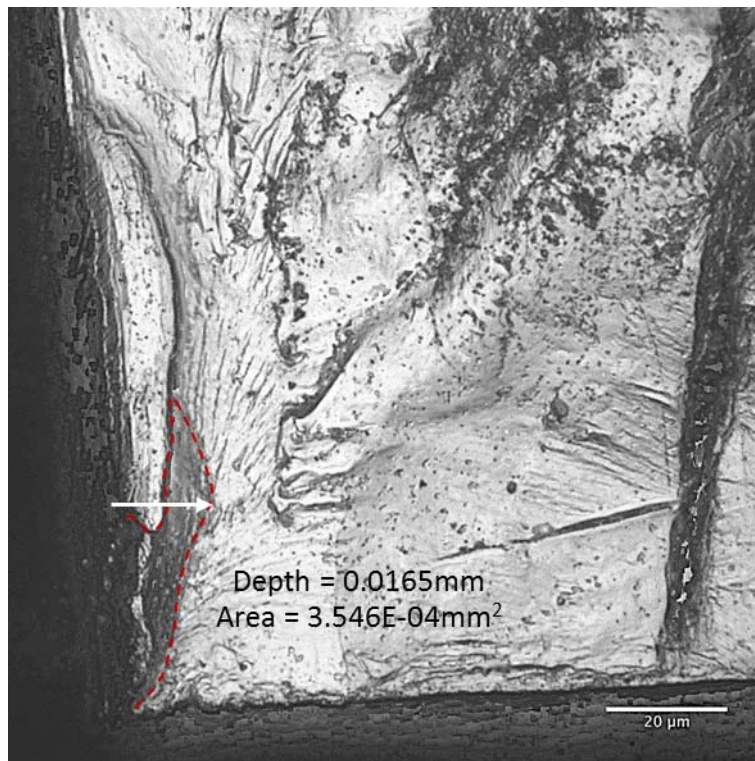
Figure C4: Initiating flaw of KK1H159
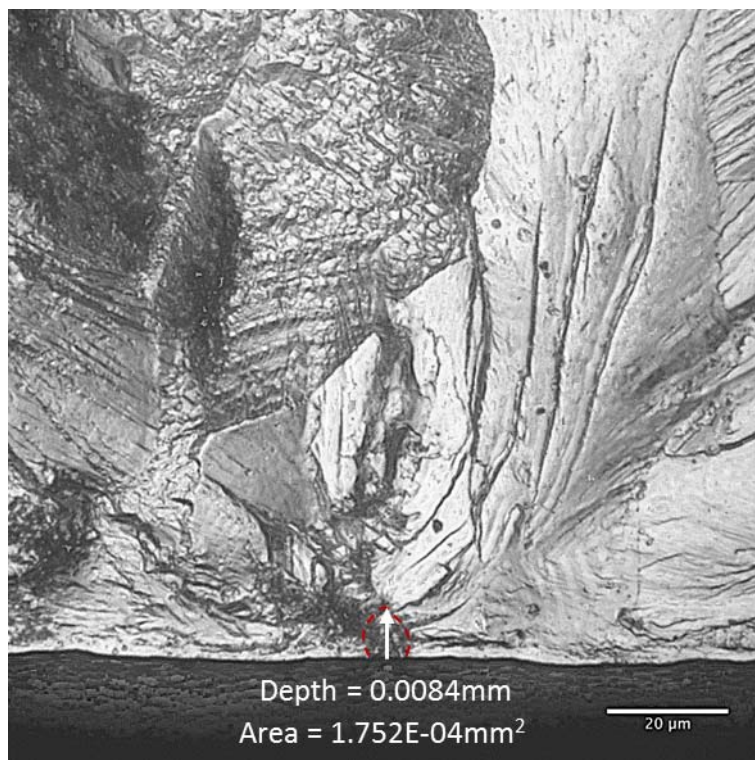
Figure C5: Initiating flaw of KK1H172

C.2   High Kt Side-Notched – Machined (#400)
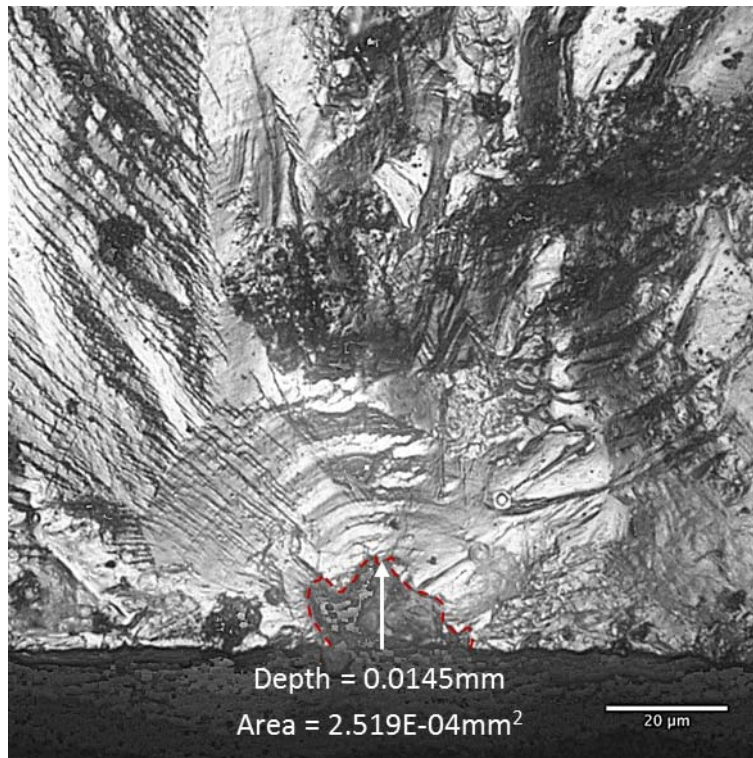
Figure C6: Initiating flaw of LM-8
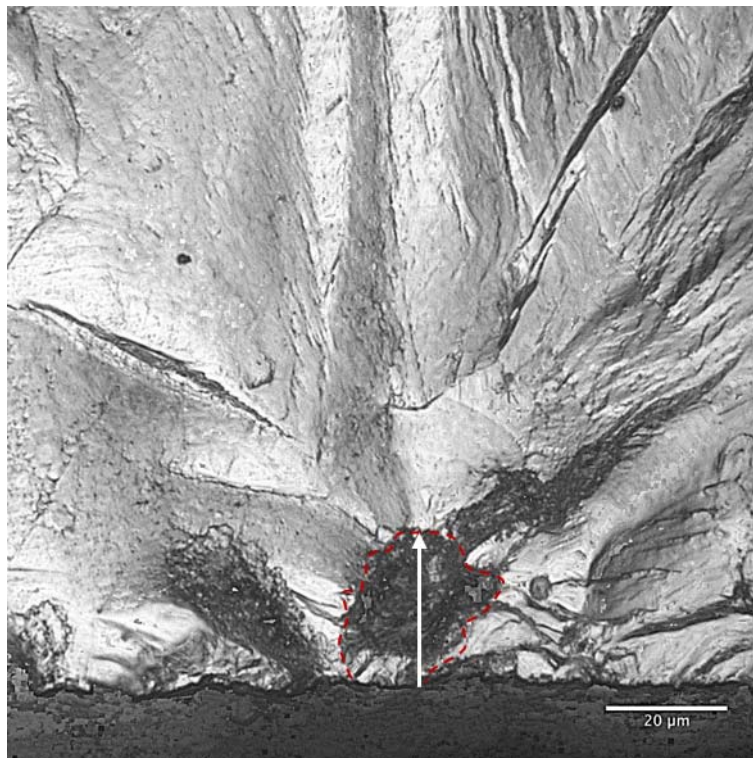
Figure C7: Initiating flaw of LM-62

Depth = 0.0111mm
Area = 1.173E-04mm²

20 µm
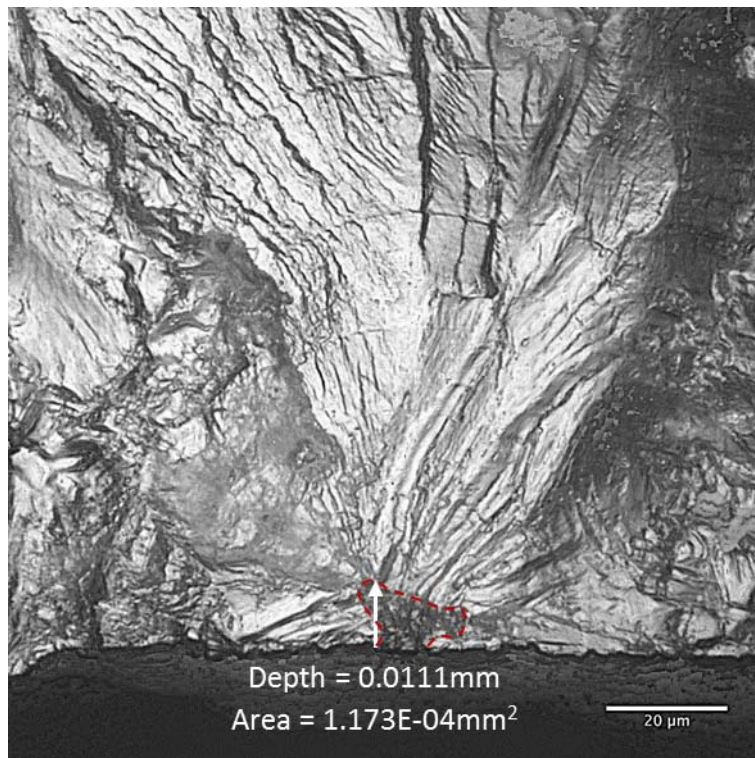
Figure C8: Initiating flaw of LM-98

Depth = 0.0530mm
Area = 5.394E-04mm²

20 µm
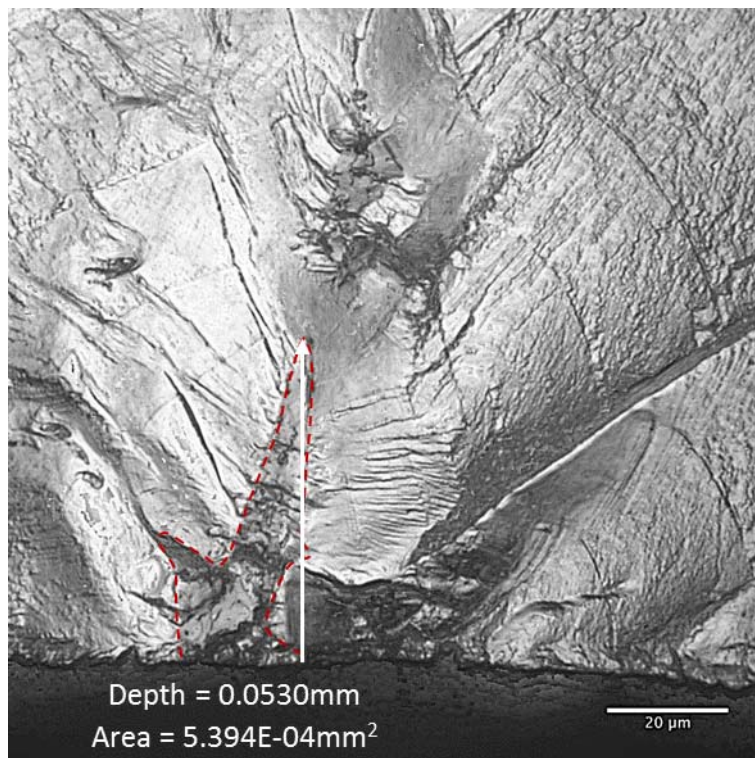
Figure C9: Initiating flaw of LM-135
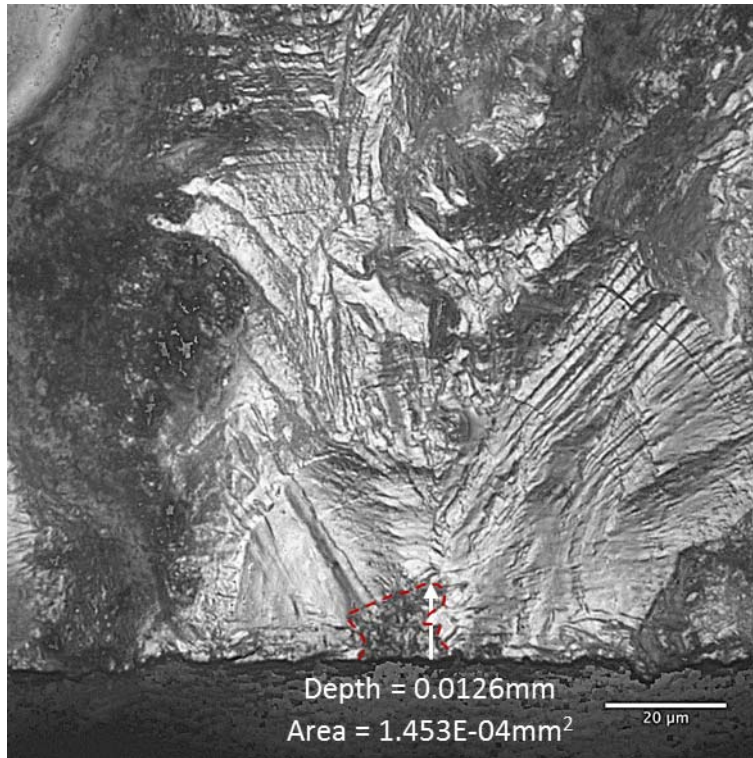
Figure C10: Initiating flaw of LM-189

C.3 High Kt Side-Notched – Machined (N6)
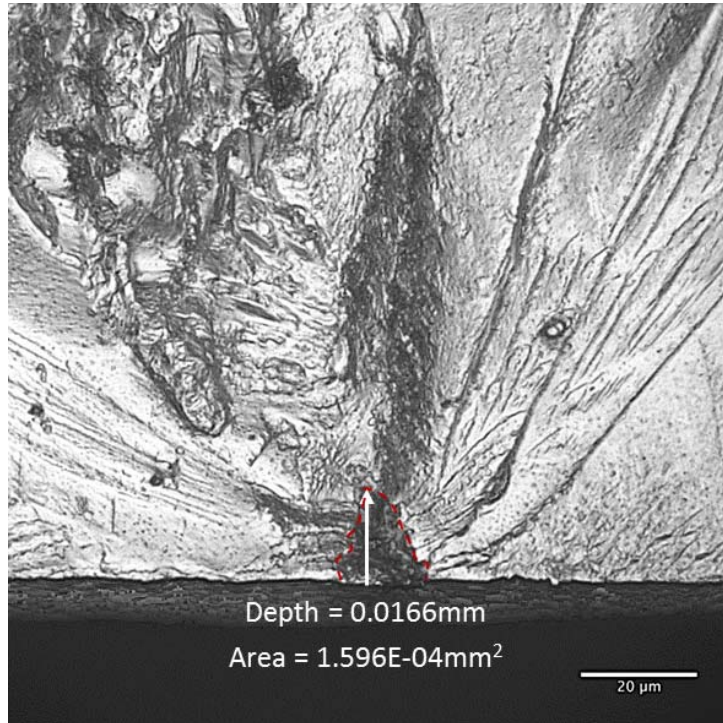
Figure C11: Initiating flaw of LMAE-01-L-T
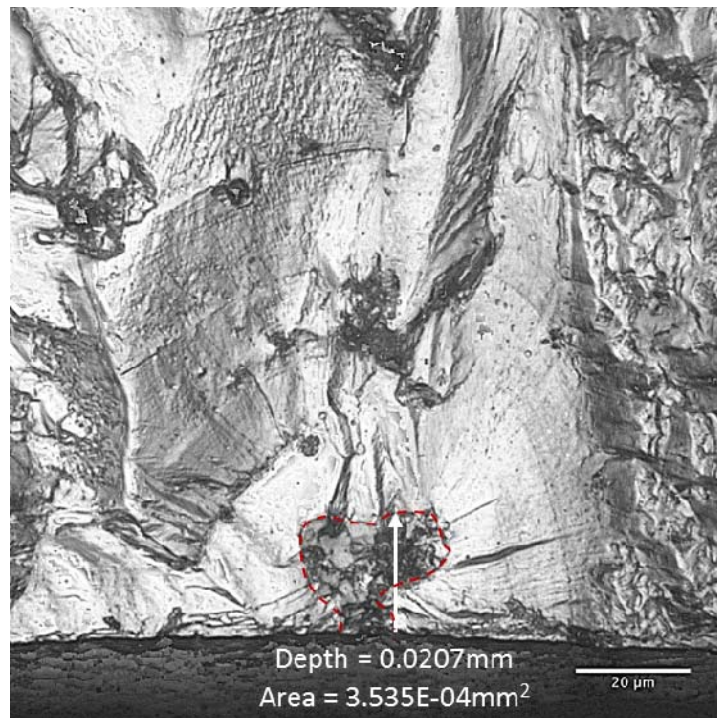
Figure C12: Initiating flaw of LMAE-03-L-T
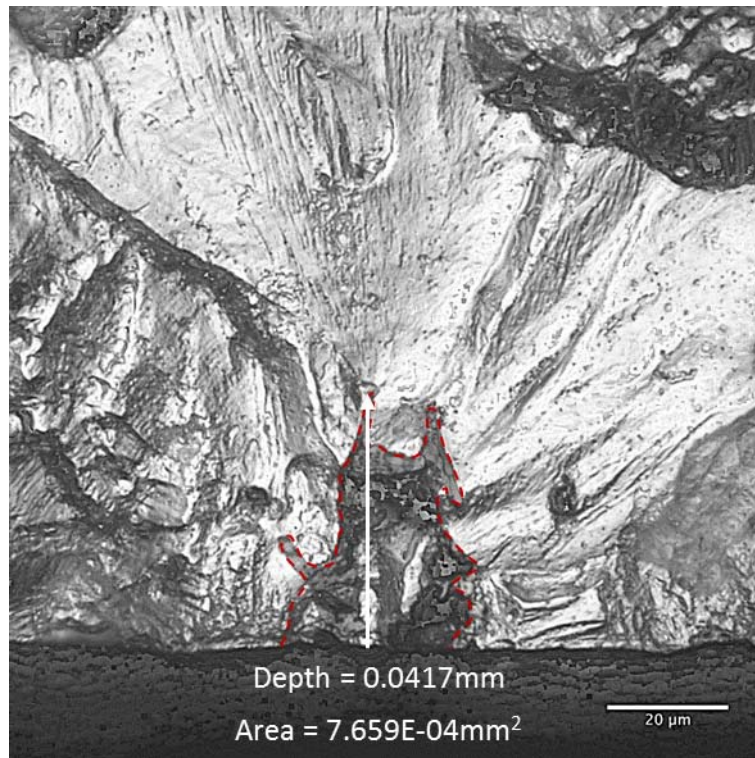
Figure C13: Initiating flaw of LMAE-05-L-T
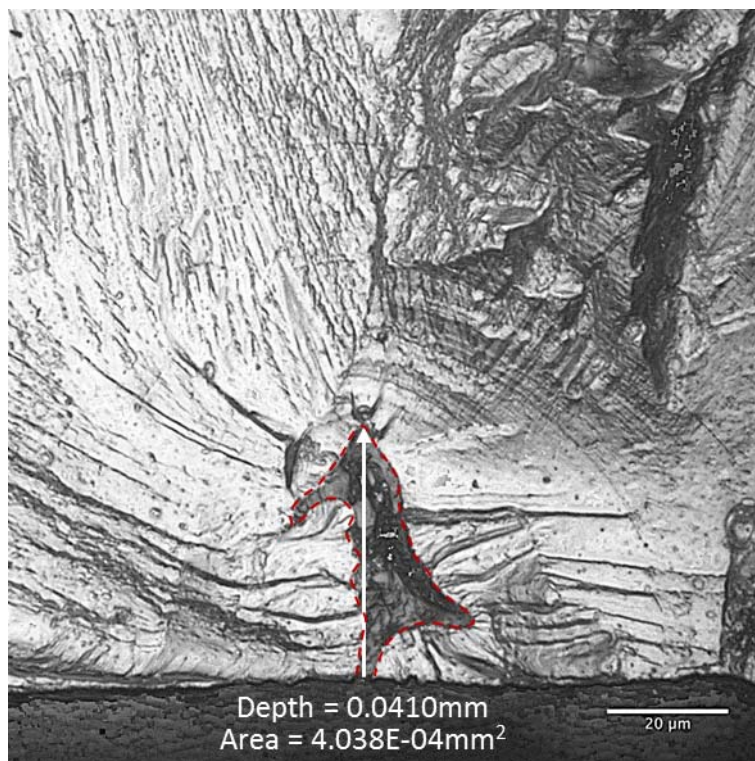
Figure C14: Initiating flaw of LMAE-07-L-T
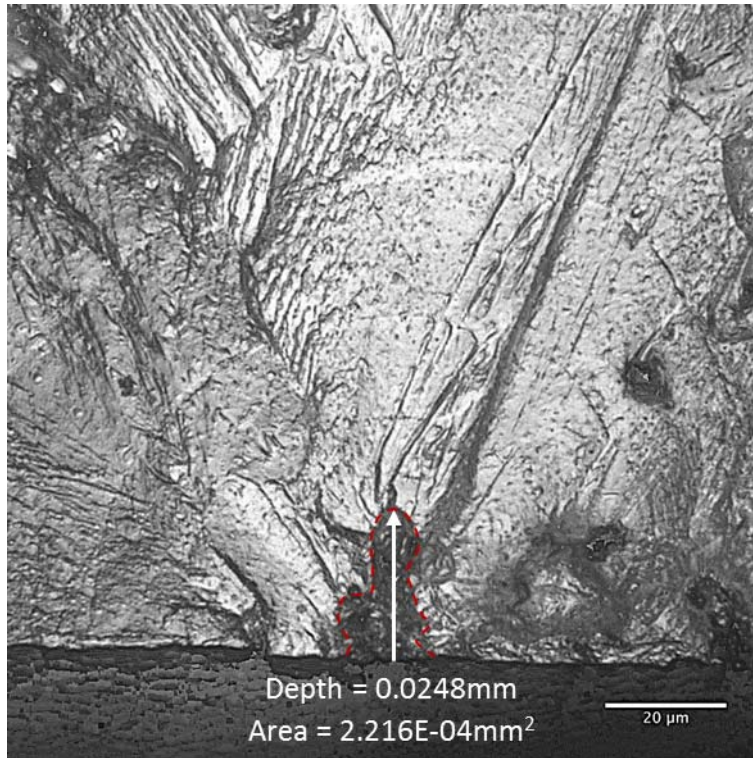
Figure C15: Initiating flaw of LMAE-09-L-T

C.4 High Kt Side-Notched – Pre-IVD Etched
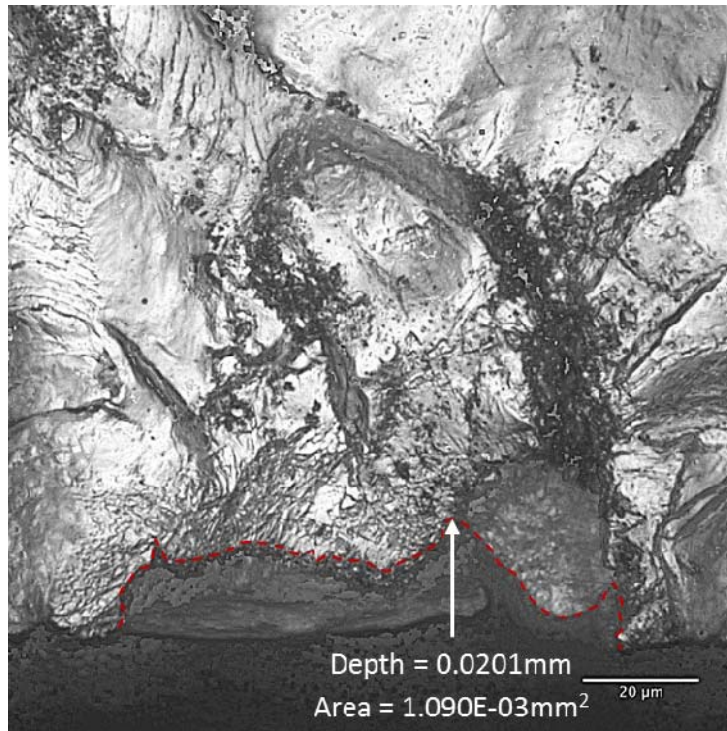
Figure C16: Initiating flaw of LM-17
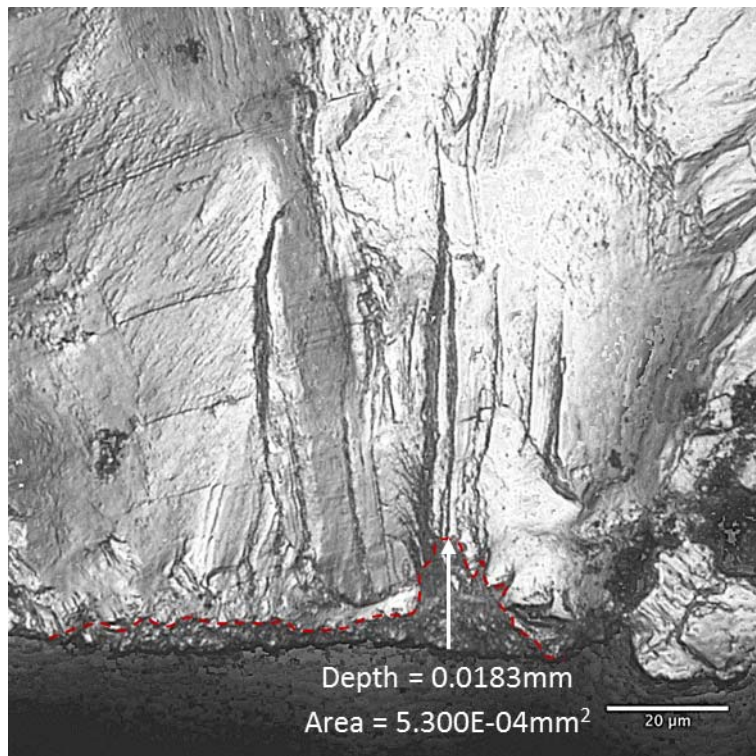
Figure C17: Initiating flaw of LM-151
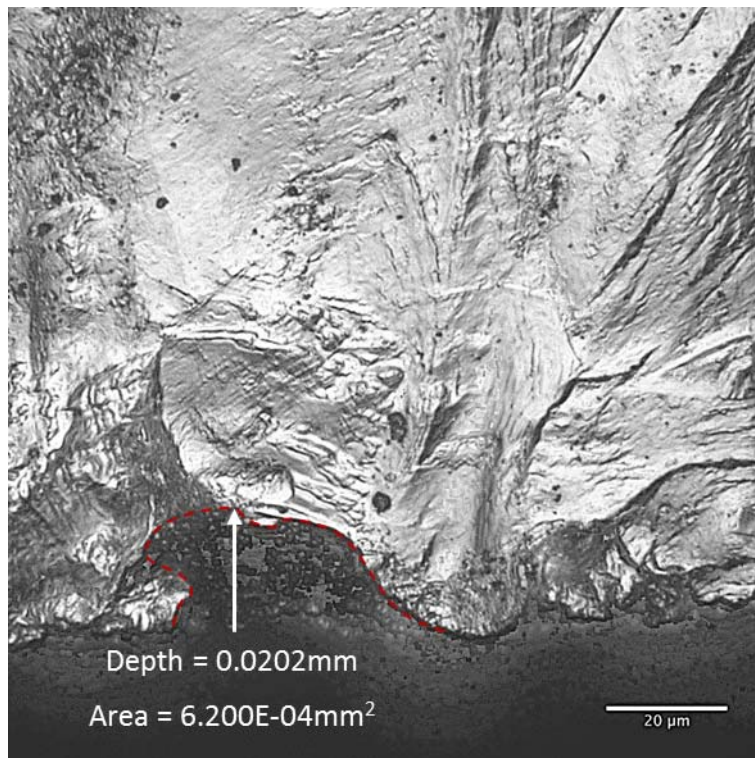
Figure C18: Initiating flaw of LM-188
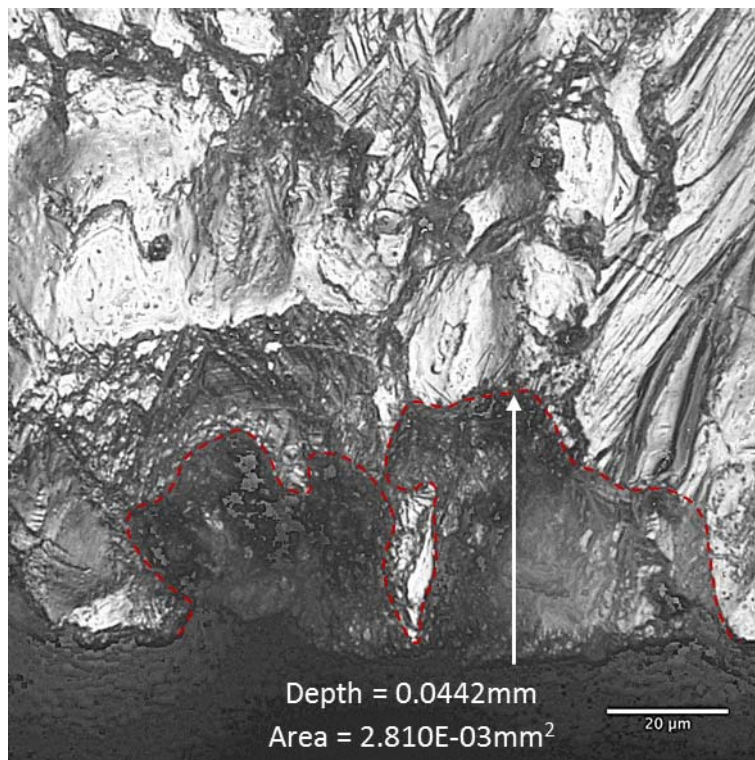
Figure C19: Initiating flaw of LM-214
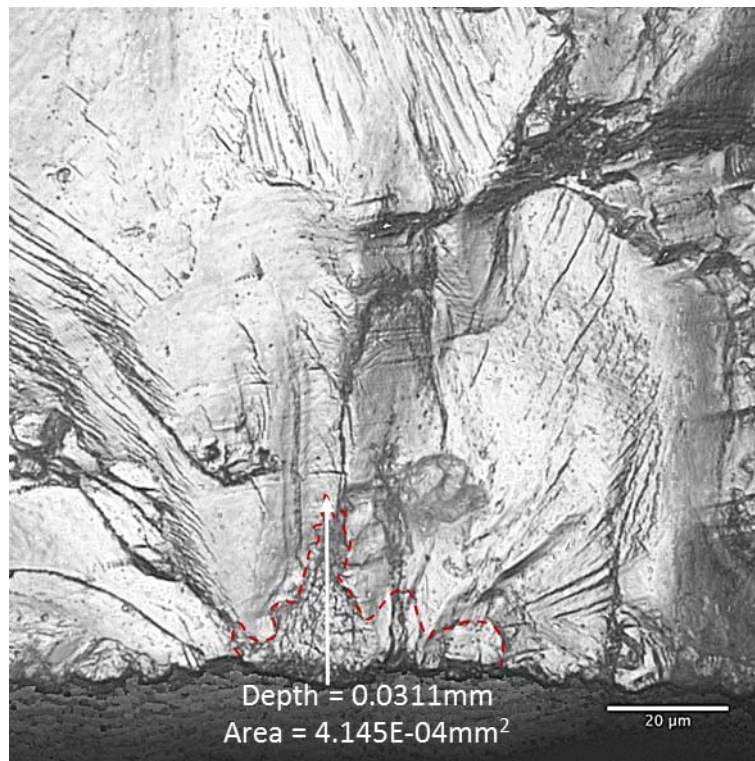
Figure C20: Initiating flaw of LM-223

C.5 High Kt Side-Notched – Anodised
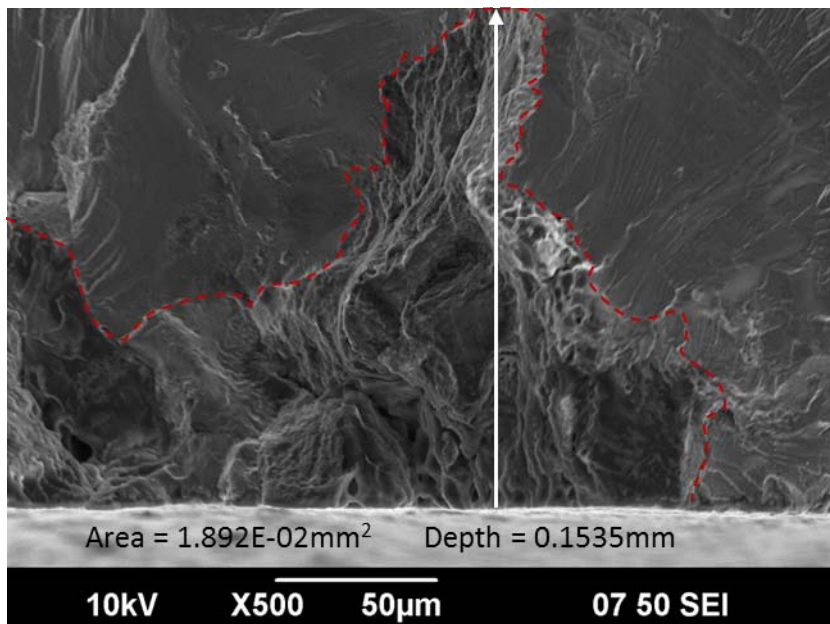
Figure C21: Initiating flaw of LM-87

Area = 2.470E-03mm²   Depth = 0.0594mm

10kV   X600   20µm   05 50 SEI
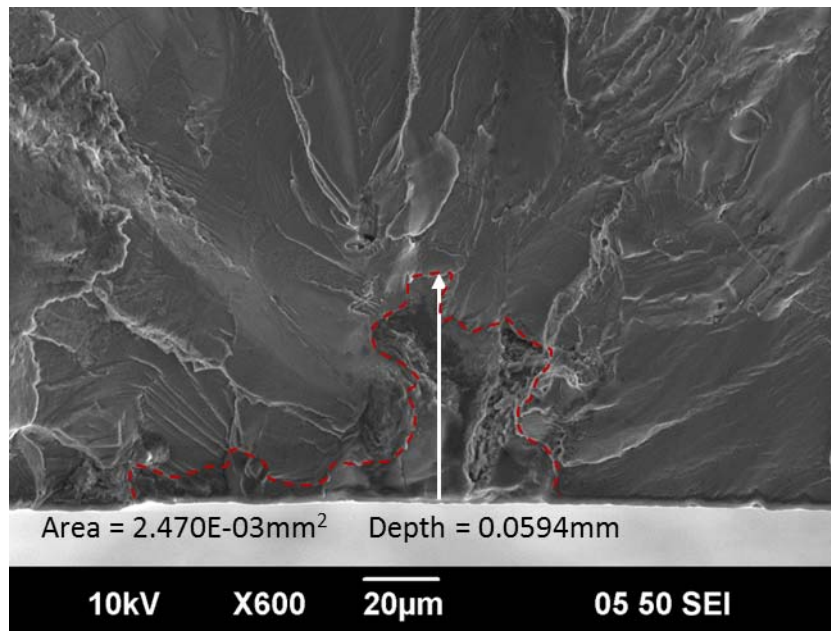
Figure C22: Initiating flaw of LM-102

Area = 3.700E-04mm²   Depth = 0.0322mm

10kV   X1,700   10µm   05 50 SEI
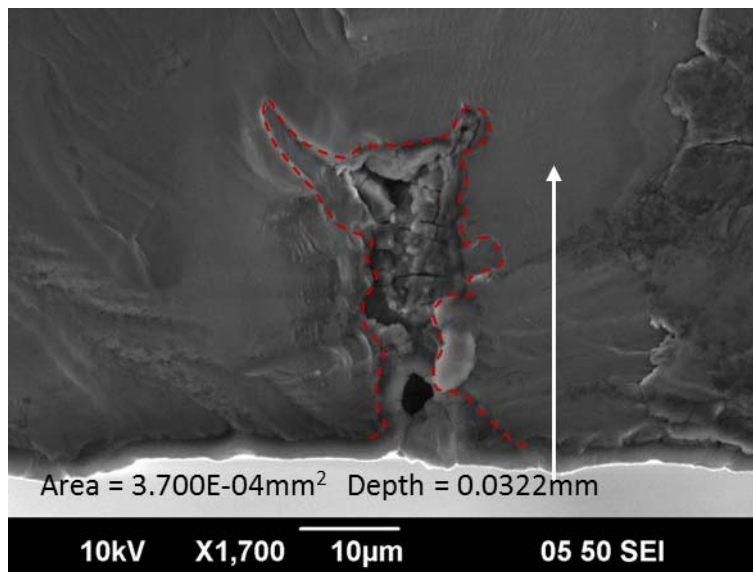
Figure C23: Initiating flaw of LM-136
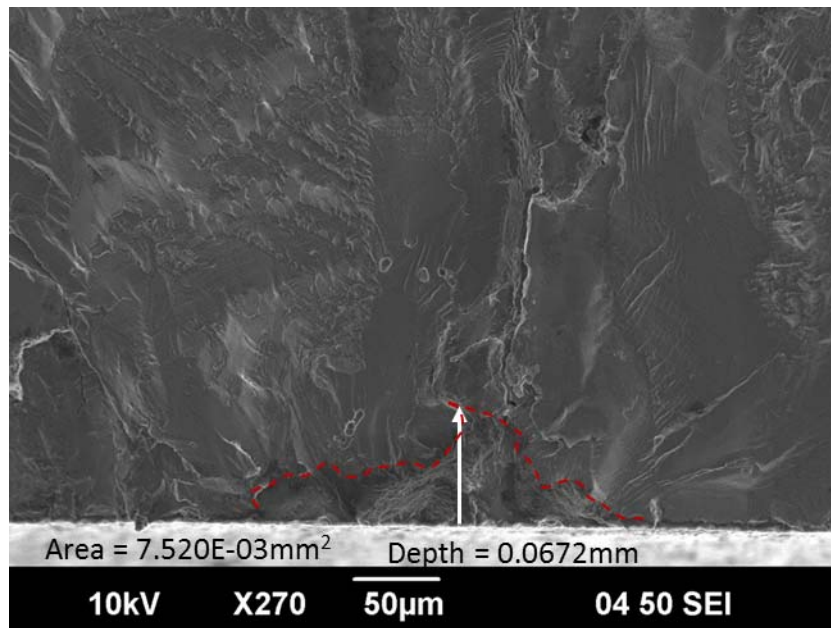
Figure C24: Initiating flaw of LM-149
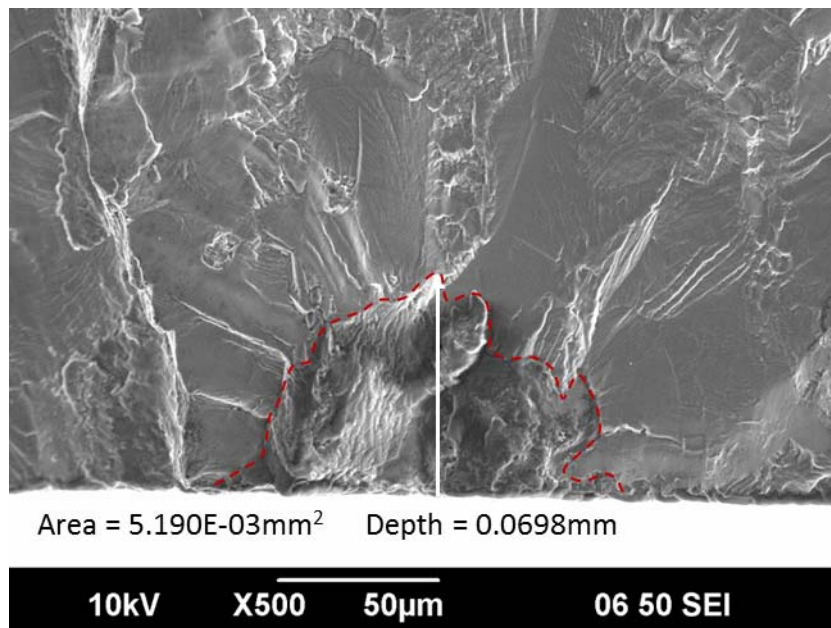
Figure C25: Initiating flaw of LM-175

C.6 Low Kt Dogbone – Machined (#400)
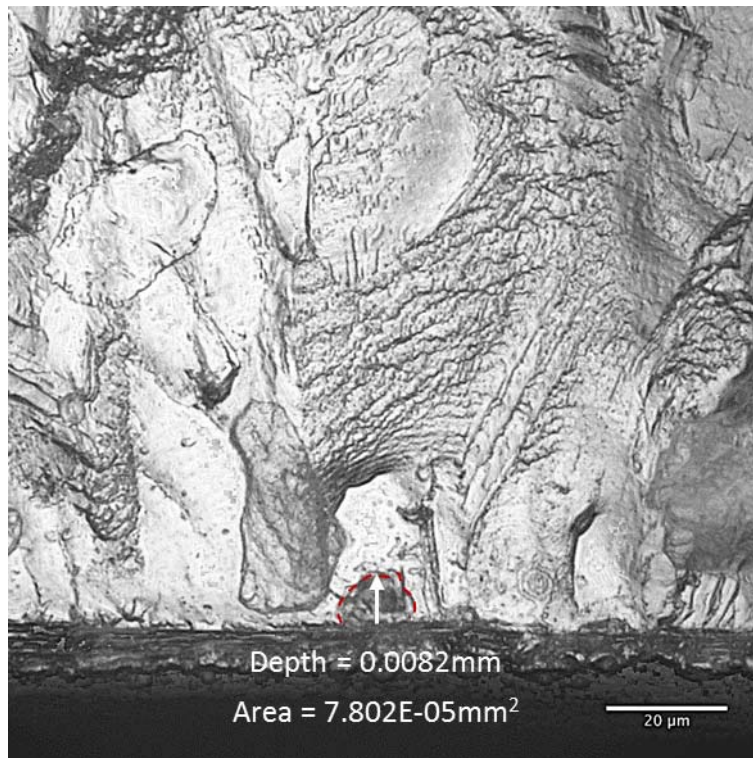
Figure C26: Initiating flaw of LM-244
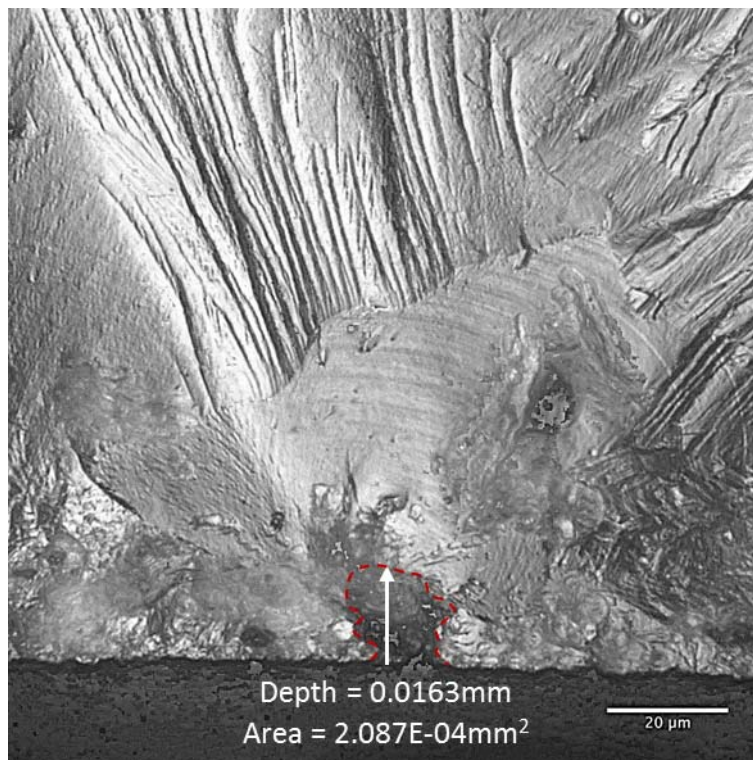
Figure C27: Initiating flaw of LM-344

Depth = 0.0262mm
Area = 1.785E-04mm^2
20 µm
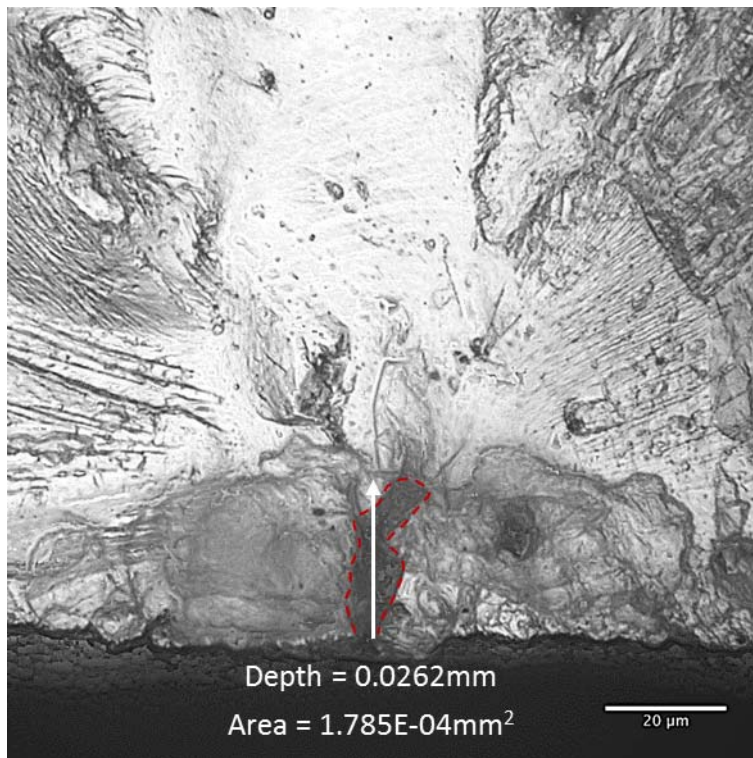
Figure C28: Initiating flaw of LM-371

Depth = 0.0086mm
Area = 3.014E-05mm^2
20 µm
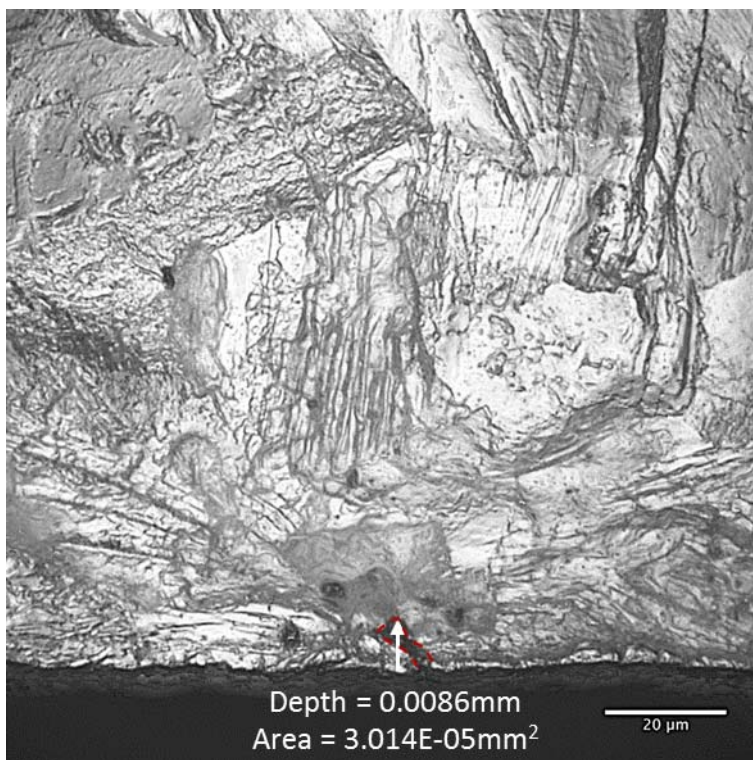
Figure C29: Initiating flaw of LM-398

C.7   Low Kt Dogbone – Machined (N6)

Depth = 0.0204mm
Area = 4.642E-04mm^2
20 µm
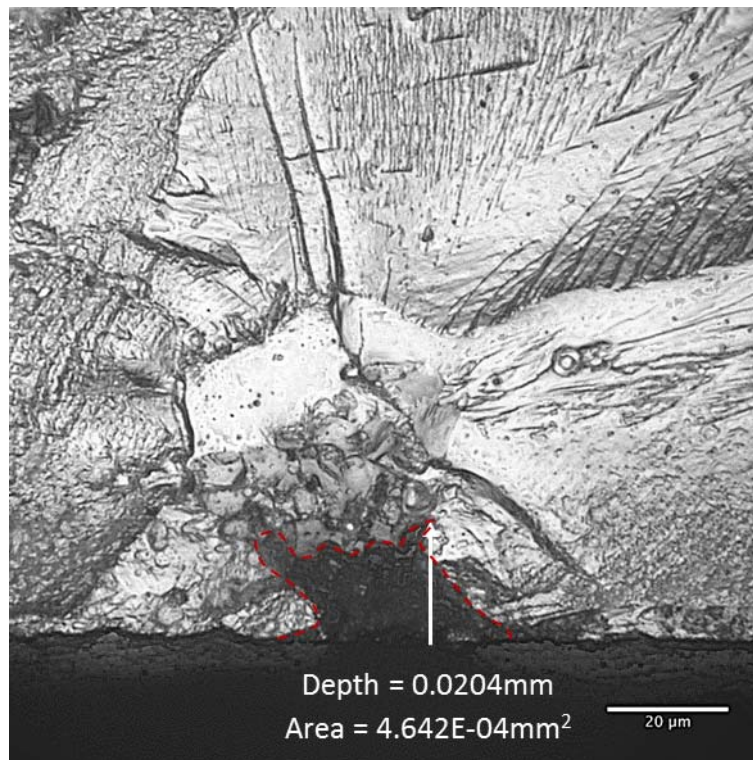
Figure C30: Initiating flaw of LMAA-01-L-T

Depth = 0.0707mm
Area = 1.525E-03mm^2
20 µm
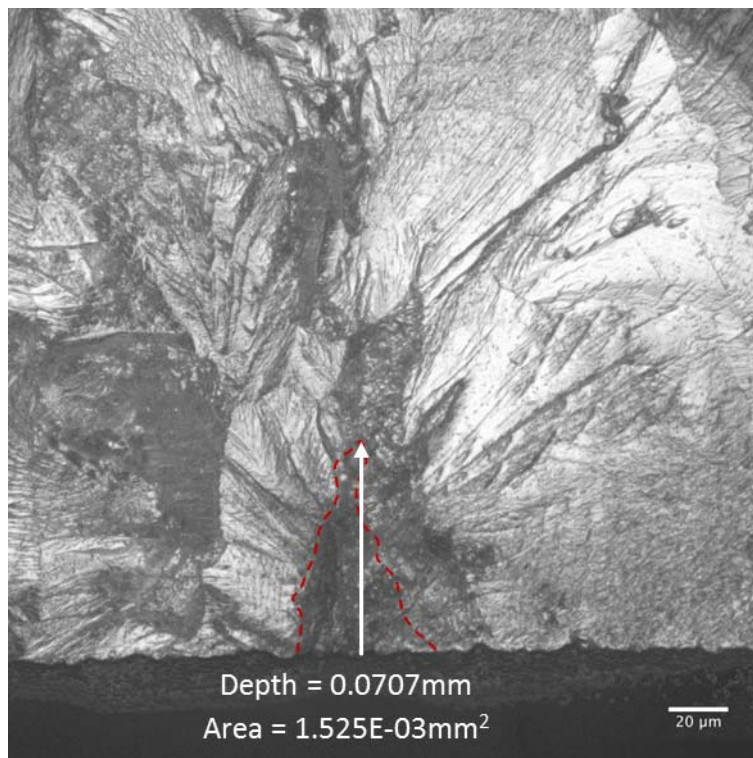
Figure C31: Initiating flaw of LMAA-03-L-T
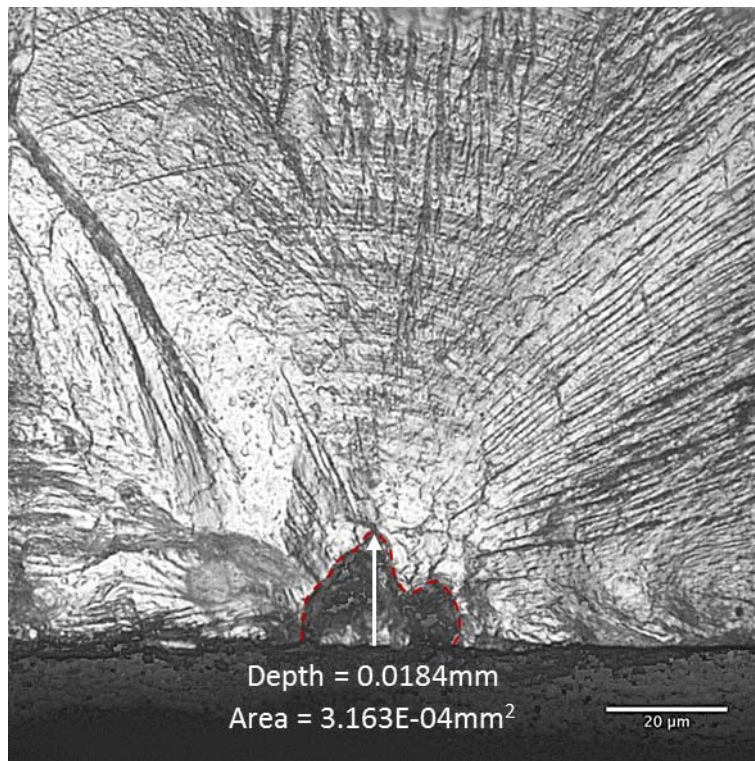
Figure C32: Initiating flaw of LMAA-06-L-T
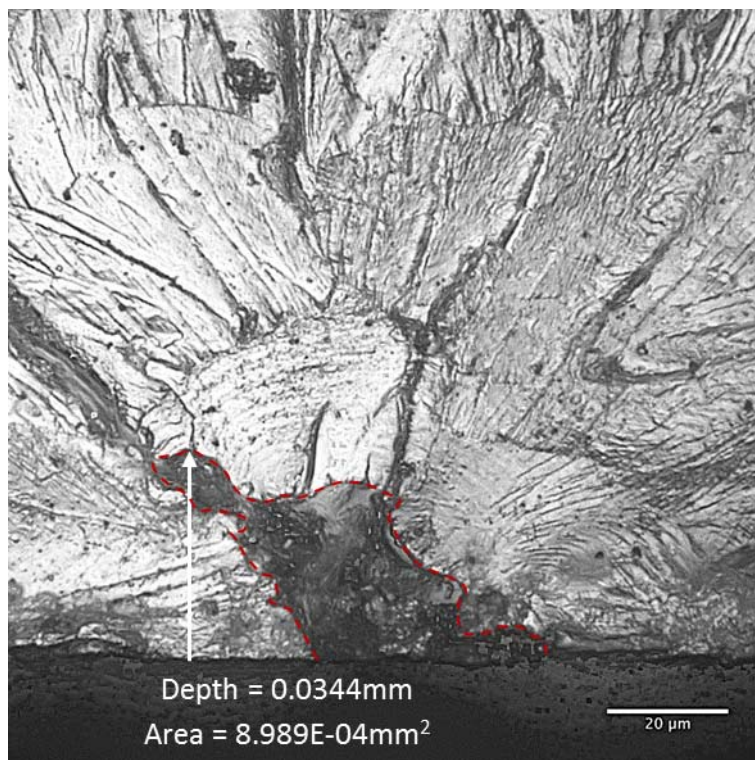
Figure C33: Initiating flaw of LMAA-10-L-T

C.8   Low Kt Dogbone – Pre-IVD Etched
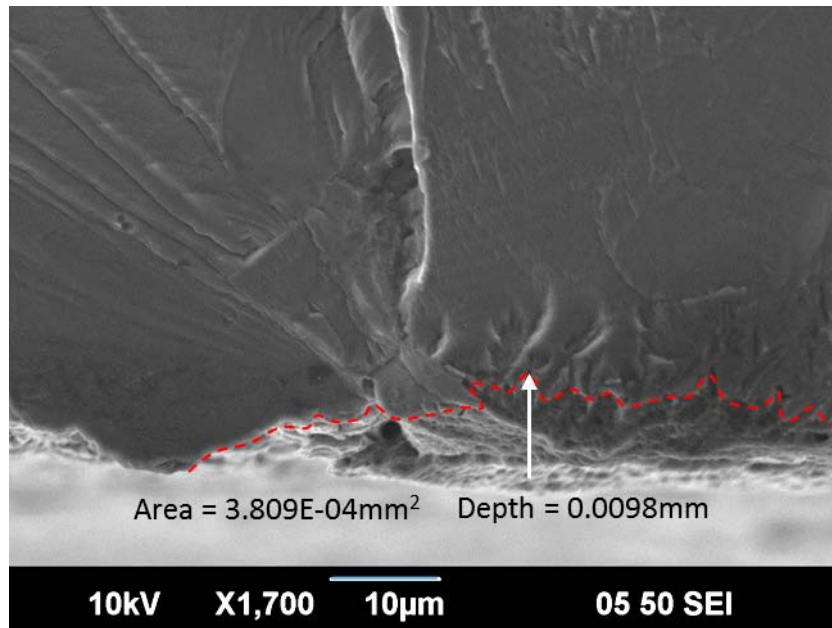
Figure C34: Initiating flaw of LM-309
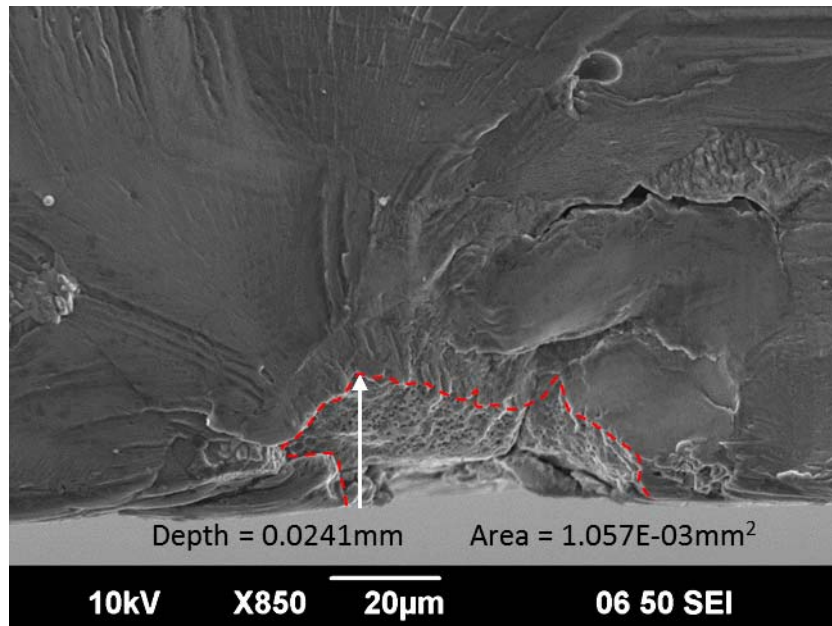
Figure C35: Initiating flaw of LM-329
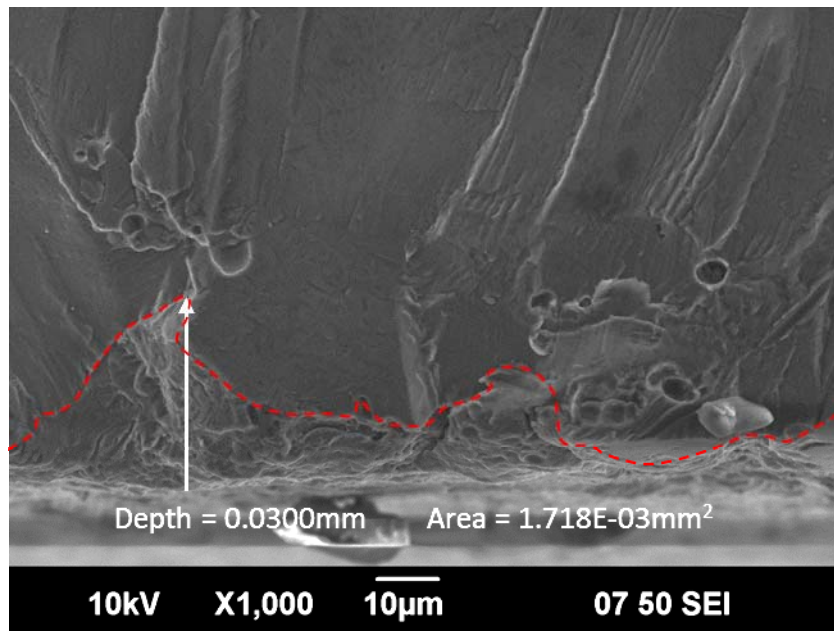
Figure C36: Initiating flaw of LM-364
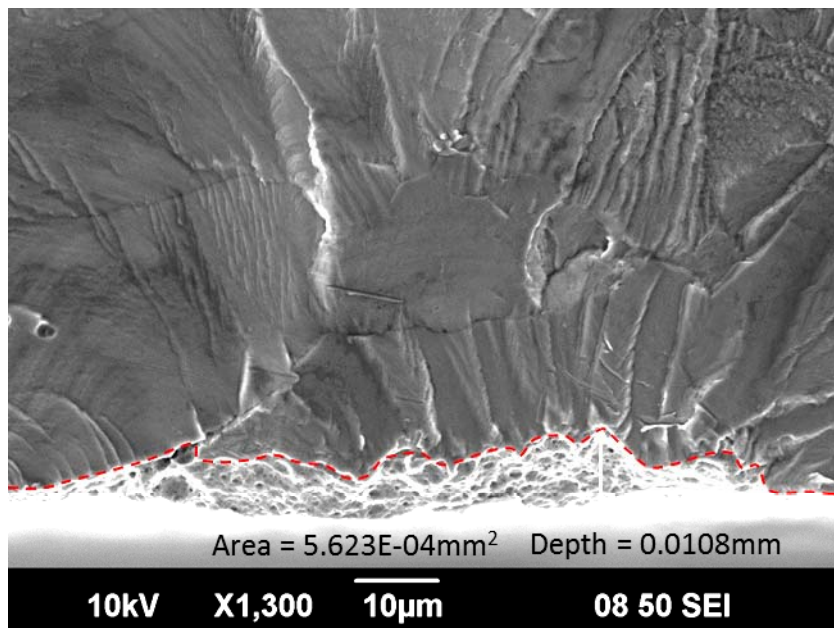
Figure C37: Initiating flaw of LM-372
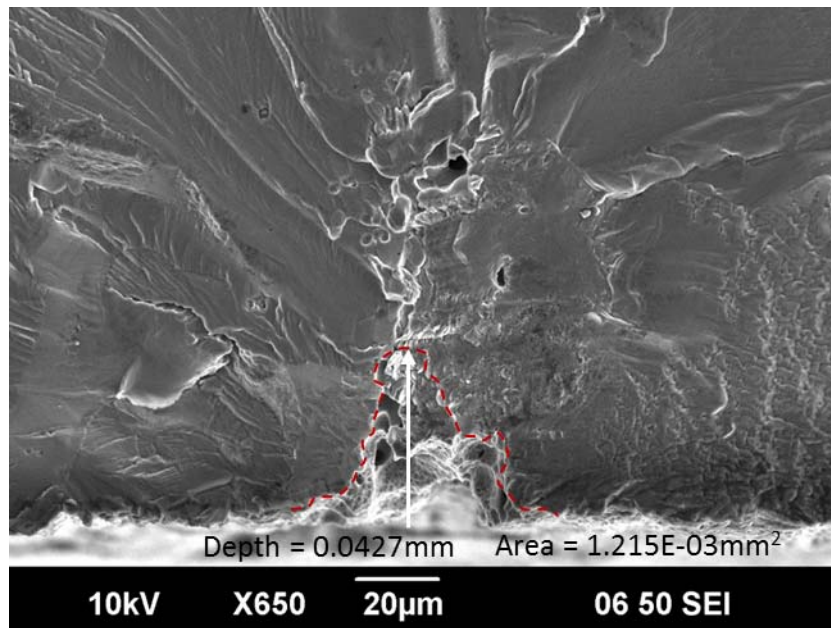
Figure C38: Initiating flaw of LM-440

C.9   Low Kt Dogbone – Anodised
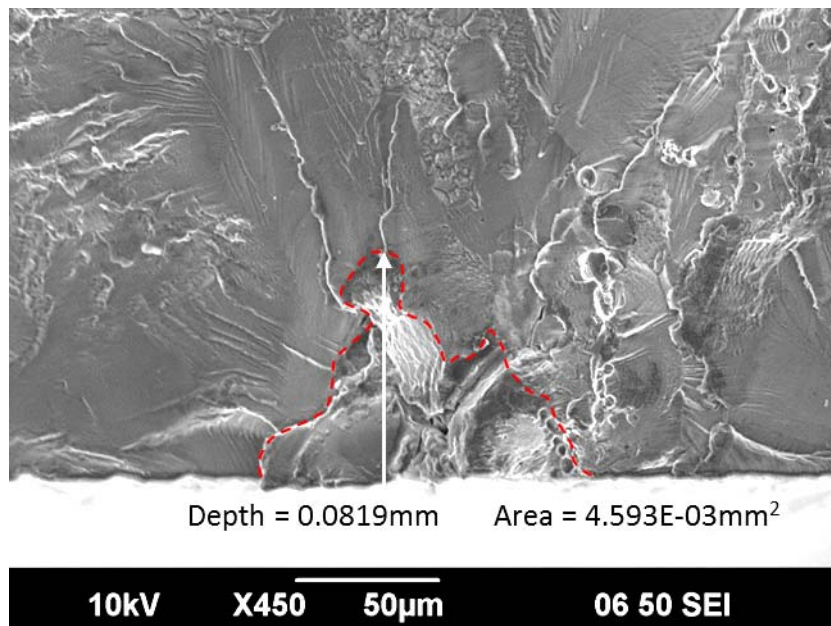
Figure C39: Initiating flaw of LM-233

Area = 6.814E-03mm² Depth = 0.0300mm

10kV   X550   20µm   05 50 SEI
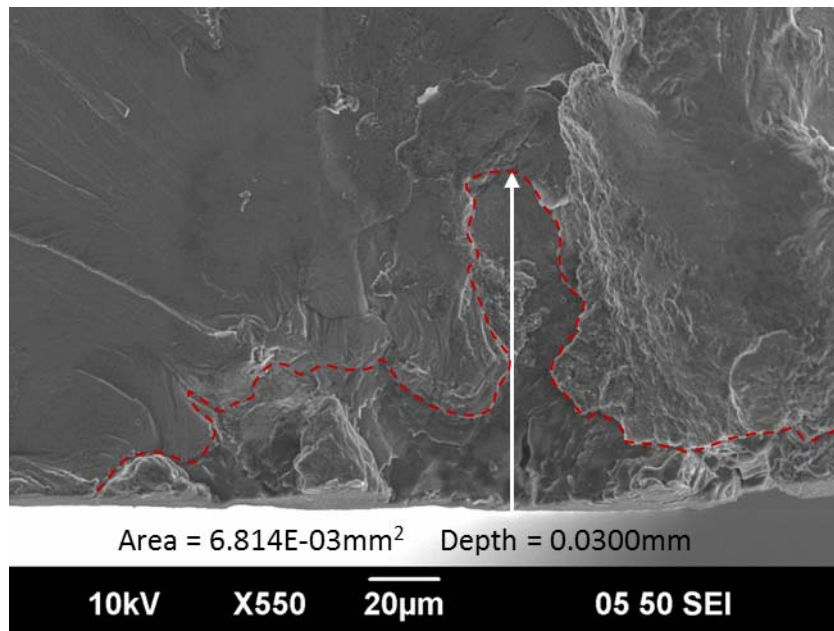
Figure C40: Initiating flaw of LM-301

Area = 9.954E-03mm²   Depth = 0.1091mm

10kV   X600   20µm   06 50 SEI
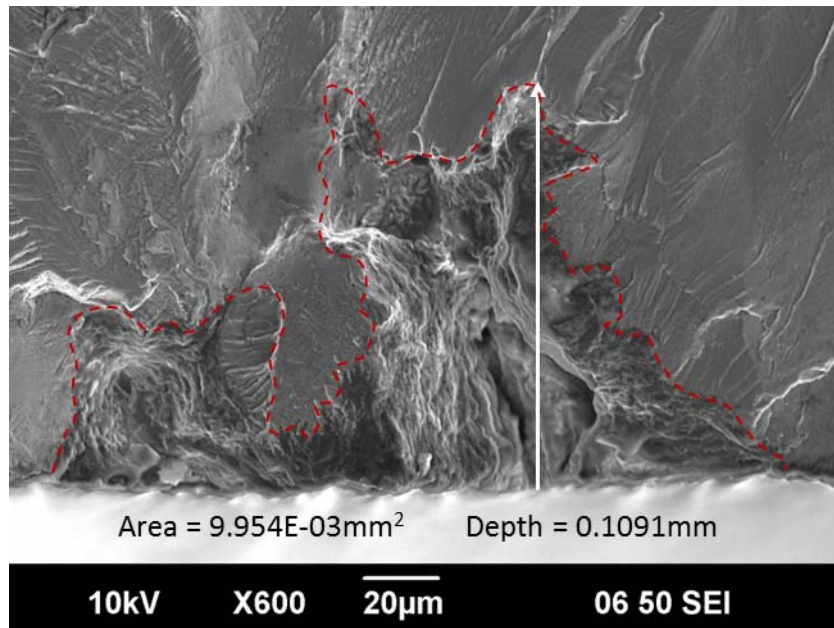
Figure C41: Initiating flaw of LM-303
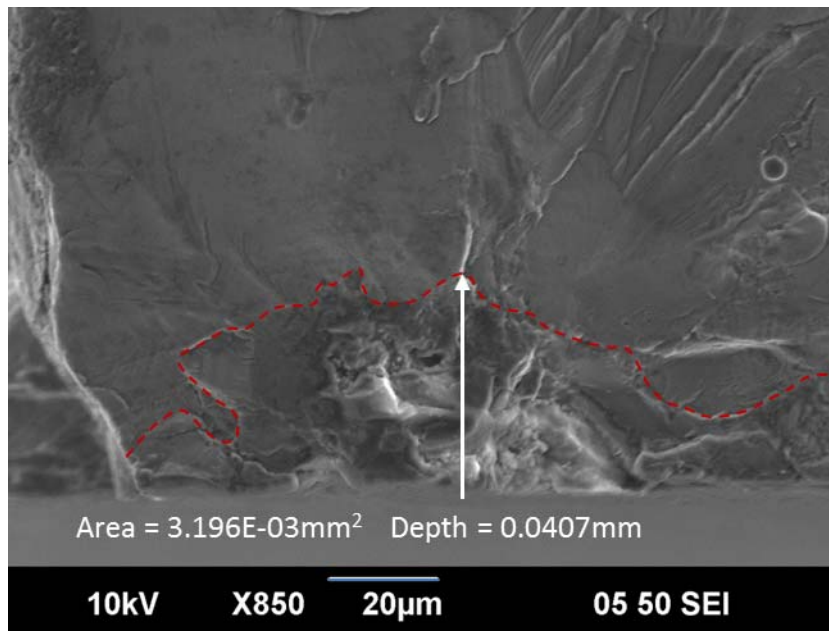
Figure C42: Initiating flaw of LM-317
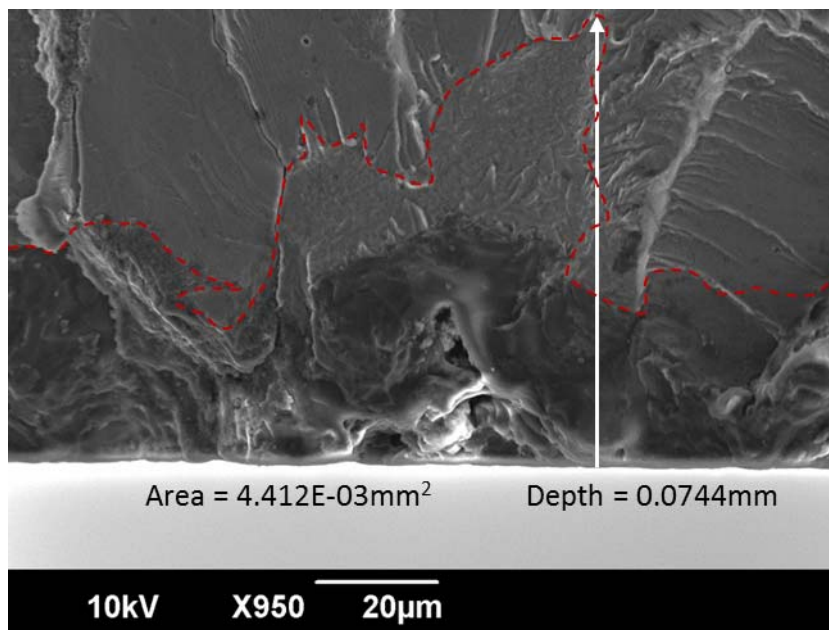
Figure C43: Initiating flaw of LM-418

Appendix D: Crack-Growth Curve Data

D.1   Crack-Growth Curve Data

D.1.1   High Kt Centre-Hole – Machined (N6)

Block Number	R (mm)				
	KF2B8	KK1H100	KK1H147	KK1H159	KK1H172
0	0.0003	0.0025	0.002	0.001	0.002
21					
22					
23					
24					0.0282
25					0.031
26					0.0371
27					0.0433
28			0.0619		0.0554
29			0.0677		0.0702
30			0.074		0.0864
31			0.0812		0.0992
32			0.0892	0.0176	0.1123
33	0.0085		0.0996	0.0193	0.1275
34	0.0102		0.1137	0.0215	0.144
35	0.0124	0.0192	0.1308	0.0233	0.1611
36	0.0145	0.0278	0.1508	0.0274	0.1817
37	0.0163	0.0335	0.1778	0.0304	0.2018
38	0.0186	0.0431	0.2209	0.0342	0.2255
39	0.0208	0.0534	0.2765	0.0384	0.2526
40	0.0233	0.0648	0.3551	0.045	0.282
41	0.0273	0.0715	0.4329	0.0512	0.3158
42	0.0312	0.0821	0.5141	0.0594	0.3567
43	0.0351	0.0959	0.6095	0.0715	0.3981
44	0.0385	0.1168	0.712	0.0859	0.4428
45	0.0429	0.1408	0.853	0.1014	0.5007
46	0.0468	0.1648	0.9648	0.1192	0.5767
47	0.0509	0.1896	1.0985	0.1336	0.6716
48	0.056	0.2129	1.2445	0.1599	0.788
49	0.0625	0.2421	1.4954	0.1861	0.8903
50	0.0685	0.2936	1.8823	0.2146	1.0418
51	0.0734	0.3425	2.4544	0.2508	1.1721
52	0.0837	0.3959	3.6012	0.2984	1.477
53	0.091	0.4792	5.1248	0.3535	1.9598
54	0.1047	0.6049		0.4321	2.6368
54.51			**8.0731**		
55	0.1175	0.7879		0.5539	3.5831

56	0.1334	0.9776		0.7188	4.7472
57	0.1598	1.2082		0.9123	6.6571
58	0.1807	1.7206		1.1315	
58.70					**11.6587**
59	0.2017	2.8798		1.4316	
60	0.2301			1.6317	
61	0.2757	6.0604		1.8058	
62	0.3193	8.7977		2.05	
63	0.3583			2.333	
63.48		**11.9162**			
64	0.3951			2.8215	
65	0.46			3.4538	
66	0.5512			4.2822	
67	0.6771			5.0553	
68	0.822				
69	1.0072				
70	1.3532				
70.09				**12.3416**	
71	1.7605				
72	2.3381				
73	2.8955				
74	3.5071				
75	4.5417				
76					
77					
77.73	**9.3813**				
78					

D.1.2 High Kt Side-notched – Machined (#400)

Block Number	R (mm)				
	LM-8	LM-62	LM-98	LM-135	LM-189
0	0.0142	0.0186	0.007	0.0154	0.0074
1			0.0283	0.0192	
2			0.0476	0.0242	
3	0.0171	0.0243	0.0675	0.0303	0.0196
4	0.0202	0.0314	0.0828	0.039	0.0282
5	0.0236	0.0382	0.1143	0.0497	0.0364
6	0.0282	0.0463	0.1459	0.0663	0.0489
7	0.0354	0.0578	0.1976	0.0852	0.0661
8	0.0425	0.0744	0.2625	0.1157	0.0878
9	0.0516	0.112	0.3679	0.1525	0.1215
10	0.0623	0.1559	0.5044	0.2098	0.1893
11	0.0912	0.2197	0.6948	0.2718	0.2745
12	0.1552	0.3056	0.9842	0.3597	0.4126
13	0.2344	0.4101	1.4493	0.5095	0.5459
14	0.3113	0.5772	1.9736	0.7551	0.7903
15	0.4513	0.899	2.9411	1.1436	1.0778
16	0.6695	1.4269		1.8805	1.5022
17	1.0744	2.294			2.1488
17.39			**14.1271**		
17.73				**8.1764**	
18	1.7525				2.9196
19	2.9313				
20	4.6219				
20.28		**11.9275**			
21.00					**12.262**
21					
21.68	**12.3238**				
22					

D.1.3   High Kt Side-notched – Machined (N6)

Block Number	R (mm)				
	LMAE-01-L-T	LMAE-03-L-T	LMAE-05-L-T	LMAE-07-L-T	LMAE-09-L-T
0	0.0026	0.0065	0.0092	0.0072	0.0083
1					
2					
3					
4		0.0293	0.0355	0.0453	
5		0.0349	0.0482	0.0544	0.0306
6		0.0398	0.0673	0.0695	0.04
7		0.0497	0.0889	0.089	0.0567
8		0.0643	0.1222	0.1169	0.0835
9		0.0826	0.1654	0.1618	0.1113
10		0.1082	0.2311	0.231	0.1605
11		0.1451	0.3057	0.3361	0.238
12		0.2105	0.4061	0.4805	0.33
13	0.0256	0.3147	0.5675	0.6697	0.4718
14	0.0355	0.4285	0.7678	0.8667	0.8539
15	0.0483	0.657	1.0269	1.1488	1.1489
16	0.0765	1.0807	1.3853	1.6303	1.521
17	0.117	1.7072	1.9937	2.5829	2.1074
18	0.1593	2.8121	2.8645	4.0268	3.0741
19	0.2267				
19.56				9.7781	
19.87		11.2869			
20	0.325				
20.51					11.8908
20.94			11.6429		
21	0.4655				
22	0.6163				
23	0.847				
24	1.1824				
25	1.7847				
26	2.9287				
27					
27.51	10.1394				
28					

D.1.4 High Kt Side-notched – Pre-IVD Etched

Block Number	R (mm)				
	LM-223	LM-214	LM-188	LM-151	LM-17
0	0.0125	0.012	0.0141	0.0047	0.0075
1		0.0279			0.024
2		0.0415	0.0332		0.0388
3		0.0599	0.0402	0.0134	0.0557
4		0.0736	0.0568	0.0288	0.0735
5	0.0373	0.1065	0.0805	0.0415	0.097
6	0.0568	0.1459	0.1137	0.0595	0.1336
7	0.0892	0.2004	0.1455	0.0856	0.1848
8	0.1496	0.2702	0.203	0.1367	0.2407
9	0.215	0.3514	0.2494	0.1943	0.3129
10	0.2837	0.4573	0.3414	0.3007	0.4112
11	0.4042	0.6134	0.4694	0.4481	0.5591
12	0.5941	0.9602	0.6373	0.6128	0.773
13	0.8338	1.4124	0.8886	0.9889	1.0026
14	1.3817		1.2436	1.5622	1.4397
15	2.8255		1.7115		
16					
16.56		12.5549			
16.73					10.4257
17					
17.12				10.5402	
18					
18.51	11.9982		10.1824		
19					

D.1.5 High Kt Side-notched – Anodised

Block Number	R (mm)				
	LM-87	LM-102	LM-136	LM-149	LM-175
0	0.0268	0.0455	0.0322	0.0322	0.0514
1				0.0541	0.0625
2		0.0538	0.0377	0.084	0.083
3		0.0785	0.0437	0.1205	0.1189
4	0.0844	0.1048	0.0504	0.1708	0.1661
5	0.1461	0.1381	0.0604	0.2319	0.2534
6	0.2479	0.1984	0.0721	0.321	0.3513
7	0.383	0.2804	0.0912	0.4653	0.5108
8	0.6191	0.4069	0.1238	0.6684	0.7514
9	0.9225	0.5871	0.1762	0.9151	1.0601
10	1.4729	0.9007	0.2746	1.3967	1.5634
11		1.4306	0.4681	1.9099	2.5032
12		2.5792	0.7277	2.4358	
12.81	**10.785**				
13		4.1994	1.066	3.9405	
13.28					**10.7811**
14			1.6747		
14.68		**10.0052**			
15			2.6717		
15.15				**13.0775**	
16			4.108		
17					
18					
19					
19.19			**14.8877**		
20					

D.1.6 Low Kt Dogbone – Machined (#400)

Block Number	R (mm)				
	LM-244	LM-344	LM-371	LM-398	LM-442
0	0.0009	0.002	0.001	0.0004	
48		0.0414			
49		0.0455			
50		0.0503	0.0518		
51		0.056	0.0538		
52		0.0631	0.0562		
53		0.0723	0.0583		
54		0.0823	0.0614		
55		0.0999	0.0638		
56		0.1092	0.067		
57		0.1201	0.0699		
58		0.1331	0.0741		
59		0.1456	0.0788		
60	0.0122	0.1628	0.083		
61	0.0128	0.1766	0.0899		
62	0.0134	0.1933	0.0966		
63	0.0145	0.2101	0.1022		
64	0.0153	0.2267	0.112		
65	0.0163	0.2456	0.1194		
66	0.0168	0.2739	0.1268		
67	0.0175	0.3138	0.1333		
68	0.018	0.3548	0.1502		
69	0.0187	0.3983	0.1598	0.02	
70	0.0191	0.4485	0.1706	0.0205	
71	0.0197	0.5044	0.1891	0.0214	
72	0.0205	0.619	0.2002		
73	0.0209	0.6903	0.2269		
74	0.0215	0.7849	0.2464		
75	0.0225	0.9274	0.2749		
76	0.0234	1.0385	0.3058		
77	0.0243	1.2015	0.3378		
78	0.0249	1.4805	0.3736		
79	0.0263	1.9665	0.4228		
80	0.0273	2.7544	0.4836		
81	0.0284		0.5584		
82	0.0298		0.646		
82.28		**6.3181**			
83	0.0308		0.7746		
84	0.0322		0.9235	0.0511	
85	0.034		1.0555	0.0569	
86	0.0356		1.2287	0.0623	
87	0.0371		1.4733	0.0691	

88	0.0391		1.7711	0.0766	
89	0.0416		2.1594	0.0868	
90	0.0443		2.6762	0.0992	
91	0.0459		3.3732	0.1125	
92	0.0487			0.124	
93	0.052			0.1402	
94	0.0562			0.155	
94.51			**9.1056**		
95	0.0616			0.1712	
96	0.0658			0.2013	
97	0.0711			0.2264	
98	0.0781			0.2531	
99	0.0855			0.2855	
100	0.093			0.3178	
101	0.1015			0.3514	
102	0.1108			0.3972	
103	0.1276			0.4604	
104	0.1414			0.5455	
105	0.1584			0.652	
106	0.1732			0.7427	
107	0.1822			0.9155	
108	0.1953			1.0685	
109	0.2098			1.2692	
110	0.2242			1.6117	
111	0.2409			1.9428	
112	0.2652			2.474	
113	0.2835			3.3286	
114	0.3126				
115	0.3517				
116	0.3895				
116.17				**7.9403**	
117	0.4335				
118	0.535				
119	0.6172				
120	0.6987				
121	0.7966				
122	0.927				
123	1.0748				
124	1.2527				
125	1.4956				
126	1.8438				
127	2.5023				
128	3.8075				
129					
130					
130.46	**8.6894**				
131					

D.1.7 Low Kt Dogbone – Machined (N6)

Block Number	R (mm)				
	LMAA-01-L-T	LMAA-03-L-T	LMAA-06-L-T	LMAA-08-L-T	LMAA-10-L-T
0	0.001	0.0093	0.0049		0.0062
7		0.0293			
8		0.0313			
9		0.0319			0.0347
10		0.0352			0.0367
11		0.0371			0.0381
12		0.0388			0.0405
13		0.0411			0.0424
14		0.0424			0.0457
15		0.0455			0.0477
16		0.0498			0.0518
17		0.053			0.0557
18		0.0619			0.0607
19		0.0707	0.0306		0.0678
20		0.0782	0.0372		0.0761
21		0.0823	0.0437		0.0908
22		0.093	0.0498		0.1175
23		0.0978	0.0556		0.1355
24		0.1027	0.0632		0.1522
25		0.1097	0.0723		0.1673
26		0.1177	0.0838		0.1824
27		0.1277	0.0964		0.2005
28		0.1382	0.1124		0.2231
29		0.15	0.132		0.2428
30		0.1623	0.1599		0.2757
31		0.177	0.2027		0.3131
32		0.1951	0.2435		0.354
33		0.2131	0.2928		0.4231
34		0.236	0.3601		0.5006
35		0.2612	0.4437		0.5885
36	0.036	0.2812	0.567		0.673
37	0.0436	0.3024	0.7284		0.7821
38	0.0566	0.3304	0.9115		0.8917
39	0.0678	0.3645	1.1521		1.0386
40	0.0762	0.4088	1.4609		1.2518
41	0.0885	0.4543	1.8977		1.4362
42	0.108	0.5034			1.744
43	0.122	0.5622			2.0379
44	0.1348	0.6584			2.3998
44.73			**6.3706**		
45	0.1477	0.7564			
46	0.1625	0.8621			

(LMAA-08-L-T: Failed in grips)

47	0.179	1.0475			
47.92					**7.4792**
48	0.1955	1.2146			
49	0.2104	1.4584			
50	0.2318	1.8404			
51	0.2639				
52	0.3075				
52.73		**6.0468**			
53	0.3484				
54	0.3827				
55	0.4294				
56	0.4869				
57	0.5653				
58	0.6362				
59	0.7368				
60	0.8917				
61	1.1214				
62	1.406				
63	1.7047				
64	2.1715				
65	2.7363				
66	3.4115				
67					
68					
68.18	**8.4071**				

D.1.8   Low Kt Dogbone – Pre-IVD Etched

Block Number	R (mm)				
	LM-309	LM-329	LM-364	LM-372	LM-440
0	0.0051	0.0065	0.0087	0.0058	0.0094
3				0.0208	
4				0.025	
5		0.0192		0.029	
6		0.0214		0.0341	
7	0.0422	0.0243	0.0148	0.0399	
8	0.0549	0.0281	0.0195	0.0445	0.0433
9	0.0677	0.0321	0.0267	0.0509	0.0469
10	0.0803	0.0376	0.0361	0.0564	0.0515
11	0.0948	0.0452	0.0496	0.0639	0.0558
12	0.1163	0.0558	0.0712	0.0718	0.0617
13	0.1348	0.0669	0.1002	0.0813	0.0668
14	0.1461	0.0801	0.1256	0.0929	0.0732
15	0.1641	0.0952	0.1495	0.1059	0.0806
16	0.1787	0.1104	0.1796	0.1229	0.0894
17	0.2061	0.1273	0.2085	0.1381	0.0986
18	0.2293	0.1467	0.2523	0.1563	0.1104
19	0.2687	0.1688	0.3278	0.1733	0.124
20	0.3066	0.1959	0.4196	0.1957	0.1394
21	0.3614	0.2237	0.5279	0.2234	0.1578
22	0.4244	0.2587	0.6333	0.2506	0.1807
23	0.4799	0.3035	0.7642	0.2787	0.2149
24	0.5647	0.3648	0.9065	0.3184	0.2636
25	0.6611	0.4111	1.1009	0.3586	0.3167
26	0.7502	0.4877	1.2575	0.4082	0.3777
27	0.8814	0.5612	1.5797	0.4664	0.4511
28	1.0274	0.7035	1.851	0.523	0.5887
29	1.18	0.827	2.3961	0.5916	0.7123
30	1.3782	0.9774		0.6753	0.9054
31	1.6818	1.256		0.8108	1.1675
31.72			**5.9821**		
32	2.0897	1.5984		0.9997	1.5825
33	2.6959	2.2057		1.2144	2.1895
34	3.4977			1.4857	2.9867
35	4.598				3.952
36					
36.2		**6.8711**			
36.99	**8.2621**				
37					
37.14					**8.2935**
38					
38.25				**4.3963**	

D.1.9 Low Kt Dogbone – Anodised

Block Number	R (mm)				
	LM-233	LM-301	LM-303	LM-317	LM-418
0	0.0553	0.0422	0.0557	0.0506	0.0258
1					
2					
3	0.0613				0.0354
4	0.0646				0.047
5	0.0683				0.0581
6	0.0729		0.0866		0.0678
7	0.0777	0.0625	0.0935		0.0803
8	0.0825	0.0691	0.102		0.0958
9	0.0884	0.0794	0.1121		0.1174
10	0.0963	0.0936	0.1253		0.1466
11	0.1048	0.1145	0.1429		0.1808
12	0.1167	0.1412	0.1671	0.0595	0.224
13	0.1323	0.1769	0.199	0.0638	0.271
14	0.1559	0.215	0.2472	0.069	0.3312
15	0.1779	0.2693	0.3091	0.0742	0.421
16	0.207	0.3324	0.4102	0.0834	0.5497
17	0.2295	0.3815	0.5766	0.0937	0.663
18	0.2619	0.5361	0.6844	0.1116	0.7949
19	0.2945	0.765	0.8183	0.1299	0.9394
20	0.333	0.8606	0.9908	0.1577	1.224
21	0.3854	1.0107	1.2175	0.2016	1.4726
22	0.4436	1.2281	1.4356	0.2567	1.7197
23	0.5084	1.5484	1.7498	0.3149	2.2359
24	0.5707	1.8492	2.2357	0.3964	
24.73					**5.9642**
25	0.6537	2.2738		0.4918	
26	0.7446	2.8088		0.6353	
26.26			**7.5959**		
27	0.813			0.8045	
28	0.9618			1.046	
28.10		**7.5413**			
29	1.1341			1.265	
30	1.2714			1.6361	
31	1.5932			2.322	
32	2.1828				
32.51				**6.4512**	
33	3.0864				
34					
35					
35.64	**7.2698**				
36					

Appendix E: Coupon Photographs

E.1 Crack Surface Photographs

E.1.1 High Kt Centre-Hole – Machined (N6)
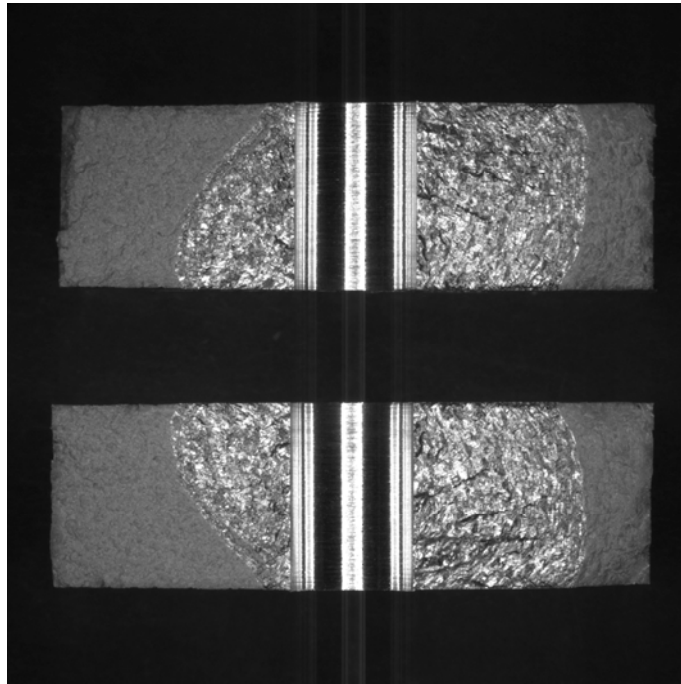
Figure E1: KF2B8
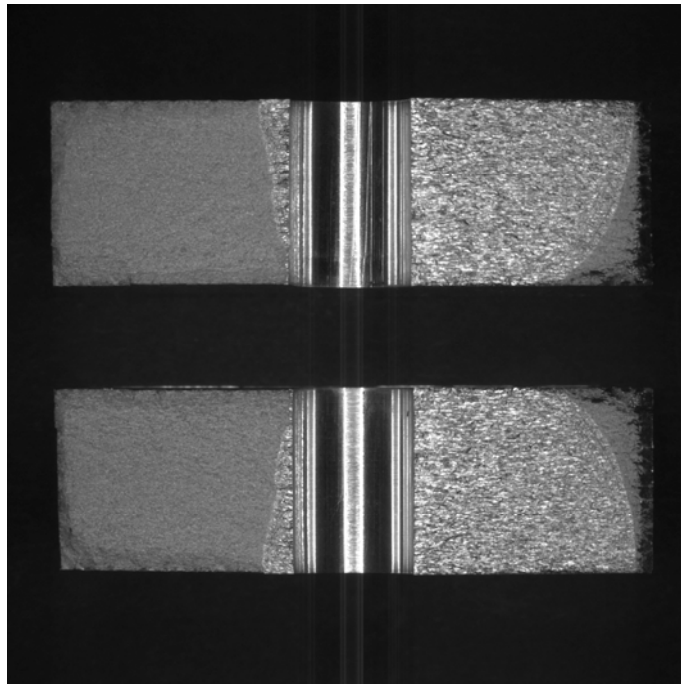
Figure E2: KK1H100
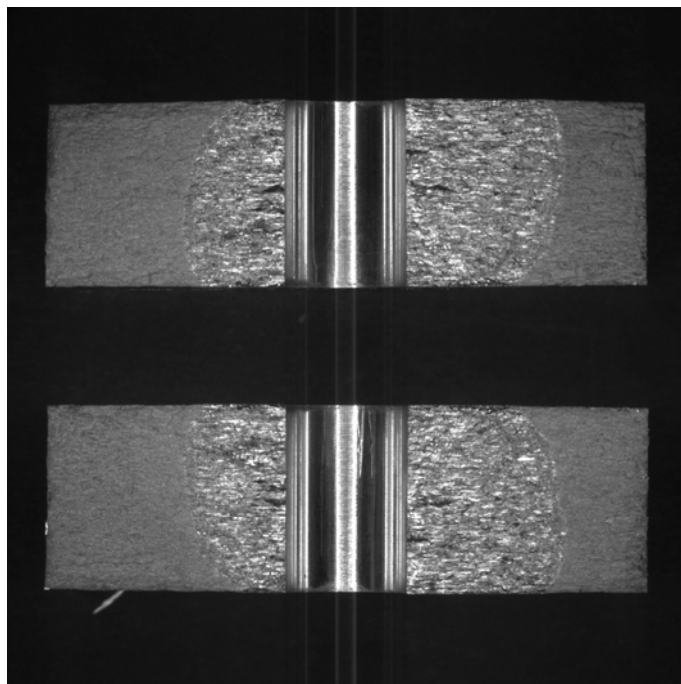
Figure E3: KK1H147
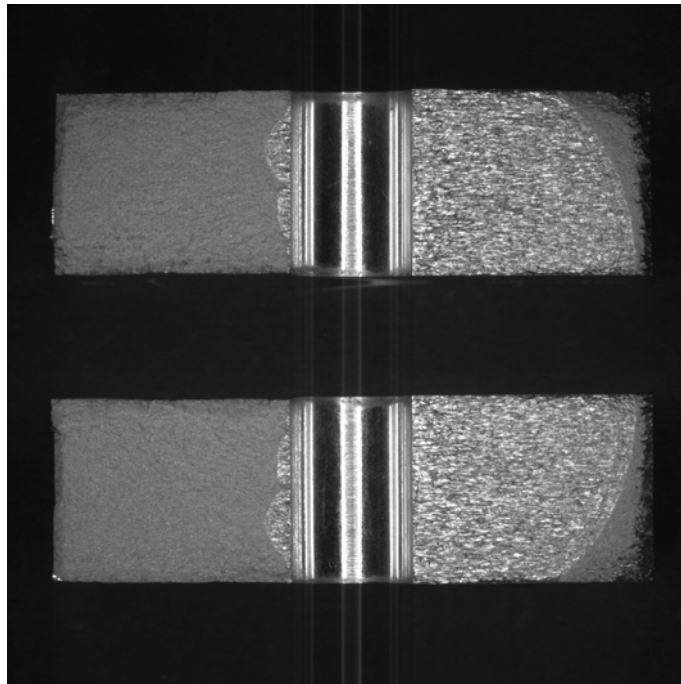
Figure E4: KK1H159
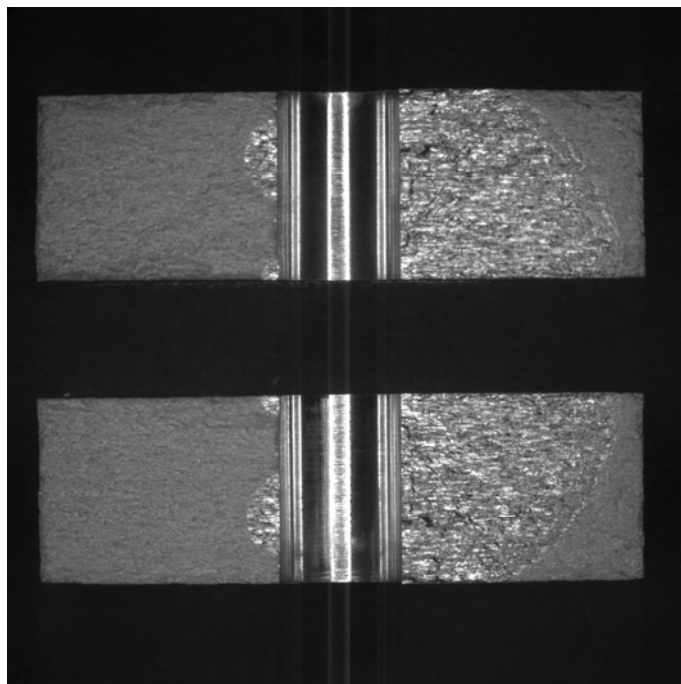
Figure E5: KK1H172

E.1.2 High Kt Side-notched – Machined (#400)
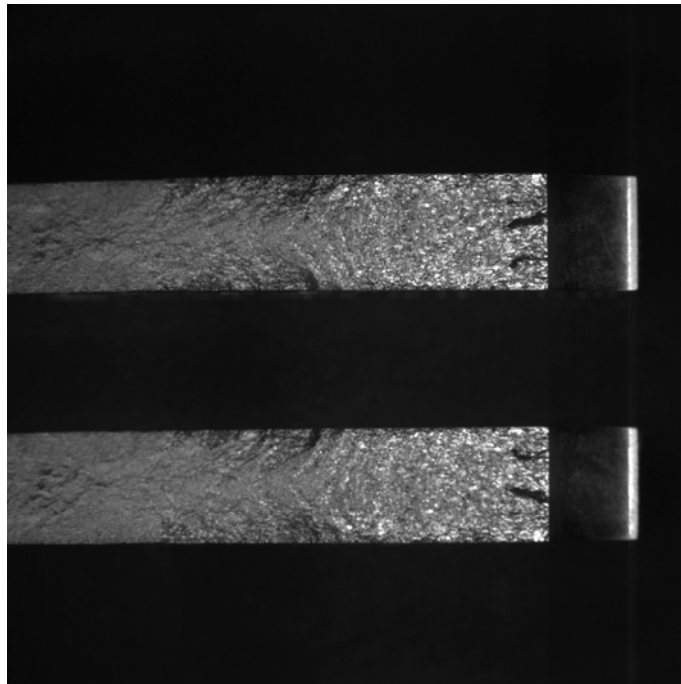
Figure E6: LM-8
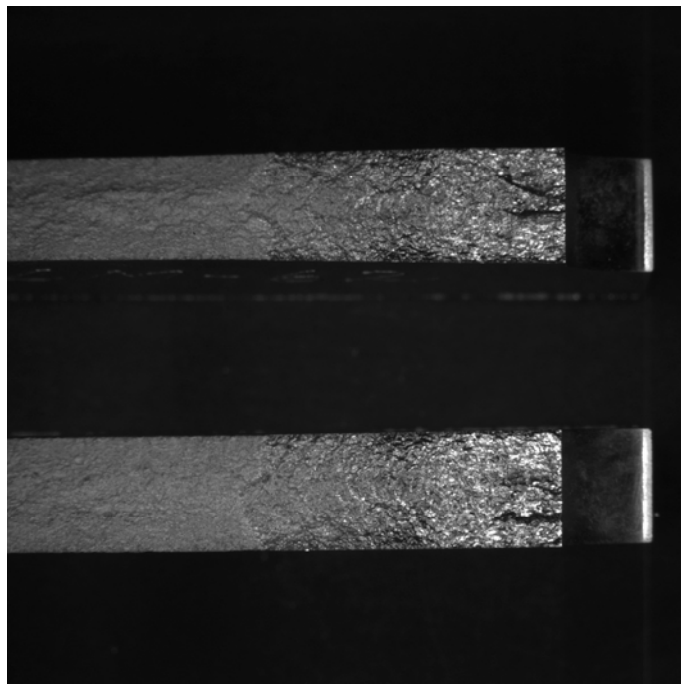
Figure E7: LM-62
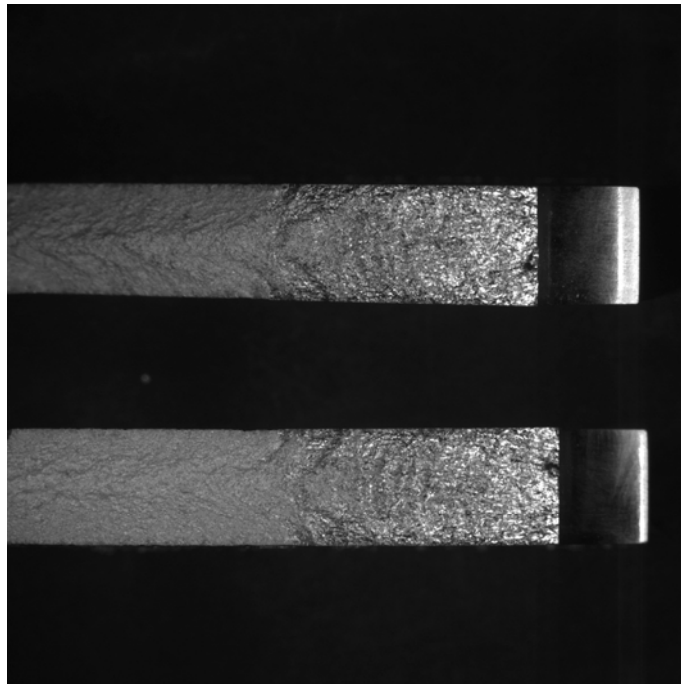
Figure E8: LM-98
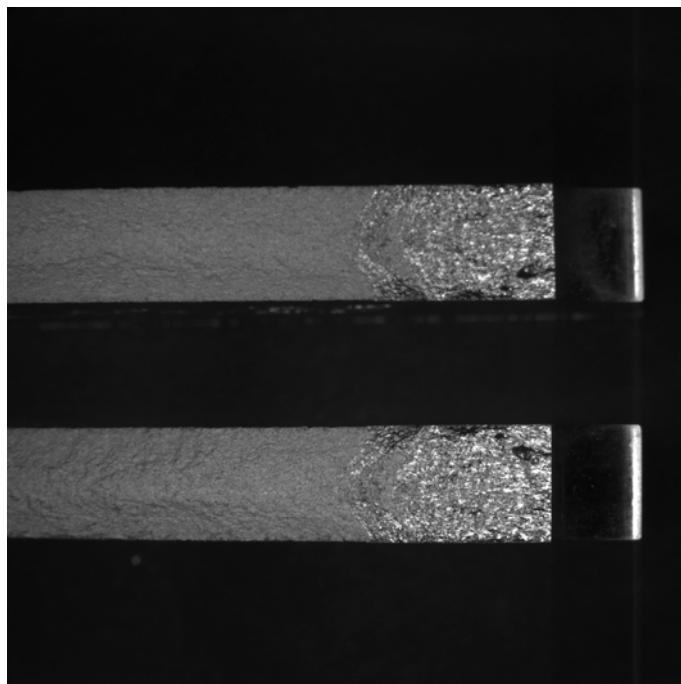
Figure E9: LM-135
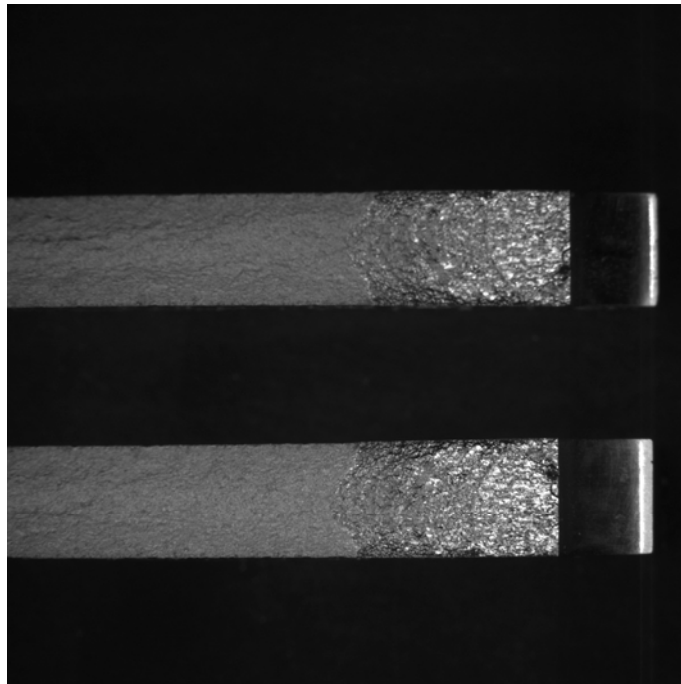
Figure E10: LM-189

E.1.3 High Kt Side-notched – Machined (N6)
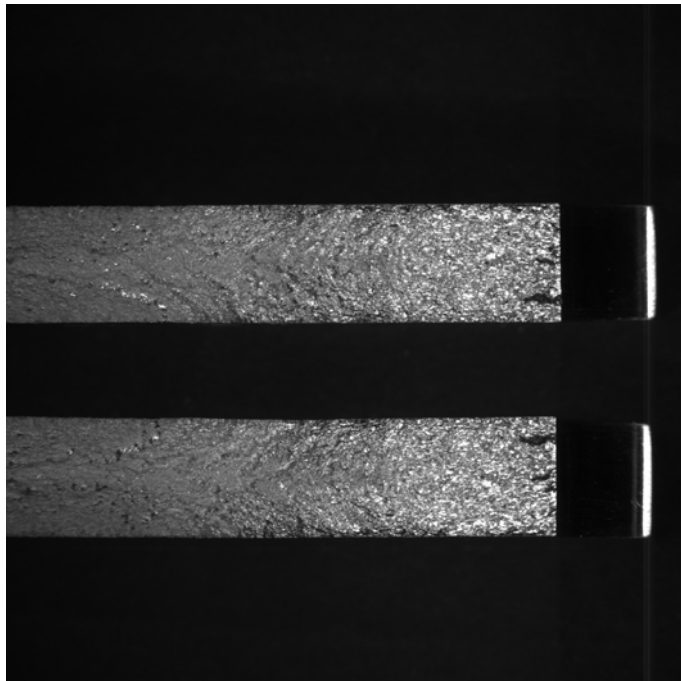
Figure E11: LMAE-01-L-T
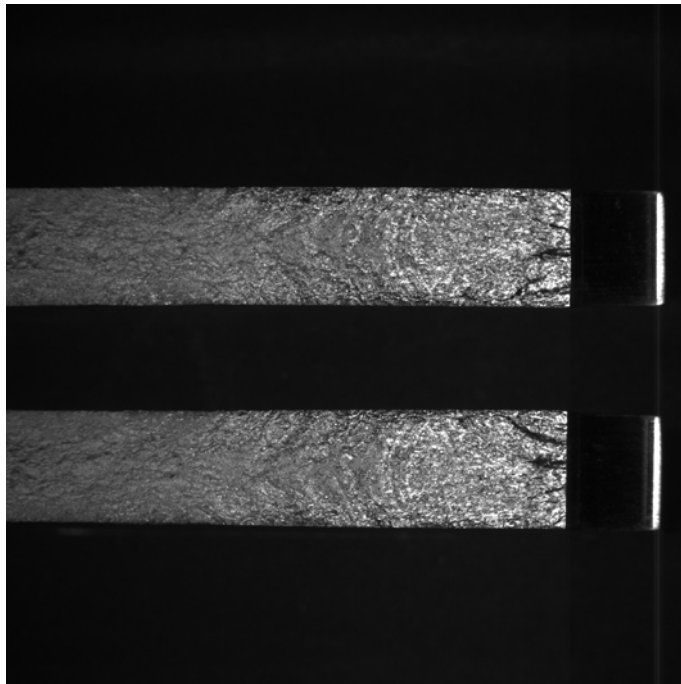
Figure E12: LMAE-03-L-T
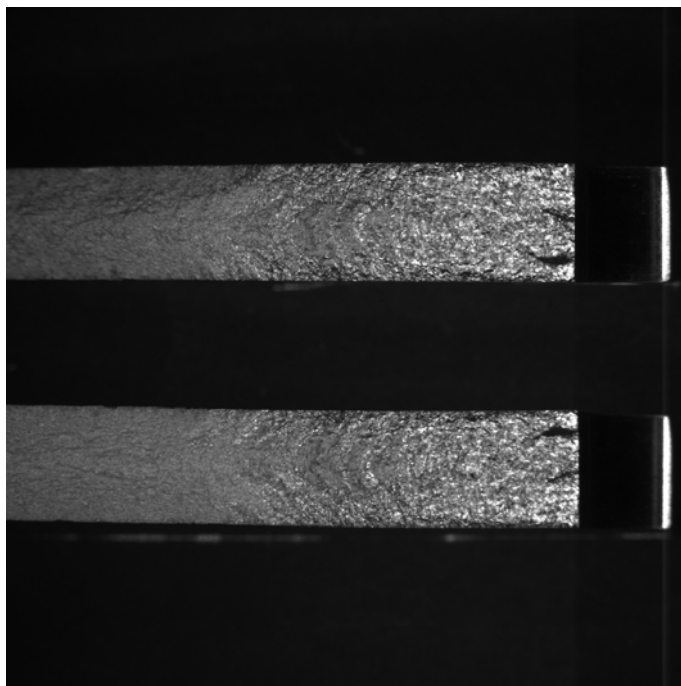
Figure E13: LMAE-05-L-T
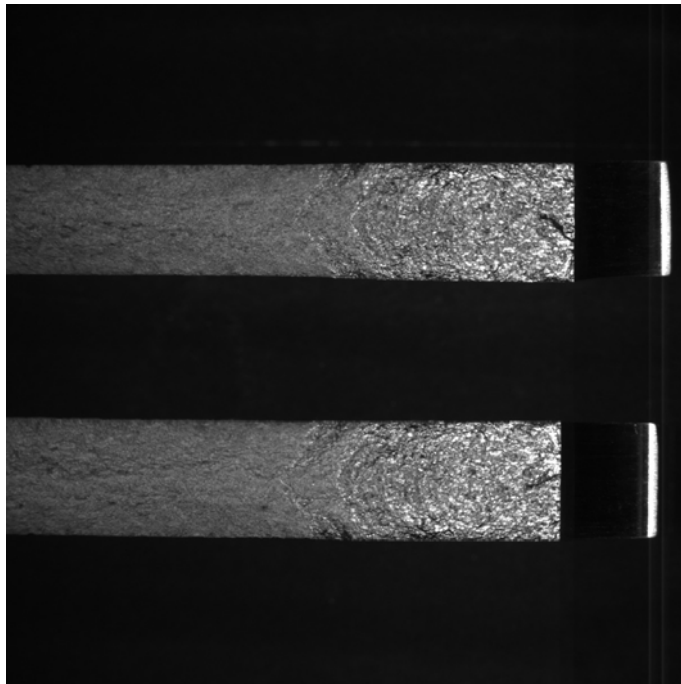
Figure E14: LMAE-07-L-T
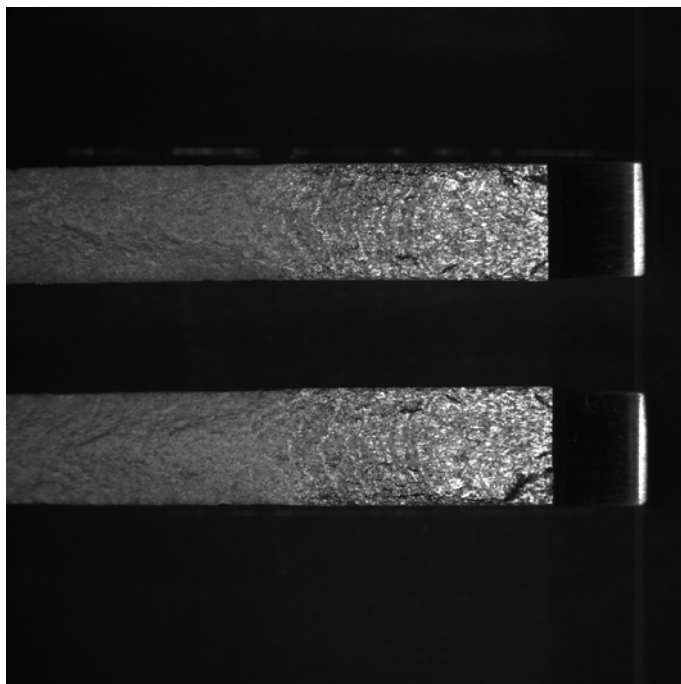
Figure E15: LMAE-09-L-T

E.1.4   High Kt Side-notched – Pre-IVD Etched
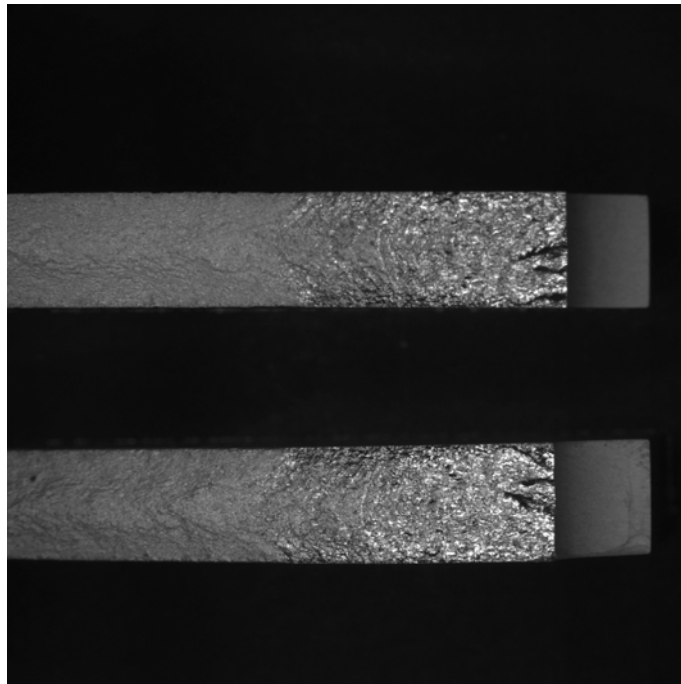
Figure E16: LM-17
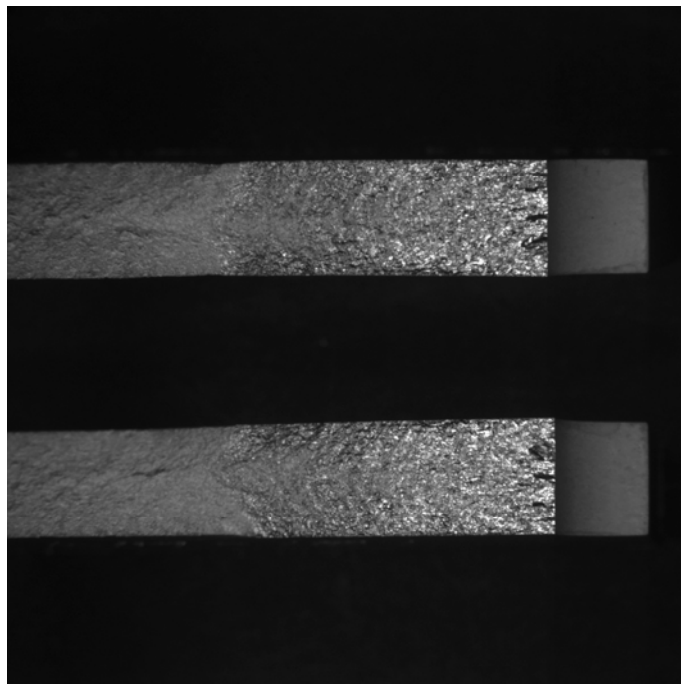
Figure E17: LM-151
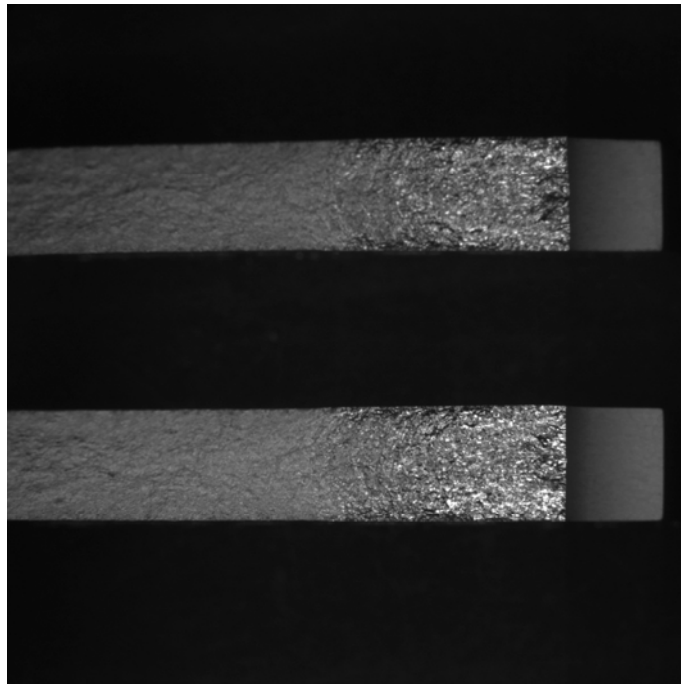
Figure E18: LM-188
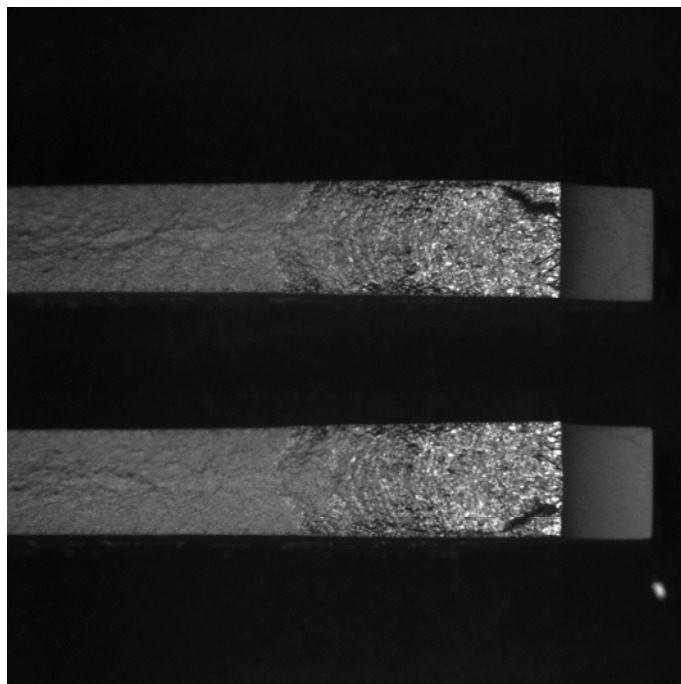
Figure E19: LM-214
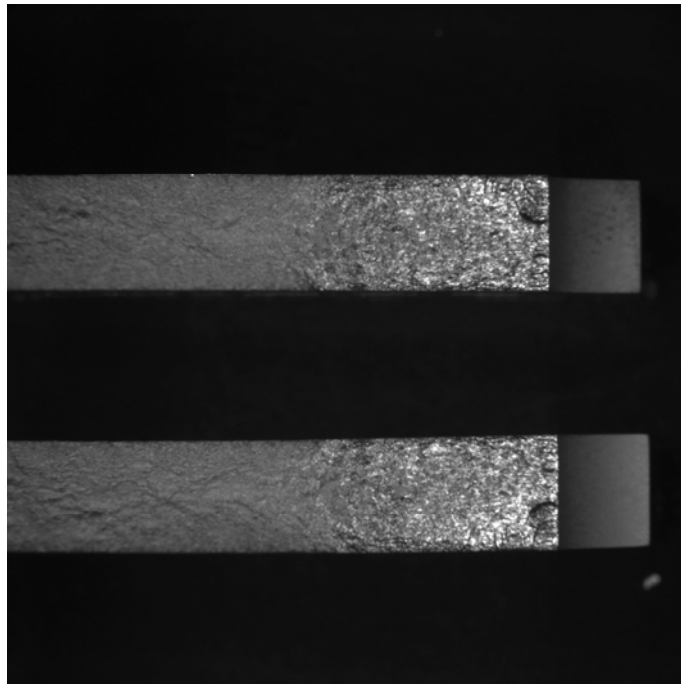
Figure E20: LM-223

E.1.5   High Kt Side-notched - Anodised
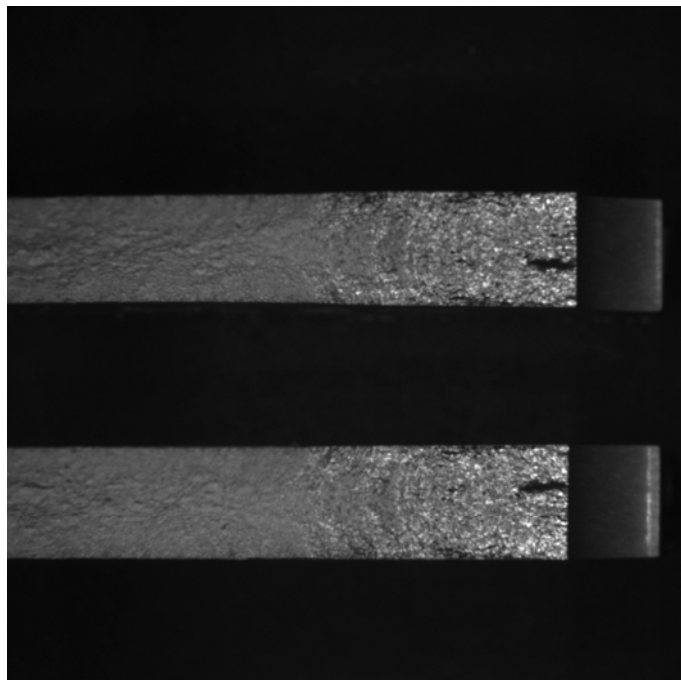
Figure E21: LM-87
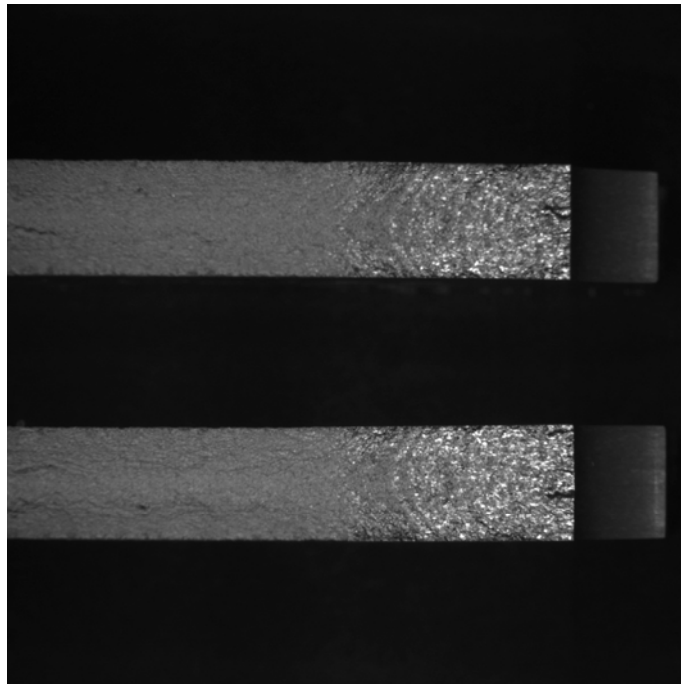
Figure E22: LM-102
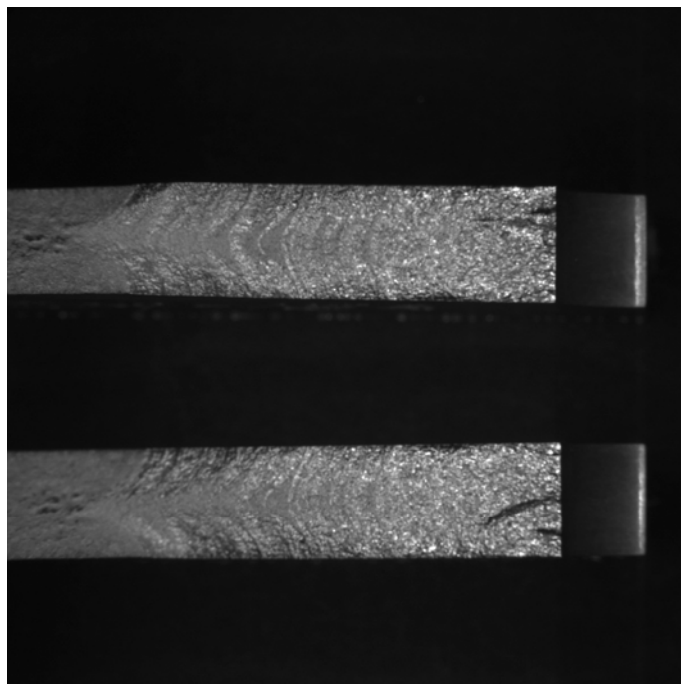
Figure E23: LM-136
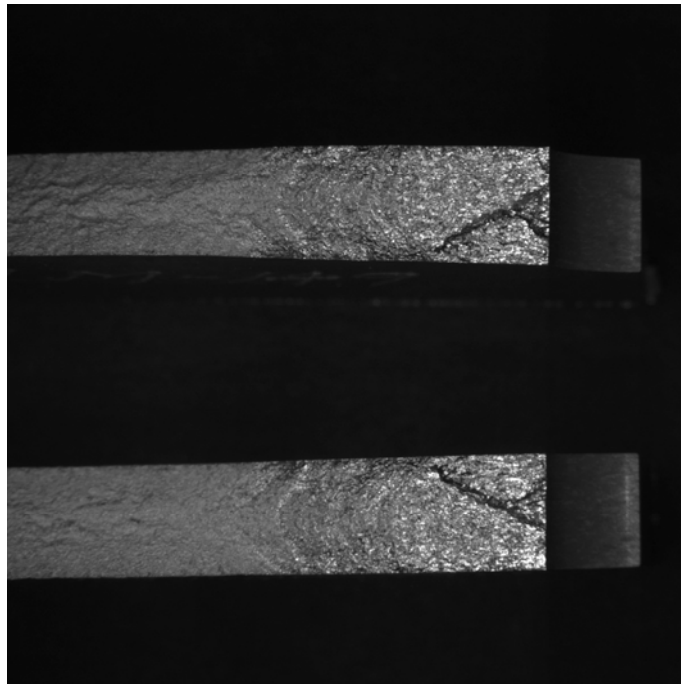
Figure E24: LM-149
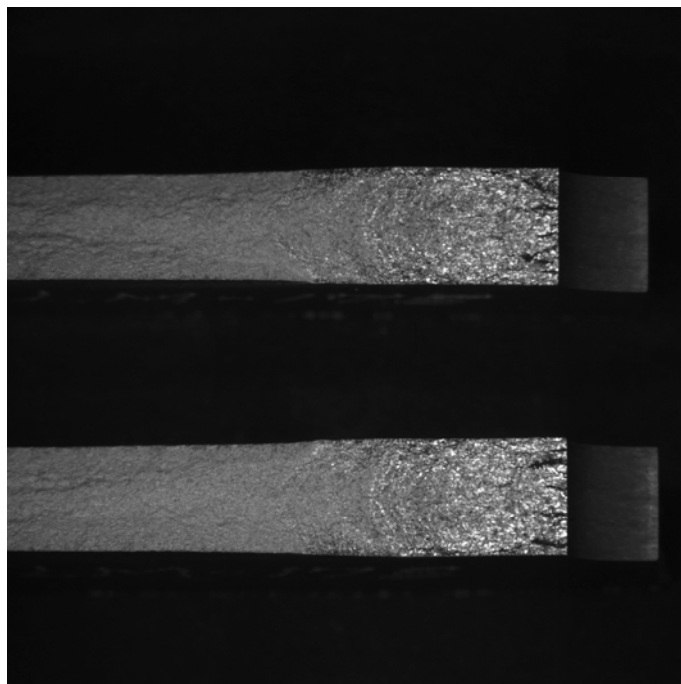
Figure E25: LM-175

E.1.6 Low Kt Dogbone – Machined (#400)
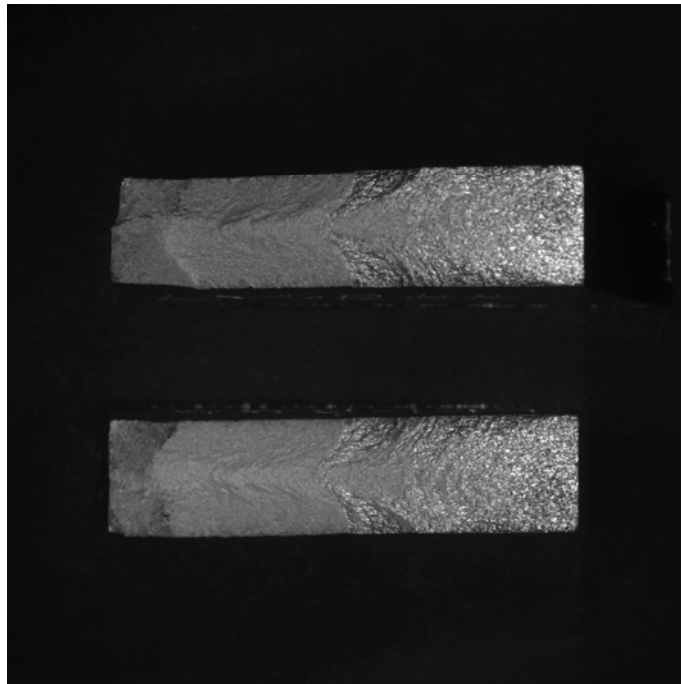
Figure E26: LM-244
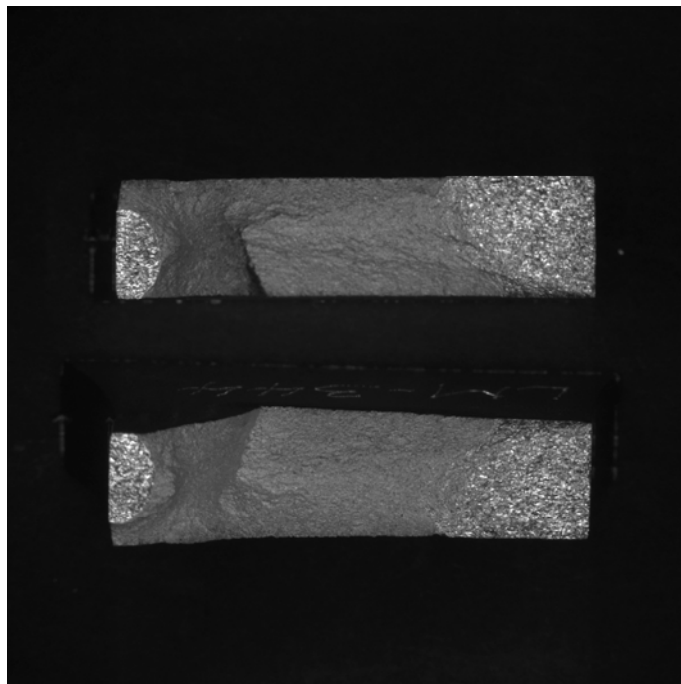
Figure E27: LM-344
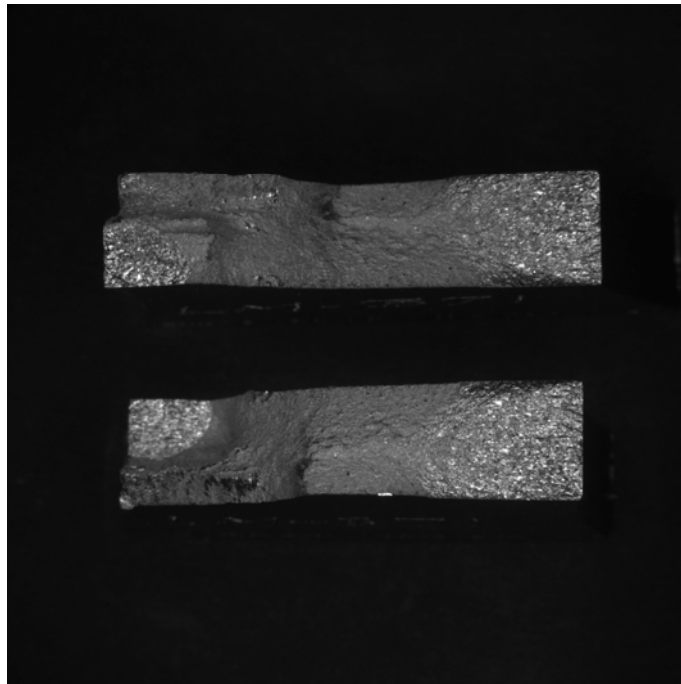
Figure E28: LM-371
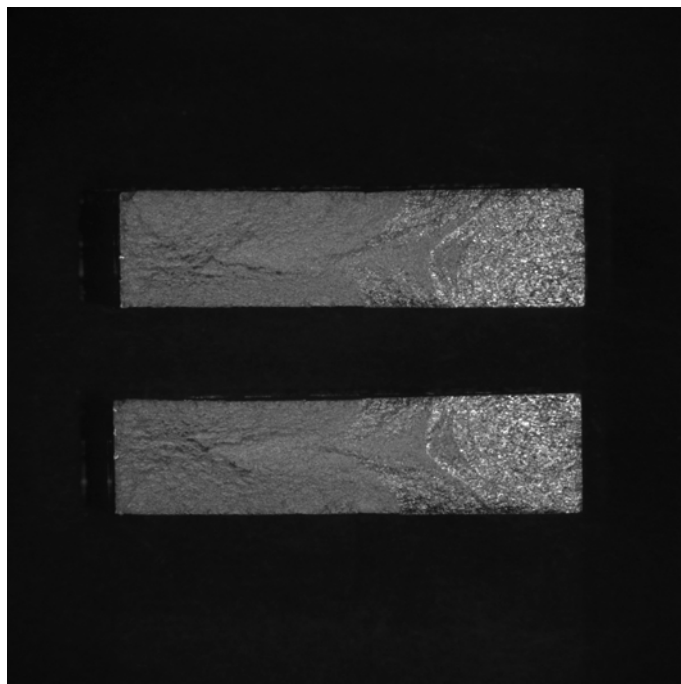
Figure E29: LM-398

E.1.7 Low Kt Dogbone – Machined (N6)
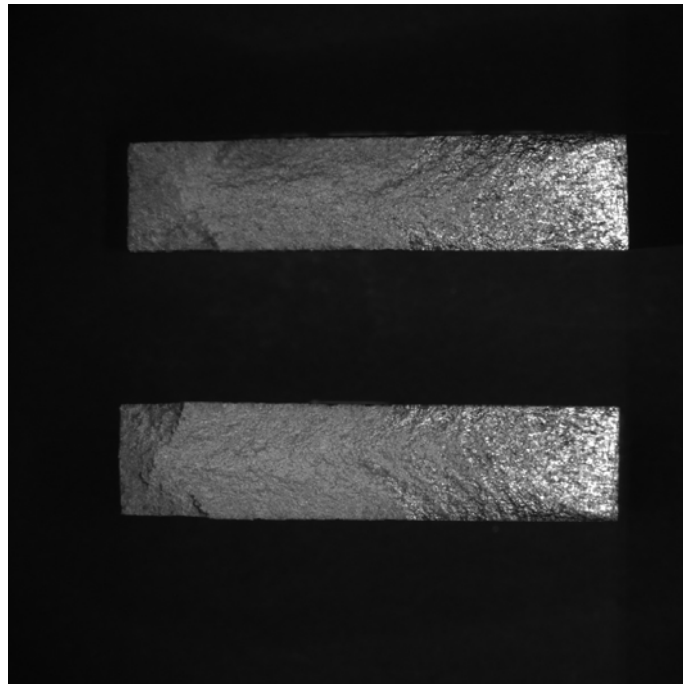
Figure E30: LMAA-01-L-T

Figure E31: LMAA-03-L-T
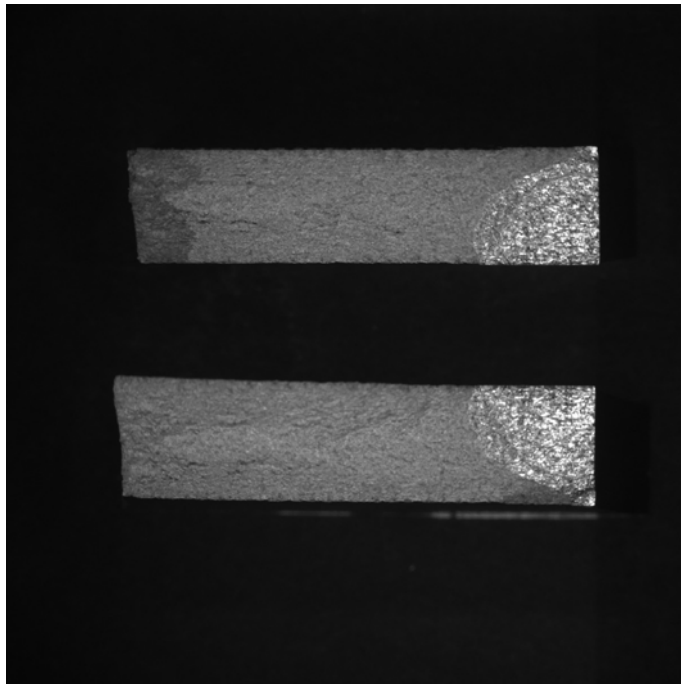
Figure E32: LMAA-06-L-T
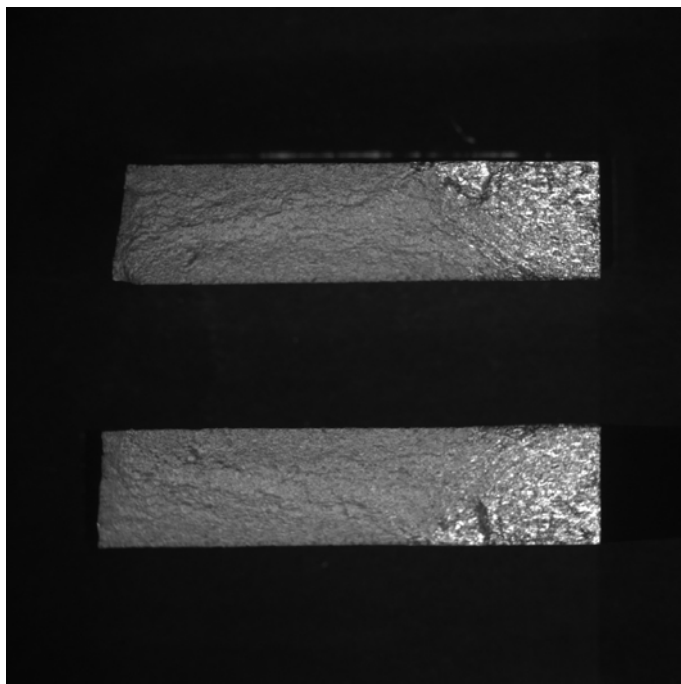
Figure E33: LMAA-10-L-T

E.1.8 Low Kt Dogbone – Pre-IVD Etched
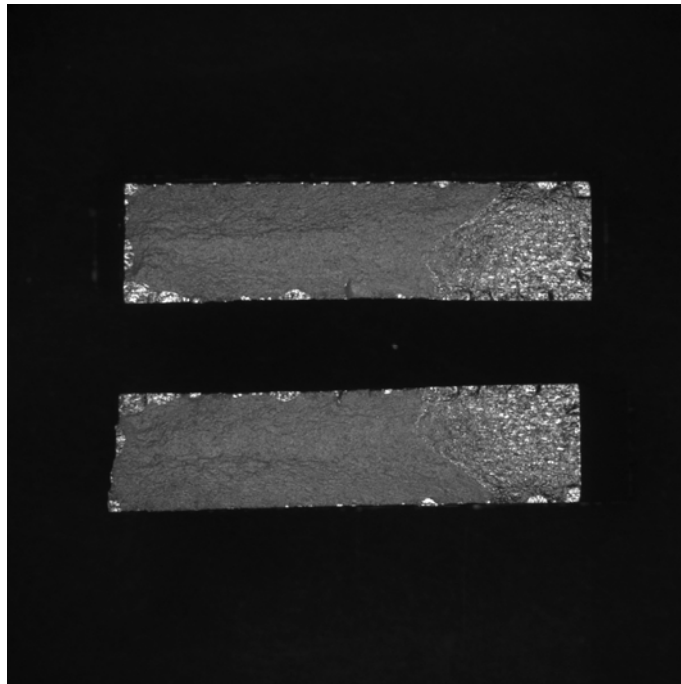
Figure E34: LM-309
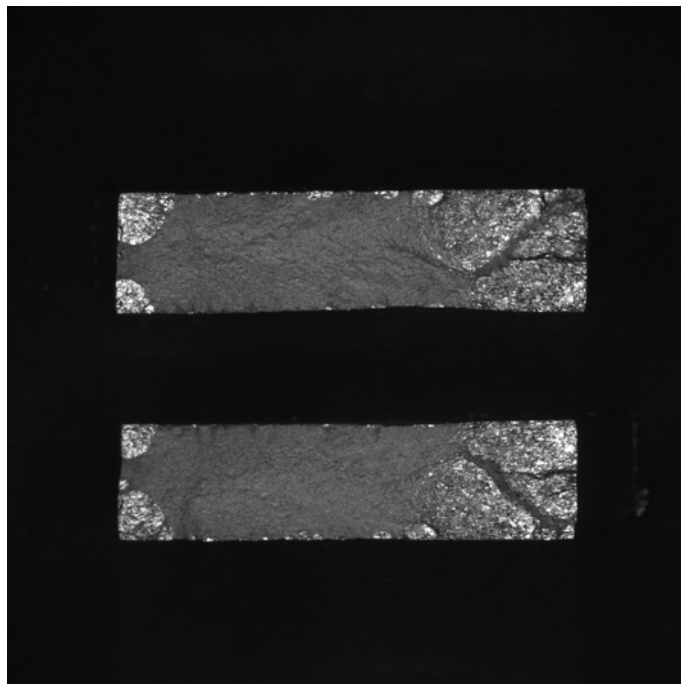
Figure E35: LM-329
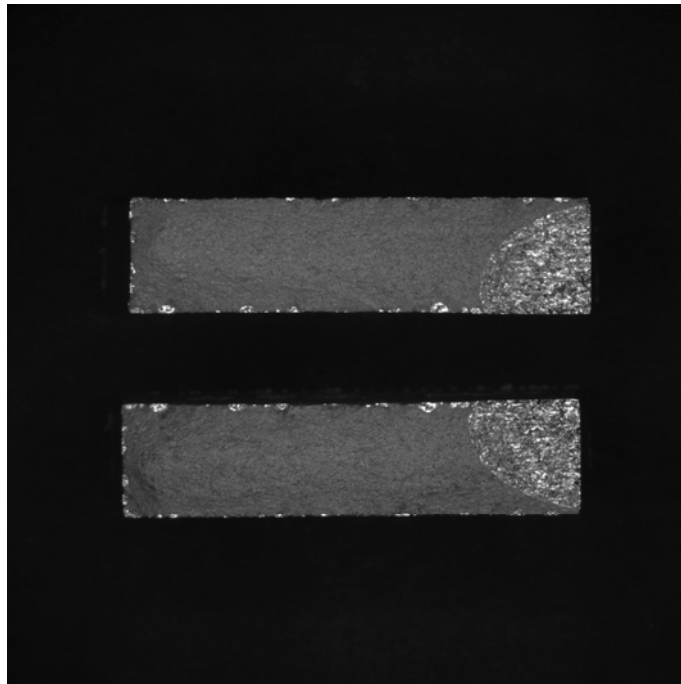
Figure E36: LM-364
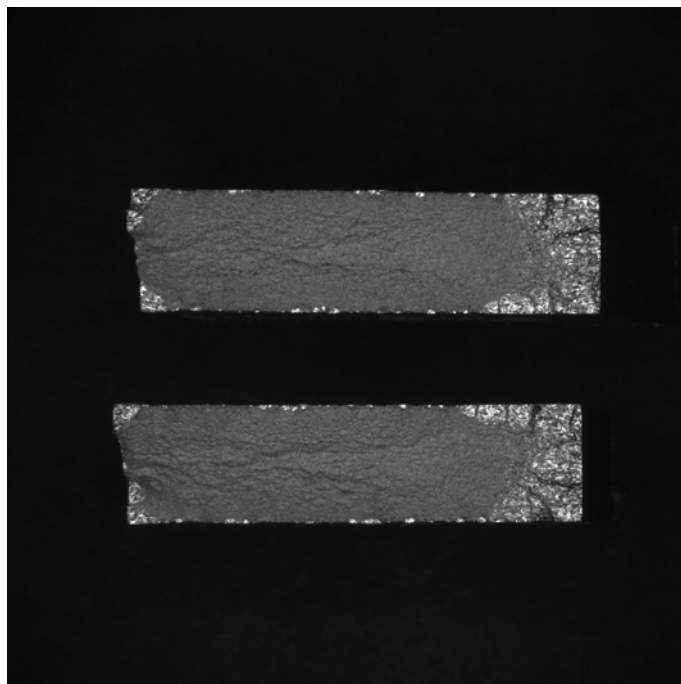
Figure E37: LM--372
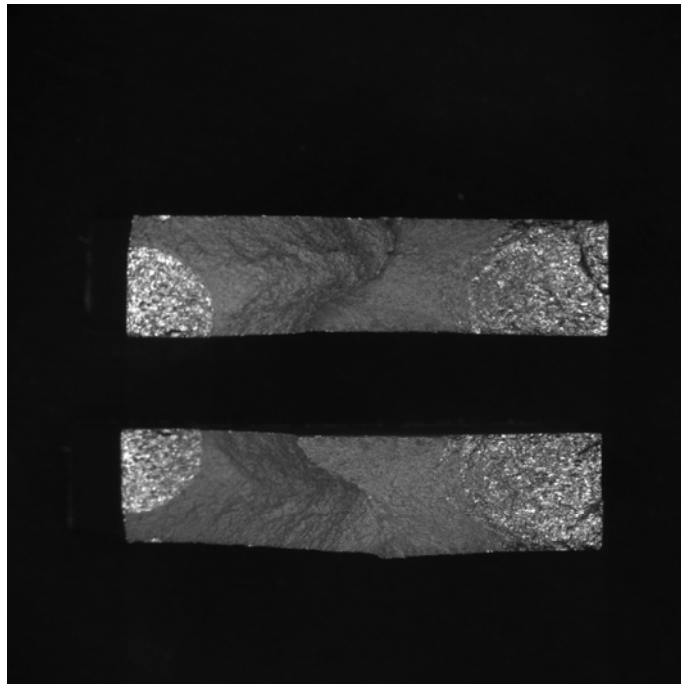
Figure E38: LM-440

E.1.9 Low Kt Dogbone – Anodised
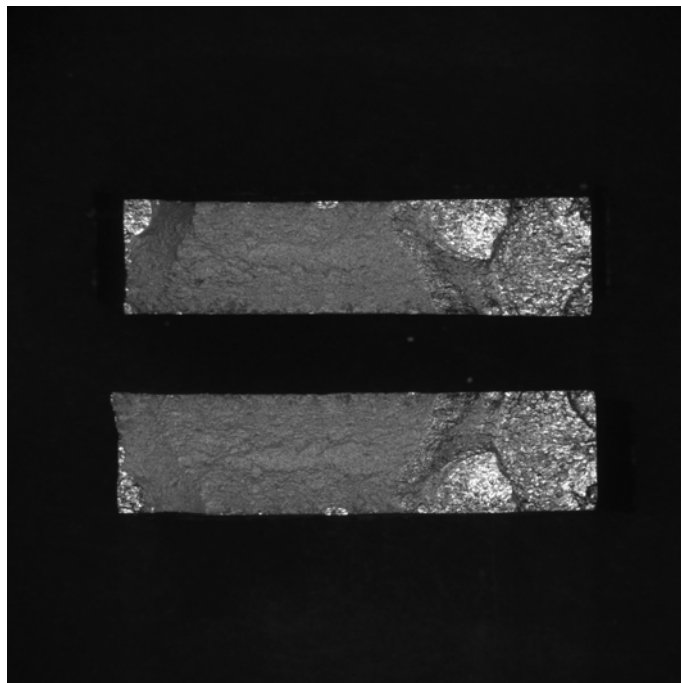
Figure E39: LM-233
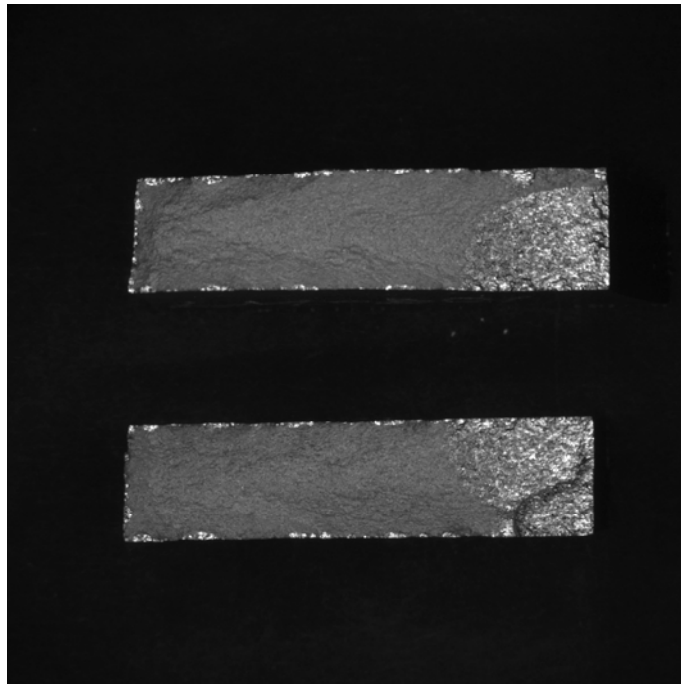
Figure E40: LM-301
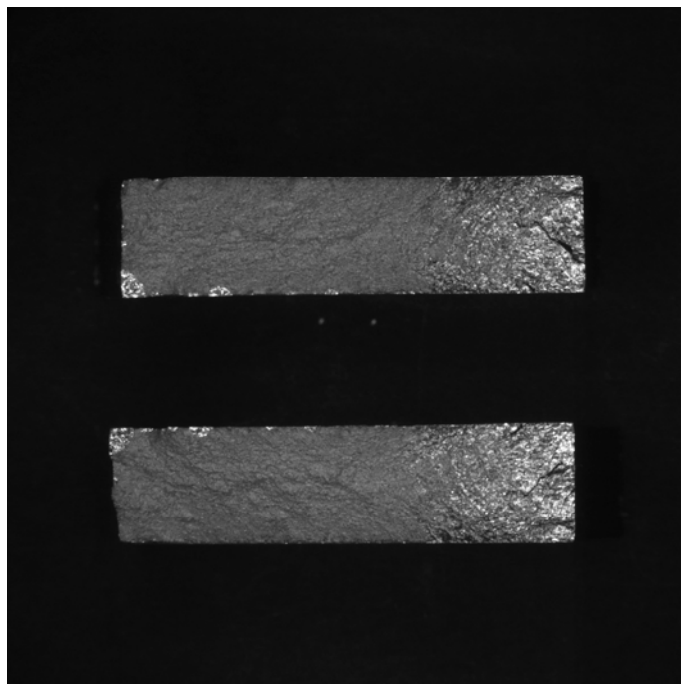
Figure E41: LM-303
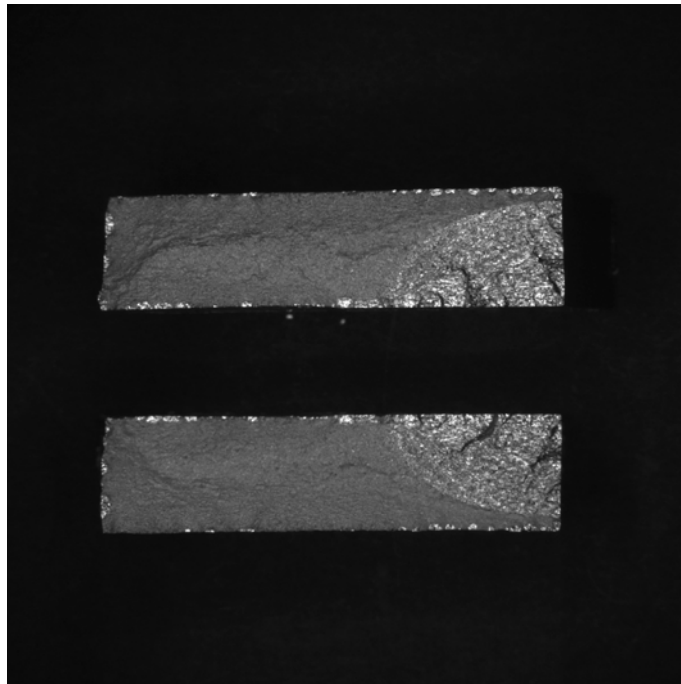
Figure E42: LM-317

Figure E43: LM-418

DEFENCE SCIENCE AND TECHNOLOGY ORGANISATION DOCUMENT CONTROL DATA		1. PRIVACY MARKING/CAVEAT (OF DOCUMENT)
2. TITLE Fatigue Testing of AA7050-T7451 with Various Corrosion Prevention Surface Treatments		3. SECURITY CLASSIFICATION (FOR UNCLASSIFIED REPORTS THAT ARE LIMITED RELEASE USE (L) NEXT TO DOCUMENT CLASSIFICATION) Document (U) Title (U) Abstract (U)

4. AUTHOR(S) Marcus McDonald, Robert Boykett and Michael Jones	5. CORPORATE AUTHOR DSTO Defence Science and Technology Organisation 506 Lorimer St Fishermans Bend Victoria 3207 Australia

6a. DSTO NUMBER DSTO-TR-2851	6b. AR NUMBER AR-015-631	6c. TYPE OF REPORT Technical Report	7. DOCUMENT DATE June 2013

8. FILE NUMBER 2011/1157777/1	9. TASK NUMBER 07/048	10. TASK SPONSOR DGTA	11. NO. OF PAGES 102	12. NO. OF REFERENCES 19

DSTO Publications Repository http://dspace.dsto.defence.gov.au/dspace/	14. RELEASE AUTHORITY Chief, Air Vehicles Division

15. SECONDARY RELEASE STATEMENT OF THIS DOCUMENT

Approved for public release

OVERSEAS ENQUIRIES OUTSIDE STATED LIMITATIONS SHOULD BE REFERRED THROUGH DOCUMENT EXCHANGE, PO BOX 1500, EDINBURGH, SA 5111

16. DELIBERATE ANNOUNCEMENT

No Limitations

17. CITATION IN OTHER DOCUMENTS	Yes

18. DSTO RESEARCH LIBRARY THESAURUS

Fatigue, corrosion prevention, fatigue testing, aluminium alloys, fatigue crack-growth.

19. ABSTRACT
The aluminium components of combat aircraft are usually manufactured with corrosion preventative surface treatments. This report presents the results of a fatigue coupon testing program carried out on AA7050-T7451 that was used to aid in the understanding of the fatigue life effect that anodising and an etching surface treatment can have in comparison to as-machined surfaces. The testing program included both high and low stress concentration geometry coupons that were subjected to a combat wing root bending moment spectrum. The results of the fatigue testing showed a reduction in the fatigue lives of anodised and etched coupons, especially in the low stress concentration geometry coupons. An investigation into the anodising process indicated the cause of the pitting found was likely chemical attack during a chemical cleaning process prior to the anodic layer being applied. These pits, which were numerous, acted as relatively large crack initiation discontinuities.